The University of Maine
DigitalCommons@UMaine

Electronic Theses and Dissertations | Fogler Library

Spring 5-8-2020

Radiometric Dating: A New Technique

Amber Emily Hathaway
University of Maine, amber.hathaway@maine.edu

Follow this and additional works at: https://digitalcommons.library.umaine.edu/etd

Recommended Citation

Hathaway, Amber Emily, "Radiometric Dating: A New Technique" (2020). *Electronic Theses and Dissertations*. 3214.
https://digitalcommons.library.umaine.edu/etd/3214

This Open-Access Thesis is brought to you for free and open access by DigitalCommons@UMaine. It has been accepted for inclusion in Electronic Theses and Dissertations by an authorized administrator of DigitalCommons@UMaine. For more information, please contact um.library.technical.services@maine.edu.

RADIOMETRIC DATING: A NEW TECHNIQUE

By

Amber Emily Hathaway

M.A., University of Maine, 2014

B.A., University of Maine, 2012

A DISSERTATION

Submitted in Partial Fulfillment of the

Requirements for the Degree of

Doctorate of Philosophy

(in Physics)

The Graduate School

The University of Maine

May 2020

Advisory Committee:

C. T. Hess, Ph.D., Professor of Physics, Advisor

Thomas E. Stone, Ph.D., Associate Professor of Mathematics and Physics, Husson University, Adjunct Graduate Faculty, University of Maine

Saima Farooq, Ph.D., Physics Lecturer, University of Maine

Andre Khalil, Ph.D., Associate Professor of Chemical and Biomedical Engineering, University of Maine

George Bernhardt, Ph.D., Research Scientist and Physics Lecturer, University of Maine

RADIOMETRIC DATING: A NEW TECHNIQUE

By Amber Emily Hathaway

Dissertation Advisor: Dr. C. T. Hess

An Abstract of the Dissertation Presented
in Partial Fulfillment of the Requirements for the
Degree of Doctorate of Philosophy
(in Physics)
May 2020

Radiometric dating is a common technique used to estimate the age of sediment and ice core samples. Lead-210 is widely used for dating sediment samples less than 150 years old. The two most commonly used lead-210 dating techniques rely on the assumption that the amount of lead-210 that is deposited in lake beds and other waterways remains constant over time. However, this assumption may not always be physically realistic, and if the rate is not constant, then age estimates derived using the constant rate assumption may not be accurate.

A new dating technique allowing for non-constant lead-210 supply rates (the NCRS model) was developed. It was implemented on 34 different sediment samples. Of these samples, 10 exhibited apparent sinusoidal fluctuations. Discrepancies in age estimates between models were most pronounced for the upper sediment layers. For the data sets which varied sinusoidally, the period was also computed and analyzed.

PREFACE

If my physics journey were a mathematical function, it would be the cosine. My foray into this discipline began auspiciously enough, with a course in calculus-based Advanced Placement (AP) Physics at Bangor High School, taught by Dr. Simon Wesley. The subject matter was challenging; I remember scoring in the 50s on my first try at a kinematics test. However, my instructor's enthusiasm for the subject was contagious. Through his lectures, I saw something beautiful hidden behind the complexity, something exciting, and I grabbled through the material, taking in what fleeting glances I could garner of that elegance. By the end of the spring semester, I was determined to major in the discipline when I started college the following fall.

I ended up earning my Bachelor's in Mathematics and Women's Studies[1] instead, with a minor in Physics, as well as one in Ethics and Social and Political Philosophy. There are many factors that influenced my departure from the physics major, some unique and personal, while others perhaps more common among those who leave physics. After earning my Master's in Mathematics, I returned to physics to pursue my Ph.D. My primary reason for choosing physics was that I wanted to remain close to home and the University of Maine did not offer a Ph.D. in any of the other disciplines I had studied. My retention is thus a fluke in many ways, the confluence of an atypical set of circumstances.

The journey to my Ph.D. involved countless tears, hours of listening to Kesha's "Praying" on repeat, and many tough decisions. However, I am immensely grateful that I was afforded this opportunity to advance science and human knowledge, and also to better understand myself. I am a small person, physically weak, and grapple with chronic anxiety which can be incredibly limiting, physically as well as mentally. However, I was blessed

[1]The precursor to the Women's, Gender, and Sexuality Studies program.

with my father's work ethic, and this journey has shown me that I am stronger and more determined that I had thought possible.

While I persisted, many others, particularly students from marginalized backgrounds, have not. I want to speak briefly on this subject, as it is dear to my heart. We, and here I mean society as a whole, as well as members of the physics community, like to view physics as objective and free of bias. However, what we study in physics, what we choose to consider physics, and who counts as a physicist are decisions made by humans who are inherently subjective. It matters who is doing physics.

Astrophysicist Jocelyn Bell Burnell credits her difference both in terms of her gender as well as the geographical location she grew up in as a contributing factor in her discovery of pulsars. Coming from outside the mainstream physics tradition, she was willing to investigate anomalies in radio telescope data which other scientists may have neglected. Making physics an inclusive space is not merely a nice thing to do; it will make for better science.

Difference made this document possible, although the ways in which it shaped my dissertation are subtle, if not indistinguishable. The most obvious difference that comes into play here is my mathematical training; the required math which was off putting to previous graduate students is what drew me in. Differences in disciplinary background may seem untethered to identity facets like gender or social class, but I have always experienced the sciences as a woman from a working class background, and my appreciation for math is inevitably intertwined with my experiences as a woman studying math. I have often felt "at home" in math, whereas in physics it took years of metaphorical couch surfing before I managed to build a place of my own. While not solely due to gender, I think my gender had its hand in making one discipline seem inviting and the other foreboding.

I want to acknowledge that most of the individuals I have met along my physics journey have been kind, many supportive, and there are but few examples I can point to as instances which have actively thwarted my interest in physics. I am also slower to

comprehend physics than I am math, and my comparative underperformance in physics has not been kind to a self which is already full of doubt. However, there is something about physics as a discipline, what I can describe best as a cultural difference, this feeling of je ne sais quoi, which permeates seemingly every facet. Each time I breathe in, it is there, not enough to suffocate, but its prevalence irritates my lungs. These days it is but a minor nuisance, but there have been times when it was all I could feel.

I am not the only person who has struggled to find a place in physics. Women, black and indigenous students, and working class students, among others, are vastly underrepresented in this discipline. In my discipline. The percentages of individuals from marginalized backgrounds receiving physics degrees has remained stagnant for years, even as the shares in other STEM fields like mathematics and chemistry have grown.

The question of how to make physics more inclusive is one that I regularly grapple with. I don't have all the answers, but I do know that ignoring this question because it is challenging will not make the situation better. We owe it to our students and to our field to foster a learning environment in which individuals from a multiplicity of backgrounds feel welcome.

My primary aim in writing this preface is to provide a sense of who the author of this document is.[2] However, in reflecting on my trajectory, I see all of the places along my path where I left or nearly left physics, and think of the others who have stood at that same juncture and found it too much, and my heart breaks. While a minority in physics due to my gender and, to a lesser extent, my socioeconomic status growing up, I still benefit from many privileges which have made my success possible, privileges that not everyone studying physics has. I felt like this document would be incomplete without some acknowledgment of the fact that not everyone is able to experience physics in the same way. Although I struggled to reach this point, my struggles likely pale in comparison to

[2]If your takeaway is that I am an anxious mess of a woman with low self esteem, you are not wrong.

what other marginalized students have had to overcome. Anything we can do to make physics more accessible will give us a step in the right direction.

I doubt this preface will be read by more than a handful of individuals,[3] but if you happen to be someone who is struggling in physics, I want you to know that you are enough. The field may feel rigid and confining at times, but it can grow and expand to fit you. You don't have to stick with physics; I don't want to force you to stay somewhere you're not happy. But if you're feeling insecure, know that my insecure self has just earned a Ph.D. in physics. Your insecure self can do incredible things too.

Amber Hathaway

April 28, 2020

[3]Hi committee!

DEDICATION

To my partner, Brian Toner, for his unwavering support and confidence in my abilities. Also, to those of you who are interested in physics, but have been led to believe that you do not belong here. Not only do you belong, you are needed. Diverse perspectives lead to better science.

ACKNOWLEDGEMENTS

First and foremost, I would like to thank my dissertation advisor, Dr. C. T. Hess for his support and mentorship throughout this process. You have believed in my abilities even when I haven't been sure of them myself, and for that I am grateful. I would also like to thank my committee members Dr. Tom Stone, Dr. Saima Farooq, Dr. Andre Khalil, and Dr. George Bernhardt for their feedback and guidance. I would like to thank my external reader, Dr. James Kaste, for his feedback on this document. I would like to thank my colleague, James Deaton, for teaching me the experimental side of things.

Thank you to my counselor, Michaele Potvin, who has helped me through some difficult times, and also the staff and faculty members who have supported me when I've been overwhelmed by my anxiety. I don't think I would have been able to make it this far into my program without your help.

I would like to thank my high school physics teacher, Dr. Simon Wesley, for inspiring my interest in physics and for supporting me from afar years after I have graduated. I would also like to thank Pat Byard for her assistance over the years and for generally being a positive and supportive force for the graduate students. I don't know how the physics department would keep going without you.

Lastly, I would like to thank my partner Brian Toner. He has been my support system throughout this whole process, encouraging me when I felt overwhelmed and sharing in my triumphs. Without his continual support, this journey would have been significantly more difficult.

TABLE OF CONTENTS

LIST OF TABLES

LIST OF FIGURES

CHAPTER 1
A BRIEF HISTORY OF RADIOMETRIC DATING

Current radiometric dating techniques are often implemented with the assumption that the amount of a radioisotope deposited annually remains roughly constant over time. However, there is evidence (e.g., [1]) to suggest that the concentration of certain radioisotopes may fluctuate. The goal of this research is to develop a radiometric dating technique that does not rely on the assumption that the rate of supply of a radioisotope remains constant.

Before this new technique can be introduced, it may be useful to have an understanding of the history of radiometric dating, as well as current dating techniques. A brief history of radiometric dating will be outlined in this chapter, while current dating techniques will be discussed in the following chapter.

1.1 The Discovery of Radiation

The existence of radioactivity as a distinct physical phenomenon was first demonstrated by Henri Becquerel (1852-1908) in 1896 [2]. His work was inspired by a 1895 discovery made by Wilhelm Conrad Röntgen (1845-1923), in which Röntgen demonstrated the existence of x rays [3, 4]. Röntgen was studying the fluorescence of cathode ray tubes. He noticed that a line appeared on a coated cardboard screen lying near his apparatus when he ran a current through the apparatus. He had shielded the tube in such a way that no visible light could pass through, so he could not attribute the fluorescence to escaped light. Subsequent experiments showed that the rays, for example, could not be polarized or separated with a prism, further suggesting that he had happened upon a new type of electromagnetic radiation.

Röntgen placed various objects such as wood and thin sheets of metal in front of the newfound fluorescence and found that it passed through many, although the thicker and

denser an object was, the harder it was for the radiation to pass through. Lead, he found, was almost impenetrable, and thus made a good shield against these new rays. Röntgen chose the name "x ray" for his discovery because the odd behavior of these rays was unlike anything else known to science at the time.

What x rays have become most well known for is the ability to image the human skeletal system without cutting the flesh. Röntgen discovered this ability while experimenting on himself, observing that when he placed his hand between the device and a screen, a silhouette of his hand bones appeared on the screen [5]. After conducting his experiments in secret for weeks, he told his wife Anna Bertha (Ludwig) Röntgen (1839-1919) [4] of his discovery on December 22nd, 1895 and took an x-ray photograph of her hand. Upon seeing the bones of her hand, she is reported to have said, "I have seen my death!" [5].

Not long after entrusting Bertha with the news of his discovery, Wilhelm Röntgen decided to publish his work. The first print of his manuscript appeared in the Sitzungsberichte of the "Physikalisch-Medizinische Gesellschaft" (session reports of the Würzburg Medical Society) on December 28, 1895 [5, 4]. Soon translations and reprints began appearing in publications all across the world (see, e.g., [6]). While the initial publication contained only a written account of Röntgen's discovery, subsequent prints often included a copy of the image Wilhelm had taken of Bertha's hand [5]. This image became the first published medical x-ray photograph [4].

After the discovery of x rays, researchers began investigating whether sources of fluorescence other than the cathode ray tube could produce x rays [3]. Henri Becquerel began experimenting with a uranium salt. He placed the salt on a photographic plate which he had covered in black paper to block out visible light and found that the plate had blackened in the spot upon which he had placed the salt. He extrapolated from his experiment that the rays came from the source of fluorescence, the uranium salt. There remained the question as to whether the uranium salt somehow garnered its abilities from illumination by the sun. In subsequent experiments, he found that regardless of whether he

Figure 1.1. X-ray image of Anna Bertha Röntgen's hand and ring. Photoprint from radiograph by W. K. Röntgen, 1895. Credit: Wellcome Collection. CC BY

had exposed the salt to sunlight, the salt still blackened the photographic plate, suggesting that the salt itself was creating the rays.

Marie Skłodowska Curie (1867-1934), who would end up coining the term "radioactivity," took interest in Becquerel's discovery and chose it as the subject of her doctoral work [3]. She wanted to test all known elements and compounds, some of which were rare and hard to obtain, to see which ones gave off this mysterious radiation. Röntgen and Becquerel had both shown that the rays they observed caused the air to become electrically conducive. Curie used an electrometer with a piezoelectric crystal that her husband Pierre had built and modified to suit her work to determine which elements exhibited this property and found that in addition to uranium, thorium also emitted radiation.

Marie Curie also observed that when testing pitchblende, an ore from which the uranium had been removed, it gave off more radiation than uranium itself. Similarly, she found that calcite was more active than pure thorium [7]. Thus, she hypothesized that there was some yet unknown element in the uranium ore that was also emitting radiation. She also discovered that radiation was a property of an element itself, as the radioactivity remained unchanged when a sample was, for example, heated or exposed to light. She wrote up her findings, using the name radioactivity for the phenomenon she had investigated. Her results were presented on her behalf at the Academy of Sciences in April of 1898.

It was at this point that Pierre joined her in her studies, and together they worked to discover the properties of the unknown element. The Curies chemically separated pitchblende and by 1898 had found evidence of a metal which they believed to be similar to bismuth. They called it polonium, after Marie's homeland, Poland. However, demonstrating its existence proved difficult, as traditional spectral analysis techniques failed to show anything new, since there was too little polonium in the samples to be observed through this technique. Later that year they found evidence of a radioactive substance different from polonium, which they called radium. A chemist colleague,

Eugêne-Anatole Demarçay (1852-1903), was able to demonstrate a unique spectral line for radium [7]. While this evidence was enough to convince many physicists that radium was in fact a distinct element, chemists required a measurable quantity of the substance.

Marie thus set out to isolate radium [7]. She proposed using slag, minerals residual after extracting the uranium from pitchblende in the production of uranium. It was from this slag that, over the course of several years, she was finally able to extract sufficient quantities of radium to demonstrate its existence as a distinct radioactive element.

The nature of radioactivity remained elusive, although Marie had a theory regarding its nature. In a manuscript published in Revue Scientifique, she put forth the idea that radiation came from the separation of atoms [8]. She stated,

> La matière radioactive serait donc de la matière où règne un état de mouvement intèrieur violent, de la matière en train de se disloquer. S'il en est ainsi, le radium doit perdre constamment de son poids. Mais la petitesse des particules est telle que bien que la charge électrique envoyée dans l'espace soit facile à constater, la masse correspondante doit être absolument insignifiante ; on trouve par le calcul qu'il faudrait des millions d'années pour que le radium perde un équivalent en milligrammes de son poids. La vérification est impossible à faire.
>
> La théorie matérialiste de la radioactivité est très séduisante. Elle explique bien les phénomènes delà radioactivité. Cependant, en adoptant cette théorie, il faut nous résoudre à admettre que la matière radioactive n'est pas à un état chimique ordinaire; les atomes n'y sont pas constitués à l'état stable, puisque des particules plus petites que l'atome sont rayonnées. L'atome, indivisible au point de vue chimique, est divisible ici, et les sous-atomes sont en mouvement. La matière radioactive éprouve donc une transformation chimique qui est la source de l'énergie rayonnée ; mais ce n'est point une transformation chimique ordinaire, car les transformations chimiques ordinaires laissent l'atome

> invariable. Dans la matière radioactive, s'il y a quelque chose qui se modifie, c'est forcément l'atome, puisque c'est à l'atome qu'est attachée la radioactivité (Curie, 70).

Her statement loosely translates as:

> The radioactive material is therefore matter in which there is a state of violent internal movement, of material being dislocated. If this is so, radium must constantly lose its weight. But the smallness of the particles is such that although the electric charge sent into space is easy to notice, the corresponding mass must be absolutely insignificant; it is calculated that it would take millions of years for radium to lose an equivalent in milligrams of its weight. Verification is impossible to do.
>
> The materialistic theory of radioactivity is very seductive. It explains the phenomena of radioactivity well. However, by adopting this theory, we must resolve to admit that the radioactive material is not in an ordinary chemical state; the atoms are not constituted in the stable state, since particles smaller than the atom are radiated. The atom, indivisible from the chemical point of view, is divisible here, and the sub-atoms are in motion. The radioactive material thus experiences a chemical transformation which is the source of the radiated energy; but it is not an ordinary chemical transformation, for ordinary chemical transformations leave the atom invariable. In the radioactive material, if there is something that changes, it is necessarily the atom, since it is to the atom that the radioactivity is attached.

It is unclear whether Marie fully ascribed to this belief at the time. Pierre was greatly opposed to this view, and a paper the couple jointly affixed their names to published two years later would caution against the hasty adoption of such an assertion [7, 9]. Nevertheless, Marie's suggestion that radiation was caused by the splitting of atoms would be validated a couple of years later.

Marie had noted in her article that there seemed to be at least two distinct types of radiation, x-ray radiation, known today also as γ radiation, and what she referred to as cathode rays, known today as β radiation. The two behaved differently; while the cathode rays were deflected by a magnetic field, the x rays were not [8].

The Curies were not the only researchers to notice distinctions between types of radiation. In 1899, about a year before Mare Curie published the manuscript in which she laid out her theory of radiation, Ernest Rutherford (1852-1908) had commented upon two types of radiation he had observed in his laboratory, which he referred to as α radiation and β radiation [3]. The α radiation, he observed, was readily absorbed, while the β radiation could travel deeper into an object. Paul Villard (1860-1934) discovered a third type of radiation coming from radium which behaved like Röntgen's x rays. This radiation he termed as γ radiation, following Rutherford's naming convention.

The nature of β particles was determined by Becquerel in 1900, when he demonstrated that they had the same charge to mass ratio as an electron [3]. However, α particles remained elusive. It was shown that they, like β particles, were deflected by a magnetic field, but in a different direction and to a lesser extend, suggesting that α particles had opposite charges and were heavier than electrons. Although speculation that α particles were related to helium was published as early as 1903 [10], it was not until 1908 when Rutherford and Thomas Royds (1884-1955) showed definitively that α particles were helium ions [11].

The Curies, Rutherford, Becquerel, and others observed that radioactive elements seemed to emit radioactive particles distinct from the original element [3]. The progeny of radium and thorium, which would come to be known during that era as radon, thoron, and actinon,[1] were radioactive, but not nearly as radioactive as the elements they had originated from. While the radioactivity of radium and thorium remained roughly unchanged over the duration of an experiment, scientists began noticing that activities of

[1] thoron and actinon are now known to be isotopes of radon

radon, thoron, and actinon decreased with time. This decrease seemed to follow an exponential trend, first decaying rapidly and then tapering off as the quantities of radon, thoron, and actinon were reduced.

In 1902, Rutherford and his assistant Frederick Soddy (1877-1956) formalized this decrease in the number of particles over time in the nuclear decay equation, [12]:

$$N(t) = N(0)e^{-\lambda t}, \tag{1.1}$$

where t is time, λ is the decay constant, $N(t)$ is the number of atoms of a given radioisotope[2] at time t, and $N(0)$ is the initial concentration.[3] The decay constant was found to be unique to a given radioisotope and governed how fast a sample of that radioisotope would decay. This paper has largely been credited as the publication that established the "disintegration of the elements" (known today as nuclear decay). Certainly, Rutherford and Soddy make a strong case for it in their paper. However, it is worth noting that a rough concept of nuclear decay existed prior to the 1902 publication, such as articulated by Marie Curie [8].

Although they did not use the term secular equilibrium in their paper, Rutherford and Soddy noticed that if thorium and one of its progeny, which they termed thorium X,[4] were kept together, the activity of thorium X would remain roughly constant after some time had elapsed. This observation supplied an important insight, namely that more atoms of a given isotope could be introduced into a sample through radioactive decay. For example, if thorium-234 was decaying in the presence of other radioisotopes including uranium-238, the creation of new thorium-234 particles through uranium-238 decay would have to be accounted for.

[2]The term radioisotope had not yet been coined at the time of Rutherford and Soddy's publication, and thus is not utilized in their manuscript.

[3]Rutherford and Soddy stated the equation in a slightly different format in their paper: $\frac{I_t}{I_0} = e^{-\lambda t}$, where I_0 and I_t are the initial activity and the activity after time t, respectively [12].

[4]Thorium X is known today as radium-224.

1.2 Radiometric Dating and the Age of the Earth

Rutherford is credited with first suggesting that radioactivity could be used to estimate the ages of minerals [2]. Prior to the discovery of radioactivity, William Thompson (1824-1907), perhaps better known as Lord Kelvin, had estimated the age of the earth based upon the premise that the earth's temperature was due to its molten origins [13]. Over time, the earth had cooled, and he estimated how long it would take for the earth to cool from its presumed original state to the surface temperature he experienced. In 1862 Thompson estimated that the earth had formed between 20 and 400 million years prior [13].

Pierre Curie and his student, Albert Laborde (1878-1968), discovered in 1903 that radium generates heat [13]. Rutherford, along with Howard T. Barnes (1873-1950), determined that the generation of heat was a direct consequence of the decay process [14]. Rutherford recognized that Thompson had not accounted for the generation of heat through radioactive decay in his calculations of the age of the earth and started looking for alternative avenues to estimate the age of the earth. Using a sample containing uranium that he had on hand, Rutherford estimated the age of the sample to be on the order of 500 million years [2], older than Thompson's estimate. Rutherford presented his findings in a lecture in 1904 [2, 15].

Although the exact nature of α particles was not yet understood, Rutherford speculated that they were related to helium. Sir William Ramsay (1852-1916) and Soddy had recently provided an estimate as to how fast radium, a product in the uranium decay series, produced alpha particles [10]. Since helium does not decay, as long as no helium leaves the sample through natural processes, Rutherford speculated that the amount of helium in a uranium sample could be used to estimate the age of the sample. This is how he made his 1904 estimate [2].

Rutherford was not the only scientist to attempt to date samples using their helium concentrations. Robert Strutt (1842-1919) conducted numerous dating experiments between 1908 and 1910 using this method [16]. A problem with this dating method soon

became apparent, however, as Strutt's estimates did not align with the accepted geological ages of his samples. It became apparent that helium was somehow escaping from the samples.

Another element used in these early dating attempts was lead. Rutherford had suggested to American radiochemist Bertram Boltwood (1870-1927) that lead was the end product of uranium decay and thus might be used to estimate the age of a sample [2, 13, 16]. Although Boltwood began investigating this idea in 1905, his first published results did not appear until 1907, as his initial age estimates proved to be inaccurate [13]. One issue with Boltwood's initial dating attempts was that the radioactive decay constants had not been accurately determined yet. Estimates of the half-life of radium in particular changed several times between 1905 and 1907, and each updated value altered Boltwood's predictions.

A reliable half-life for uranium[5] had not yet been established, so Boltwood used the half-life of radium to provide an estimate [17]. At the time, the best estimate for the half-life of radium was 2600 years, an estimate Rutherford had come up with. Since half-life is computed as

$$t_{\frac{1}{2}} = \frac{\ln[2]}{\lambda}, \tag{1.2}$$

to find the decay constant λ,[6] Boltwood divided ln[2] by 2600 years to obtain the estimate that in a given year, the fraction of all radium isotopes that would decay would be $\lambda = 2.7 \times 10^{-4}$. Rutherford and Boltwood had previously estimated that for every gram of uranium in a sample, there were about 3.8×10^{-7} grams of radium [18]. In other words,

$$\frac{m_{Ra}}{m_U} = 3.8 \times 10^{-7}. \tag{1.3}$$

To provide a rough estimate for the half-life of uranium, Boltwood recognized that the radium and uranium in his samples should be in secular equilibrium,[7] so that at any

[5]Isotopes were not yet understood, but uranium-238 is the most commonly occurring isotope, so it is likely that Boltwood's samples contained uranium-238 primarily.

[6]Boltwood used few symbols or equations in his original paper. His process has been rewritten using contemporary mathematical expressions and notation to make it easier to follow

[7]Boltwood used the term "radio-active equilibrium."

moment in time, equal amounts of uranium and radium atoms should be decaying. That is,

$$\lambda_U N_U = \lambda_{Ra} N_{Ra}. \tag{1.4}$$

Instead of using the atomic masses of radium and uranium to extrapolate the number of particles of each type, he assumed that the masses were the same. If the atomic masses were the same, then the ratio he and Rutherford had computed of radium to uranium in a sample would be the same as the ratio between the number of particles in each. In other words,

$$\frac{m_{Ra}}{m_U} \approx \frac{N_{Ra}}{N_U} \tag{1.5}$$

and thus

$$\lambda_U = \lambda_{Ra} \frac{N_{Ra}}{N_u} \approx \lambda_{Ra} \frac{m_{Ra}}{m_U}. \tag{1.6}$$

Multiplying λ_{Ra} by $\frac{m_{Ra}}{m_U}$, he arrived at the conclusion that the decay constant for uranium was on the order of 10^{-10} decays per year [17]. This implied that the half-life of uranium was on the order of 10^{10} years.

To estimate the age of the minerals in his sample, he took the ratio of lead to uranium in each sample and multiplied it by 10^{10}. Boltwood did not explain why this should yield the age of the sample. His approach was perhaps more heuristic than what follows, but the same equation can easily be derived mathematically using appropriate approximations. From the nuclear decay equation,

$$N_U(t) = N_U(0)e^{-\lambda_U t} \approx (N_U(t) + N_{Pb}(t))e^{-\lambda_U t}, \tag{1.7}$$

where N_{Pb} is the number of lead atoms in the sample. The latter part of the equation relies on the assumption that all of the uranium in the sample that has decayed has decayed to a stable isotope of lead that has remained in the sample, and that there is no lead in the sample from other sources. Rearranging,

$$N_U(1 - e^{-\lambda_U t}) = N_{Pb}e^{-\lambda_U t} \tag{1.8}$$

and thus

$$\frac{N_{Pb}}{N_U} = e^{\lambda_U t} - 1. \tag{1.9}$$

Using a Taylor series expansion,

$$\frac{N_{Pb}}{N_U} \approx (1 + \lambda_U t) - 1 = \lambda_U t. \tag{1.10}$$

Ignoring the atomic mass differences between lead and uranium,

$$\frac{m_{Pb}}{m_U} \approx \lambda_U t. \tag{1.11}$$

By his estimates, his samples ranged in age from 410 million to 2.2 billion years. This implied that the earth had to be at least 2.2 billion years old, significantly older than previous radiometric dating efforts had suggested.

There were several problems with Boltwood's approach. The biggest issue was that many of his samples contained thorium as well as uranium. Thorium also decays to lead, but Boltwood assumed that it did not [17]. His flawed assumption was premised on the fact that, while he found roughly constant uranium to lead ratios in his mineral samples from a given location, the thorium to lead ratios varied substantially from one sample to another. By assuming that all of the lead in his samples came from uranium, his results for samples with high thorium to uranium ratios were necessarily skewed. Furthermore, the samples likely contained various isotopes of both lead and uranium. While this could not have been accounted for at the time, as isotopes had not yet been identified, it may have skewed his results, as different isotopes have different half-lives and come from different decay chains. Boltwood also made many simplifications, such as ignoring mass differences between uranium and radium, which denied the method the rigor that would be needed for accurate age estimates. Nonetheless, Boltwood had provided the framework that would lead to modern lead-uranium dating.

While Boltwood and Rutherford occasionally toyed with the question of the age of the earth, neither one published extensively on the subject following Boltwood's 1907 paper.

Arthur Holmes (1890-1965), one of Strutt's students, was inspired by Boltwood's work and set out to improve upon Boltwood's techniques. His first publication, in 1911, utilized Boltwood's basic technique, using equation [1.11] to compute the age of his sample, but with a newly calculated half-life of uranium of 8.2 billion years [19]. While this value does not match the currently accepted value, Holmes's half-life calculation was closer than Boltwood's 10 billion year estimate. Two years later, Holmes published a book examining the different methods that were being used at the time to estimate the age of the earth [20]. Using a further refined half-life of uranium of 5.4 billion years, he estimated that one of his samples was 1.6 billion years old.

Discoveries during the 1910s led to complications in the radiometric dating technique established by Boltwood and refined by Holmes [13]. One issue was that it was discovered that lead was a decay product of thorium, thus adding challenge to dating samples containing both uranium and thorium. In 1913, Soddy introduced the concept of the isotope, showing that there existed atoms with the same proton number but different neutron numbers. The term isotope was suggested to Soddy by the physician Dr. Margaret Todd[8] (1859-1918), from the Greek *iso topos*, which means "same place" [22]. The term was fitting because isotopes of an element occupy the same place on the periodic table. It was found also that isotopes of the same radioactive element had different half-lives. Recognizing that there were different isotopes of both uranium and lead, and that different isotopes of uranium decayed into different isotopes of lead meant that Boltwood's method could no longer be expected to provide a reliable age estimate. Although Holmes was forced

[8]Todd is an intriguing figure in the history of medicine. She did not show much of a passion for medicine, but rather seemed to pursue it because medical school was one of the highest educational attainments available to women [21], becoming one of the first students at the Edinburgh School of Medicine for Women. There she met the woman who would become her life partner, Dr. Sophia Jex-Blake, a physician and one of the founders of the school. While attending medical school, Todd wrote and published the novel *Mona Maclean, Medical Student* under a male pseudonym. The novel was significant in part because it received much praise as well as support for the movement to integrate women into the medical profession. Although she did practice medicine at times, it was her writing that seemed to compel her, as she went on to publish several more books and stories. She died by suicide in 1918, three months after her final book, a biography of Dr. Jex-Blake, had been published.

to leave academia for years at a time due to low wages offered to him as a student and later as an instructor [15], he continued to pursue a reliable technique for lead-uranium dating.

It was not until the late 1930s when American physicist Alfred Nier (1911-1994) provided the insight which would make accurate radiometric dating possible. Previously, due to the observed unchanging atomic weight of lead in various samples, it was assumed that lead isotopes existed in roughly the same ratios in all samples. Nier examined the abundance of lead isotopes in various samples and found that the lead composition was not uniform [23, 24]. Since different lead isotopes have distinct half-lives, the assumption of uniform abundance led to incorrect notions regarding the age of samples. Nier's work provided the insight to account for variations in lead isotopes between samples. Arthur Holmes used the ideas put forth by Nier to estimate the age of the Earth. He concluded that the Earth was about 3 billion years old [25], much closer to the currently accepted 4.5 billion years than any previous calculations. At about the same time, German physicist Fritz Houtermans (1903-1966) independently produced a similar estimate of the age of the Earth based upon Nier's work [2, 26].

The current estimate for the age of the Earth was determined by American geochemist Clair Patterson (1922-1995) in 1956 not by dating terrestrial samples, but rather by dating meteorites [27, 13]. Patterson analyzed the lead compositions of five different meteorites, two iron meteorites and three stone meteorites. Iron meteorites do not contain uranium, so the lead composition should theoretically remain unchanged over time. The two iron meteorites in Patterson's study had almost identical compositions. Using the idea that all three stone meteorites had started with the same lead composition, he estimated the age for each of the stone meteorites and found the age estimates ranged from 4.5 billion to 4.6 billion years [27].

1.3 Radiometric Dating on Shorter Timescales

While early radiometric dating efforts focused on objects which had existed for hundreds of millennia, interest soon turned to using radioactivity to determine the age of more recent samples. Carbon-14, which was first proposed as a radioactive dating tool in the late 1940s by American nuclear chemist Willard Libby (1908-1980) [28, 29], has a half-life of 5730 years, much shorter than the half-lives of uranium-238, uranium-235, and thorium-232. This shorter half-life makes it useful for dating objects which have existed for a few millennia, such as archaeological artifacts and glaciers.

Carbon-14 is produced when cosmic rays collide with nitrogen [30]. It, along with stable carbon-12, is taken in and released by organisms during their lifetime, for example by inhalation and exhalation. Thus, living organisms typically have the same ratio of carbon-14 to carbon-12 as the atmosphere. When an organism dies, it no longer takes in new carbon-14 and the carbon-14 present in its system slowly decays. Carbon-12, which is not radioactive, will also be present in the organism's system and the carbon-12 levels will remain the same as time elapses. Thus, the ratio of carbon-14 to carbon-12 will decrease over time. By examining the ratio of carbon-14 to carbon-12, an estimate of the age of the organism or artifact can be made. Mathematically, this works as follows. From the decay equation,

$$N_{C14}(t) = N_{C14}(0)e^{-\lambda_{C14}t}, \tag{1.12}$$

where $\lambda_{C14} = 1.21 \times 10^{-4}$ decays per year. The amount of carbon-14 remaining at the present time, N_{C14} can be measured directly from the sample. To determine the initial amount of carbon-14, the atmospheric ratio of carbon-14 to carbon-12 at the time of the organism's death must be known. Multiplying the atmospheric ratio by the amount of carbon-12 in the sample can provide an estimate of how much carbon-14 was present in the organism's system at the time of its death, $N_{C14}(0)$. Once that final quantity has been determined, equation [1.12] can be solved for time.

While carbon-14 has many uses, its half-life is still long enough that it may be difficult to date very recent phenomena due to the fact that very little carbon-14 will have decayed. Other radioisotopes with still shorter half-lives can be useful for this purpose. One of the most widely used of these radioisotopes is lead-210.

Lead-210 is a naturally occurring isotope of lead which is a product of the uranium-238 decay series [31], with a half-life of about 22.3 years [32]. Lead-210 was first used in radiometric dating in 1963 by E. D. Goldberg, who used it to estimate the age of glacier ice [33]. Almost a decade later, it was used by Krishnaswamy et al. to date lake sediment samples [34]. Dating lake sediment samples remains one of its most common uses in radiometric dating.

The method of dating lake cores or ice cores differs from artifact dating in a significant way. It is generally assumed that the entirety of an artifact was constructed at a particular instance in time, so the date that is estimated from the analysis of a sample of the object can often be understood to stand for the age of the artifact as a whole. With core samples, however, layers of sediment or ice build up over time. Thus, the sediment at the bottom of a lake core sample would be expected to be older than the sediment at the top of the sample. To estimate the age, certain assumptions must be made regarding the manner in which the sediment was deposited.

To utilize Krishnaswamy et al.'s model, it must be assumed that the rate of supply of lead-210, that is, the flux of lead 210 reaching the surface of the sediment, and the sedimentation rate remain constant in time [34, 35]. While these assumptions work reasonably well for many samples, they may be too restrictive to be used to analyze others. A new technique for lead-210 dating, known as the constant rate of supply (CRS) model, was introduced in 1978 by Appleby and Oldfield [36]. This model required only that the rate of supply remain constant. The CRS model will be discussed in detail in a subsequent chapter.

Krishnaswamy et al. also investigated the possibility of using several other radioisotopes for dating, namely cesium-137 and iron-55 [34]. Many dating techniques such as those used in carbon-14 and lead-210 dating rely on the assumption that deposits of the radioisotope have remained roughly constant over time, but this assumption must often be eschewed when using cesium-137 for radiometric dating. Cesium-137 is a product of nuclear fission [2] and has a half-life of about 30.2 years [32], indicating that cesium-137 could be used on timescales similar to the ones lead-210 is used for. Since cesium-137 is part of the fallout from nuclear testing, it would be expected that in regions where nuclear testing has occurred, increases in the cesium-137 content of the soil can be mapped to the time period in which the testing occurred. However, in practice, cesium-137 dating has proven inconsistent [37]. Davis et al. examined the cesium-137 profiles of lakes in northern New England and Scandinavia. Lead-210 dating was performed on 14 of the 16 New England lakes and the chronostratigraphic pollen markers of the New England lakes were analyzed as well. Cesium-137 was observed at depths corresponding to dates that the lead-210 and pollen markers estimated were prior to the fallout. These results suggest that cesium-137 may be more mobile than lead-210, moving through the sediment layers instead of remaining stationary, which could make it difficult to extrapolate accurate ages from the cesium-137 profile of a sample.

Another fallout radionuclide used in radiometric dating is strontium-90 [38]. As with cesium-137, prior to the testing of nuclear weapons, very little strontium-90 would be expected to be found in the soil. Strontium-90 was deposited in the Great Lakes region from 1953 through 1964 through fallout from weapons testing and precipitation. After 1964, major above ground nuclear weapons testing was discontinued, thus diminishing the amount of Sr-90 deposited in the region annually. Some Sr-90 could still be expected to be observed in post-1964 samples, as radioactive remnants of nuclear weapons testing would be delivered via precipitation, but the amount of Sr-90 being added would show a significant decrease compared to the nuclear testing years.

Lerman examined the Sr-90 concentration in the Great Lakes between 1954 and 1969 [38]. Because the Great Lakes are interconnected, the Sr-90 concentration could be decreased by outflow as well as radioactive decay and increased by inflow from multiple sources, requiring a more complicated mathematical relation than is used to describe isolated lakes. Lerman proposed a system of differential equations describing the concentration of Sr-90 in the Great Lakes as a function of time. The differential equations took into account the various sources of inflow and outflow for each lake, as well as loss due to radioactive decay. Lerman's model did not fit the collected concentration completely. He was able to obtain a better fit for three of the Great Lakes by increasing the input for the years 1962-1964 by a small amount and increasing the outflow by $6 - 8\%$. The need to increase the outflow suggested that there were additional mechanisms by which Sr-90 was removed, although what those mechanisms would be was not immediately clear.

CHAPTER 2
A DEEPER LOOK AT LEAD-210 DATING

2.1 The Lead-210 Decay Process

Lead-210 is part of the uranium-238 decay series [31], as shown in Figure 2.1. It has a half-life of about 22.26 years [32], and can decay to bismuth-210 through electron emission or to mercury-206 through α emission. Compared to many other naturally occurring radioisotopes, lead-210 has a relatively long half-life, which makes it useful for dating sediment samples that are no more than 100-150 years old.

Since lead-210 is part of the uranium-238 decay chain, if uranium-238 or one of its progeny, such as radon-222, are present in a sample, new lead-210 atoms will be continually introduced into the sample through radioactive decay. If the system is in secular equilibrium, the amount of lead-210 in the sample will remain nearly unchanged as time passes. Since the amount of lead-210 stays constant, it is not useful for radiometric dating. This type of lead is referred to as supported lead-210 because there is a source that replenishes it.

If, however, lead-210 is separated from its source, then over time, the lead that is present in the sample will decay. There are multiple mechanisms by which this separation occurs in nature. It may, for example, be swept away by wind or be deposited in precipitation. Some lead-210 particles separated in such a manner may reach the bed of a lake. Over time, sediment will accumulate atop this lead-210, sealing it into the lake bed. This lead is referred to as unsupported lead-210 and it is this lead which is used to date samples.

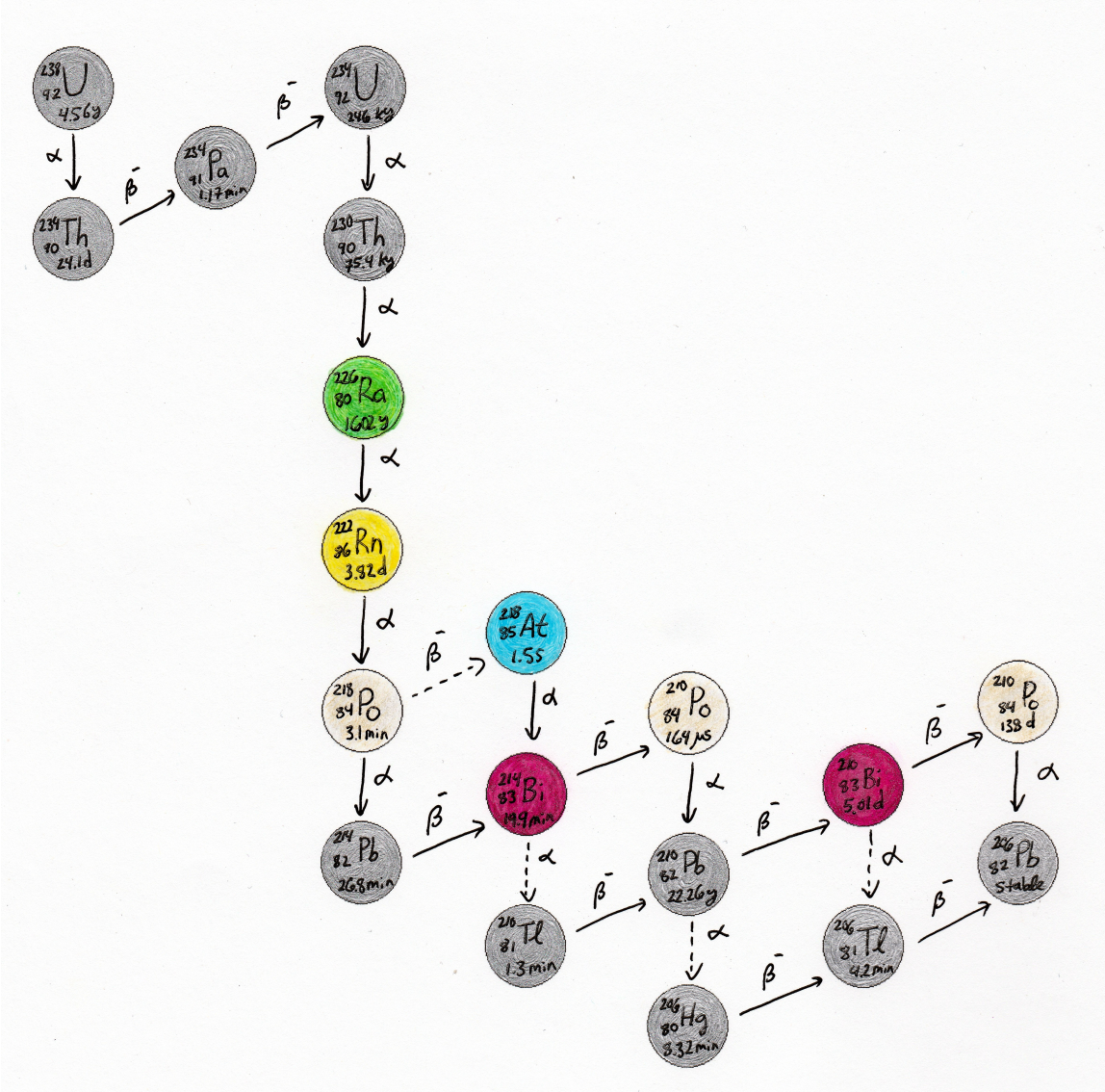

Figure 2.1. The uranium-238 decay series.
For isotopes that have two possible decays, the most common decays are shown with solid arrows, while less frequently occurring decays are represented with dashed arrows. Some infrequent decays have been omitted from the chart for readability.

2.2 Obtaining and Counting a Lead-210 Sample

To begin the dating process,[1] a core sample must be taken. The site for the core sample may be chosen for a variety of reasons. However, there are several features that

[1]Although this chapter refers primarily to the lead-210 dating process, because all radioisotopes decay similarly, many steps of the process of radiometric dating are the same, regardless of the isotope used for dating. Variations may exist in, for example, what type of detector is used to count the particles. However, the general process of collecting a core sample, counting the decays of radioisotope, and modeling the age of the sample follows similarly.

may make for a more ideal sample site [39]. Relatively undisturbed bodies of water[2] are preferable because if there is too much mixing of the upper sediment layers, the lead that exists in these sediments may migrate between layers, making it difficult to estimate the surface concentration accurately. In a naturally formed lake, cores are often taken from the center of the lake to minimize disturbances caused by shoreline activity. Choosing bodies of water with other geological or temporal markers that can corroborate age estimates can also be useful.

In reservoirs, it is advisable to take core samples that reach the layers of sediment that existed prior to the creation of the reservoir. Since the reservoir was created in a specific time frame, the creation of the reservoir can serve as a check on age estimates provided by radiometric dating. Samples with higher sedimentation rates are desirable because a higher sedimentation rate decreases the amount of mixing of the sediment after it has been deposited [40] and also minimizes the adverse effects of diagenesis on the sample [41]. Nonetheless, bodies of water with less desirable attributes may be of interest to scientific study, and with the appropriate mathematical tools, it may be possible to analyze these samples as well.

The core samples analyzed by the Environmental Radiation Lab (ERL) at the University of Maine are sometimes provided by external agents, while at other times are collected by students. The coring tools used vary depending on the department or institution that is collecting the core sample. For a brief discussion of which coring tools are desirable for what types of bodies of water, see [39].

When a lake core sample is taken, it is cut into thin slices, often half an inch in thickness. The slices are weighed once when wet to find the wet weight and again when dried to find the dry weight, M [1]. The individual slices are then ground and placed inside tubes to be analyzed for their lead-210 content.

[2]Most ideal are lakes containing varved sediment, that is, a collection of thin sediment layers that alternate in color. In such bodies of water, there is so little mixing of the sediment that each stratification corresponds to the summer or winter of a given year. Thus, the age of the sediment can be determined by counting the layers.

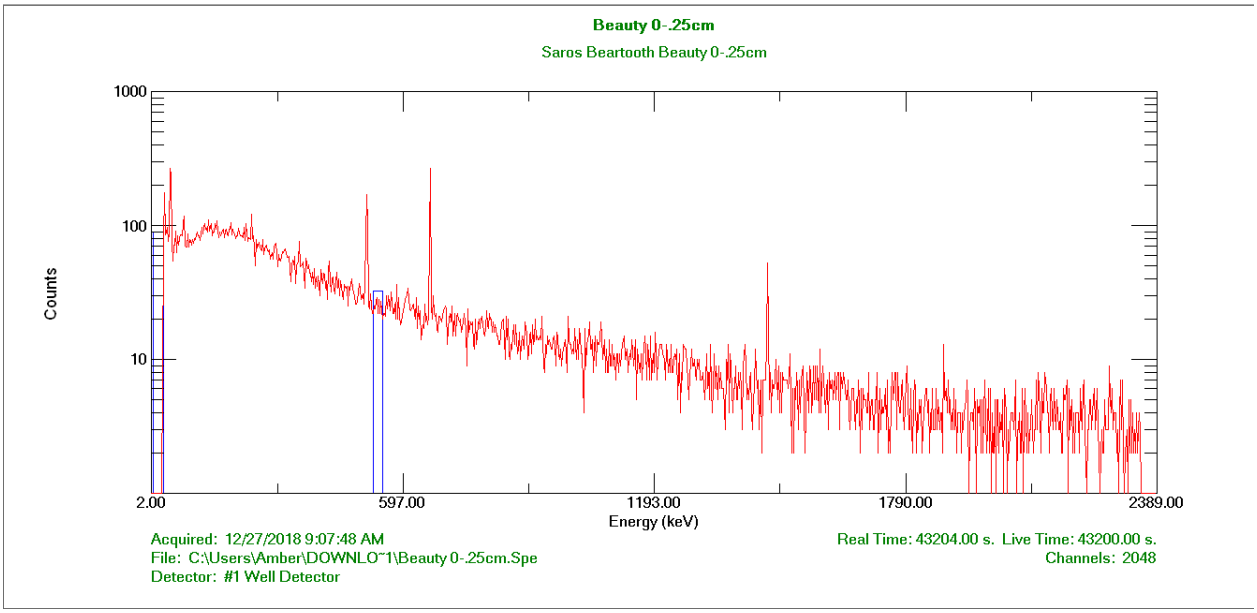

Figure 2.2. An example spectrum produced by MAESTRO.

In the Environmental Radiation Lab, germanium detectors are used to count gamma particles. Germanium is an optimal material for gamma counting because its large absorption coefficient makes it useful for detecting a wide range of particle energies [42]. The tube containing the sediment sample is placed in one of the germanium detectors and counted for 12-24 hours. While lead-210 is of primary interest to our laboratory, the detector counts γ emissions at all energies within the energy range of the detector, making it possible to determine counts for other radioisotopes, such as cesium-137.

The germanium detectors are connected to a computer running the MAESTRO software program.[3] MAESTRO provides data for the number of counts obtained at various energies, producing a spectrum of energies, such as shown in Figure 2.2. There may be multiple energy peaks corresponding to different radioisotopes present in the sample, as Figure 2.2 demonstrates, so before analysis can begin, the peak corresponding to the desired radioisotope must be determined. Common gamma energy peaks can be found in [43].

[3]MAESTRO is a multichannel analyzer produced by ORTEC

Table 2.1. Example counting data.

Energy (keV)	**Counts**)
505	26
506	25
507	30
508	27
509	85
510	177
511	234
512	110
513	34
514	25
515	19
516	20

Once the appropriate energy peak has been identified, the peak area must be computed. For example, suppose the fictional data presented in Table 2.1 were the counts collected for energies around 510 keV (Note that lead-210 has a peak around 47 keV and thus this fictional data is not meant to be representative of lead-210).

This data is represented graphically in Figure 2.3. As the histogram shows, while there is a clear peak at 511 keV, the counts at 510 keV and 512 keV are also higher than the background radiation counts. To calculate the value of the peak, the first step is to compute the gross area corresponding to the energies from 510 keV to 512 keV. This is done by adding the individual counts, i.e.,

$$G = \sum_{i=510}^{512} c_i = 177 + 234 + 110 = 521, \tag{2.1}$$

where G denotes the gross area and c_i denotes the count at the ith energy. In general, for a peak starting at some energy L and ending at some energy R, where L and R stand for left and right, respectively, the gross area is given by [42]

$$G = \sum_{i=L}^{R} c_i. \tag{2.2}$$

However, the gross count G is not the value of the peak, as the background radiation has not been taken into account. We will assume that the background radiation does not have

a peak at the location of the peak of interest and thus is approximately constant throughout the peak, a reasonable assumption in many situations. (For instances in which there is significant overlap between the peaks of the sample and background radiation, see e.g., [42].)

To determine the background count, m channels immediately to the left and m channels immediately to the right will be selected. For the purposes of this example, we will choose $m = 4$. In general, as long as the background counts are close to uniform, choosing three to five channels on either side of the peak should generally be sufficient to estimate the background counts [42]. To find the background count under the peak, the background counts are averaged and then multiplied by n, the number of channels under the peak. In this case, $n = 3$. In general, the background counts are given by [42]

$$B = \frac{n}{2m}[\sum_{i=L-m}^{L-1} c_i + \sum_{i=R+1}^{R+m} c_i]. \tag{2.3}$$

Note that $2m$, the averaging factor, has been moved to the front of the equation for ease of notation. The background counts in this example are then given by

$$B = \frac{3}{2 \cdot 4}[\sum_{i=510-4}^{510-1} c_i + \sum_{i=512+1}^{512+4} c_i] = \frac{3}{8}[\sum_{i=506}^{509} c_i + \sum_{i=513}^{516} c_i] = 77.25 \approx 77. \tag{2.4}$$

To then find the area of the peak, the background must be subtracted from the gross peak. In other words, the area N, which represents the total number of counts, is given by [42]

$$N = G - B = \sum_{i=L}^{R} c_i - \frac{n}{2m}[\sum_{i=L-m}^{L-1} c_i + \sum_{i=R+1}^{R+m} c_i]. \tag{2.5}$$

In this particular example, $N = 521 - 77 = 444$.

Once the number of counts in the peak has been determined, the uncertainty of the peak must be computed. Since each peak tends to form a distribution that is close to a Poisson distribution, a rough estimate for the uncertainty would be $\Delta N = \sqrt{N}$ [1]. However, because there is also some uncertainty in the estimation of the background counts, that uncertainty must be accounted for as well. For this reason, the uncertainty is given by [1]

$$\Delta N = \sqrt{N + \frac{B}{m}}. \tag{2.6}$$

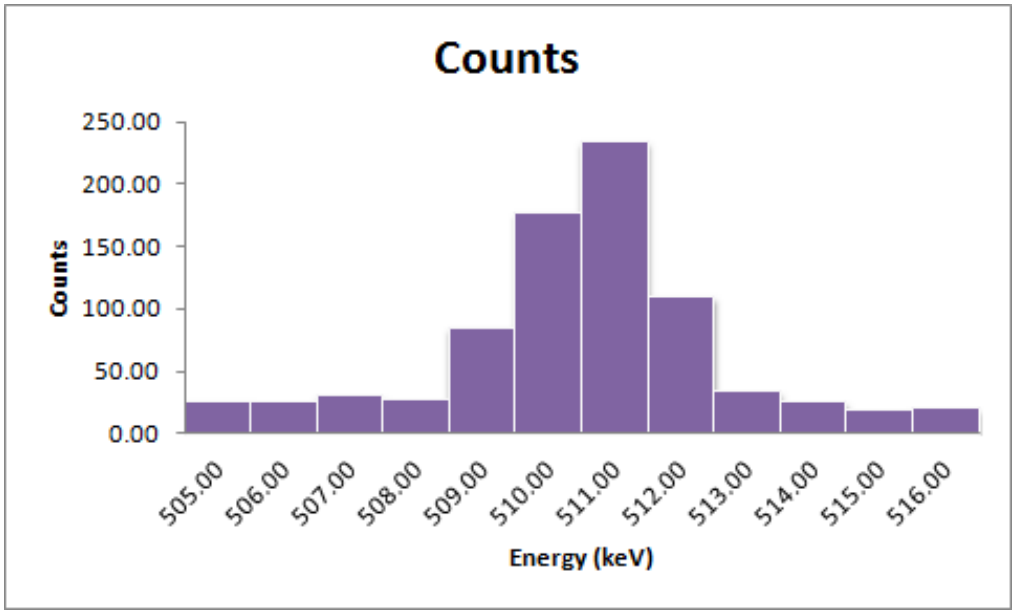

Figure 2.3. A graphical representation of the sample counts.

One thing to be aware of is that the number of counts measured by the detector in a given time interval is not the same as the number of decays that have happened in that time interval. Only a fraction of lead-210 decays produce a γ ray, which means that most decays will be unable to be detected. Furthermore, no detector is perfectly efficient, meaning that the detector itself will fail to account for some of the decays that have occurred. Thus, corrections must be made to estimate the number of decays that have occurred in a given time interval.

Lead-210 has a low branching ratio of about 4% [44], meaning that only about 4% of the decays produce a γ ray. Thus, to estimate the number of decays that have occurred during an interval of time, the number of counts must be divided by .04. Suppose, for example, that $N = 781$. Then

$$N_e = \frac{N}{.04} = \frac{781}{.04} = 19525. \tag{2.7}$$

However, the efficiency of the detector must also be accounted for. The efficiency depends upon the geometry of the detector as well as the energy peak and can be determined by calibrating with a known source. This process is described in [45]. Once the efficiency of

the detector has been determined for the given energy peak, the total number of decays can be determined by dividing the modified number of counts N_e by the efficiency γ_e,

$$N_t = \frac{N_e}{\gamma_e}. \tag{2.8}$$

For the example above, assuming a detector with efficiency $\gamma_e = .25$, the total number of decays in the given time interval would be

$$N_t = \frac{19525}{.25} = 78100. \tag{2.9}$$

Thus, for our hypothetical example, while the detector measured only $N = 781$ counts, about $N_t = 78100$ lead-210 decays occurred during time interval in which the data was collected.

For radiometric dating, it is not the actual activity at each depth that is essential, but rather a proportional representation of how many counts there are at each depth. In other words, it does not matter so much whether we use the 50 and 25 count estimate without the efficiency at two depths or the 200 and 100 counts that would be expected once efficiency is taken into account; the ratio between the two depths is the same. As long as all measurements are taken using the same detector, all measurements will be reduced by the same efficiency factor γ_e. For this reason, the efficiency of the detector is sometimes omitted from the activity calculations. That is, N_e is used in place of N_t in activity calculations. Making this change will not affect age estimates, but the calculated "activity" will not be a true activity, and thus could not be used for comparing against activity calculations from other detectors.

From the number of total decays N_t, the activity can be determined. The activity is defined as the number of decays per unit time [45],

$$A = \frac{dN}{dt} = \frac{d}{dt}N(t) = -\lambda N_0 e^{-\lambda t} = -\lambda N(t). \tag{2.10}$$

In practice, activity is generally obtained by taking the number of decays N_t and dividing it by the time that elapsed as the detector counted. For example, if it took 12 hours (or 43200

s) for the detector to complete its counting, then, continuing with the example above,

$$A = \frac{N_t}{t} = \frac{78100}{43200} = 1.8079. \tag{2.11}$$

Thus the activity would be 1.81 Bq.

The specific activity is what is used for radiometric dating. The specific activity is the activity per unit mass of a sample [45], or

$$C = \frac{A}{M}, \tag{2.12}$$

where M is the dry mass of the sample, as mentioned previously.

Beyond a certain depth, the concentration of lead-210 will remain roughly unchanged. The specific depth at which this occurs varies from one body of water to the next, and can be approximated by looking for a point in the data beyond which the fluctuations in lead-210 are small. The tail of the data is averaged to determine an estimate of the supported lead-210 in the sample.[4] Once the specific activities have been computed, an estimate of the specific activity of supported lead-210 is determined by averaging the specific activities for depths deeper than the chosen cut off depth. This activity estimate is then subtracted from the specific activities to obtain an estimate of the unsupported lead-210 present in each layer of the sample. A plot of concentration of unsupported lead-210 versus depth can then be constructed.

Although the rationale may not become clear until the CRS model has been described, a modified activity A_m in units of $\frac{Bq}{cm^2}$ must also be computed. This value is obtained by multiplying the specific activities by what is called the dry mass, M_d, which itself a mass but rather has units of $\frac{g}{cm^2}$. The process of obtaining the dry mass is described below.[5]

[4]To use this technique, it is worth noting that the deviation between different data points in the tail of the curve should be fairly small. If the standard deviation is greater than about 10 %, then another technique may be needed. Dr. James Kaste recommends calculating the radium-226 content in each sediment layer and using that to determine a unique supported lead-210 value for each data point.

[5]The following technique is the one which was outlined to me. Dr. Kaste suggests a more straightforward approach. His recommendation is to use the thickness of the layer and the radius of the core tube to determine the volume of the core slice. Dividing the dry mass by the volume will then yield the bulk density.

The loss on ignition must also be computed to determine how much of the sample is composed of organic versus inorganic matter. The samples are sent to the Sawyer Environmental Chemistry Laboratory at the University of Maine, where the are heated to 500°C [1]. The organic sediment in the sample will burn off, while the inorganic matter will remain. Since the organic and inorganic constituents of the samples have different densities, the percentages of each will be needed to determine the dry mass densities of the samples.

It is assumed that the organic matter has a density of 1.6 $\frac{g}{cm^3}$ and that the inorganic sediment has a density of 2.5 $\frac{g}{cm^3}$ [1]. The solid density S is the sum of the organic and inorganic densities by their respective percentages, given mathematically as [1]

$$S = 1.6O + 2.5I, \tag{2.13}$$

where O and I denote the percentages of organic and inorganic matter in the sample, respectively.

The presence of water in the sediment sample must be accounted for. To begin with, the percent sediment by weight is computed. If the dry weight is denoted by d and the wet weight by w, then the percent sediment by weight, s_w, will be the ratio of the two multiplied by 100%, i.e.

$$s_w = \frac{d}{w} \cdot 100\%. \tag{2.14}$$

Likewise, since the sample is made up of sediment and water, the percent water by weight is given by

$$f_w = 100\% - s_w. \tag{2.15}$$

From here, the percentages of sediment and water by volume must be computed so that the mass density and ultimately the dry mass can then be determined. The percent water by volume f_v is given by [1]

$$f_v = \frac{f_w}{f_w + \frac{s_w}{S}}. \tag{2.16}$$

The percent sediment by volume s_v is thus

$$s_v = 100\% - f_v. \tag{2.17}$$

Table 2.2. Cumulative Activity.

Depth (cm)	**Modified Activity** ($\frac{Bq}{cm^2}$)	**Cumulative Activity** ($\frac{Bq}{cm^2}$))
1	.48	1.29
3	.37	.81
5	.21	.44
7	.16	.23
9	.07	.07

The mass density ρ_M is given by [1]

$$\rho_M = S \cdot s_v. \tag{2.18}$$

Once the mass density has been calculated, the dry mass M_d can be determined. The dry mass is the solid density of the sample in $\frac{g}{cm^3}$ multiplied by the depth of the interval, D, in cm. From [1],

$$M_d = S \cdot D. \tag{2.19}$$

Observe that the units of M_d are $\frac{g}{cm^2}$.

Now that M_d has been determined, the desired conversion can be made. The specific activities S are multiplied by M_d to obtain a modified activity in units of $\frac{Bq}{cm^2}$,

$$A = S \cdot M_d. \tag{2.20}$$

Note that although A_m had been previously used in this paper to distinguish the activities from the modified activities, the subscript is omitted from the above equation as well as throughout the remainder of this document to remain consistent with conventional notation.

One final calculation remains to be computed, namely the cumulative activities. To obtain cumulative activities, the modified activities of a layer are summed with all of the modified activities of lower depths. As an example, consider the fictionalized activity data given in Table 2.2. The lowest depth is 9 cm, with a corresponding modified activity of .07 $\frac{Bq}{cm^2}$. Since there are no sediment layers beneath this layer, the cumulative activity is the same as the modified activity. The 7 cm sediment layer has one layer beneath it, so the

cumulative activity is the sum of the modified activities of the 7 cm and 9 cm layers, or $A_c = .07 + .16 = .23\ \frac{Bq}{cm^2}$. Similarly, the cumulative activity of the 5 cm layer is the sum of the modified activities of the 5, 7, and 9 layers, the cumulative activity of the 3 cm layer is the sum of the modified activities of the 3, 5, 7, and 9 cm layers, and the cumulative activity of the 1 cm layer is the sum of all of the modified activities. The sum of all modified activities is generally used as the initial condition $A(0)$ when estimating the age of a sample. More detail on the typical dating technique used will be presented in the following section.

As mentioned in the introductory chapter, there are two commonly used methods for dating samples based on their lead-210 content. The Constant Flux, Constant Sedimentation (CFCS) model was introduced by Goldberg [33] and refined by Krishnaswamy [34]. As the name suggests, this model assumes that, for a given sample, the flux and the sedimentation rate are constant. A second model, the Constant Rate of Supply (CRS) model, proposed by Appleby and Oldfield, assumes that the lead-210 flux is constant. This assumption means that the dry mass sedimentation flux multiplied by the activity per gram is constant. Derivations of the CFCS model can be found in many sources (e.g., [34, 35, 1]), but since it is more restrictive than the CRS model, it will not be analyzed in detail here. A derivation of the CRS model will be provided in the following section.

2.3 The Constant Rate of Supply Model

In 1978, Appleby and Oldfield introduced a mathematical model for dating sediment samples assuming a constant supply rate of lead-210, which they termed the Constant Rate Supply (CRS) Model [36]. Their derivation is as follows: Suppose that the initial concentration of unsupported lead-210 C_0 in $\frac{Bq}{g}$ satisfies the equation

$$C_0(t)r(t) = \zeta, \tag{2.21}$$

where ζ is constant and $r(t)$ $\frac{g}{cm^2 yr}$ is the dry mass sedimentation rate at time t. If x is the depth of the sediment of age t, then the concentration of lead-210 at depth x, in accordance with the nuclear decay equation, is given by

$$C(x) = C_0(t)e^{-kt}, \tag{2.22}$$

where

$$k = \frac{\ln 2}{22.26} = .03114 \tag{2.23}$$

is the radioactive decay constant of lead-210 in inverse years. Then, rearranging the concentration equation,

$$C_0(t) = C(x)e^{kt}. \tag{2.24}$$

If the sediment is laid down during a small period of time δt, then the thickness of this layer is given by

$$\delta x = \frac{r(t)}{\rho(x)}\delta t, \tag{2.25}$$

where $\rho(x)$ is the dry mass per unit wet volume of the sediment at depth x in $\frac{g}{cm^3}$. Then the rate of change of depth is

$$\dot{x} = \frac{r}{\rho}. \tag{2.26}$$

Solving for r,

$$r(t) = \rho(x)\dot{x}. \tag{2.27}$$

Substituting (2.24) and (2.27) into (2.21),

$$C(x)e^{kt}\rho(x)\dot{x} = \zeta, \tag{2.28}$$

or

$$C(x)\rho(x)\dot{x} = \zeta e^{-kt}. \tag{2.29}$$

Consider the function

$$A(x) = \int_x^\infty \rho(x)C(x)dx, \tag{2.30}$$

where A is the total residual unsupported lead-210 beneath sediments of depth x. By the Fundamental Theorem of Calculus,

$$\dot{A} = \frac{d}{dt}(\int_x^\infty \rho(s)C(s)ds) = [\rho(s)C(s)]_{s=\infty} - \rho(x)C(x)\dot{x}. \tag{2.31}$$

Since the unsupported lead-210 concentration decreases with depth, $[\rho(s)C(s)]_{s=\infty} = 0$, and thus

$$\dot{A} = -\rho(x)C(x)\dot{x} = -\zeta e^{-kt}. \tag{2.32}$$

Hence,

$$A = -\int_{-\infty}^{t} \rho(x)C(x)\dot{x}ds = -\int_{-\infty}^{t} \zeta e^{-ks}ds. \tag{2.33}$$

Using the negative sign to flip the limits of integration,

$$A = -\int_{-\infty}^{t} \zeta e^{-ks}ds = \int_{t}^{\infty} \zeta e^{-ks}ds \tag{2.34}$$

and thus

$$A(x) = \frac{\zeta}{k}e^{-kt}. \tag{2.35}$$

Given the initial condition $A(0)$,

$$A(x) = A(0)e^{-kt}. \tag{2.36}$$

Solving (2.36) for t,

$$t = \frac{1}{k}\ln\frac{A(0)}{A(x)}, \tag{2.37}$$

where t is the age in years of the layer of depth x. For a given sample, the age can thus be estimated from $A(x)$, assuming that the flux of unsupported lead-210 is nearly constant.

2.4 Problems with Current Dating Techniques

Both the CFCS and CRS models work relatively well in certain situations, but neither one applies universally to all sediment samples. Consider the following data, used by Douglas Cahl in his master's thesis [1] and presented in Figure 2.4. Under the CRS model, the relationship between activity and depth should follow an exponential decay curve, but

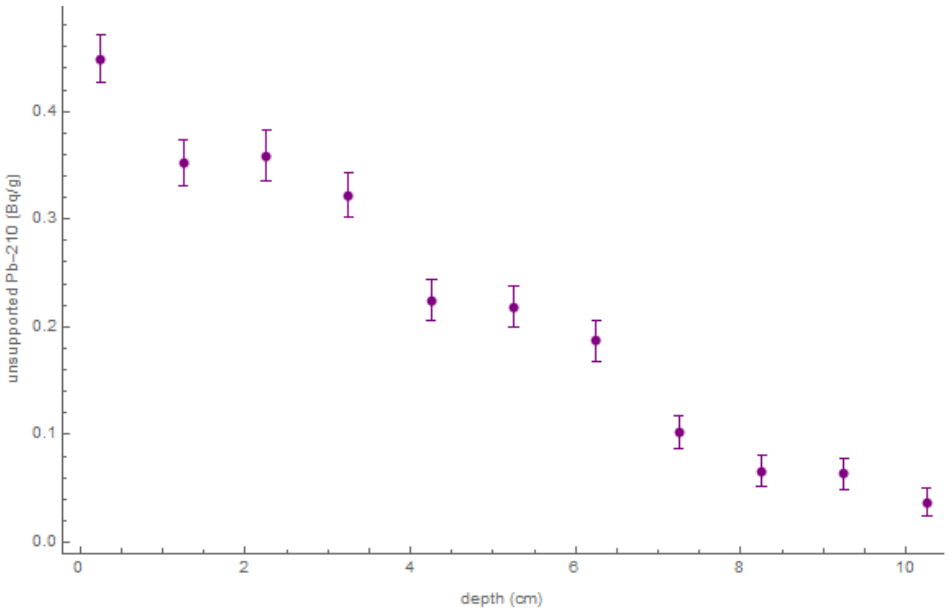

Figure 2.4. Data presented in Douglas Cahl's master's thesis of unsupported lead-210 vs. depth.

there appear to be sinusoidal fluctuations as well. Neither the CRS model nor the CFCS model account for periodic fluctuations in activity such as the one observed here.

While this project was initiated with lead-210 in mind, since all radioisotopes decay in accordance with the nuclear decay equation, with slight modifications it could be applied to many other radioisotopes. Of particular interest is cesium-137, which exists in the environment primarily as fallout from nuclear weapons testing. Cesium-137, which has a half-life of about 30.2 years [32], theoretically should be usable for estimating the age of samples on similar timescales to those dated using lead-210. However, it has proven an unreliable dating source due in part to an ability to permeate the soil layers in a manner that other radioisotopes generally do not demonstrate [37].

The behavior of cesium-137 varies considerably from one lake to another, depending on the biological, chemical, and geological properties of the lake [46]. For example, the type of water in a lake has been shown to influence the mobility of cesium-137 [47]. In a study of Lake St. Clair in Michigan, it was found that sorbed cesium-137 was more mobile in anoxic soft water, that is, soft water with depleted levels of dissolved oxygen, and less mobile in

oxic, or oxygen rich, soft water [47]. Hard water was found to fall between oxic and anoxic soft waters in terms of cesium-137 mobility, although there was little difference between oxic and anoxic hard water. Other factors such as the composition of the lake bed may also influence the mobility of cesium-137, as it is readily absorbed by some minerals such as clay and mica [47, 48].

Although cesium-137 may sometimes provide unreliable age estimates under the CRS and CFCS models, it can play a crucial role in radiometric dating. Due to losses from the top of a core sample that may occur in coring, lead-210 age estimates may fail if not calibrated against another radioisotope such as cesium-137 [49]. Additionally, in regions in which the watershed and lake bed have undergone disturbances, using lead-210 alone can provide inaccurate age estimates [50], so an additional radioisotope such as cesium-137 may be needed to confirm the estimates. While a piecewise approach employing CRS techniques and comparing against chronostratigraphic markers has been been applied to a sampling of cesium-137 samples with some success [49], a model that handles all cesium-137 samples remains elusive. If the mobility of cesium-137 could be modeled mathematically, then a more comprehensive model for cesium-137 dating which does not require a constant rate of supply of cesium-137 could perhaps be devised.

Additional radioisotopes of interest could include beryllium-7 and strontium-90. Beryllium-7 deposits have been shown to vary seasonally [51]. With a half-life of about 53.3 days [32], it might not be as useful for dating lake core samples, but it could provide information for short timescale analyses. Like cesium-137, strontium-90 is a radionuclide introduced into the environment primarily as fallout from nuclear weapons testing [38]. With a half-life of 28.8 years [32], it can be used for aging samples of similar timescales to those aged using lead-210. In particular, changes in concentration of strontium-90 in the Great Lakes over time have been studied in some detail by Lerman [38]. While Lerman devised a model specific to the Great Lakes, a more general model that could encompass strontium-90 dating might be useful.

Devising a general model that can be used for cesium-137 and strontium-90 is a pressing matter in North America. Very little cesium-137 and strontium-90 present in lake sediment samples is naturally occurring. Nuclear weapons testing in the United States introduced large quantities of these radioisotopes into the environment beginning in 1952 and continuing through the mid-1960s [50]. In the years since above ground nuclear weapons testing ended, little new cesium-137 and strontium-90 has been introduced into North American lake beds. Since these two radioisotopes have half-lives on the order of 30 years, much of the cesium-137 and strontium-90 introduced into the environment through weapons testing has decayed. These diminishing levels have added an additional layer of difficulty to cesium-137 dating [52]. Thus, it is imperative to develop techniques to accurately age sediment samples using these radioisotopes while the levels of these isotopes are still detectable in North American sediment samples.

In addition, for lead-210 samples exhibiting sinusoidal fluctuations, the period of the oscillations will be calculated and analyzed. It is hypothesized that the oscillations are caused by changes in wind and rainfall due to climate cycles, such as perhaps the North Atlantic Oscillation, which has been speculated to create periodic fluctuations in atmospheric lead-210 in parts of Europe [53]. However, further study would be needed to assess the nature of the sinusoidal behavior.

The aim of the following chapters is to devise a mathematical model for radiometric dating that does not require a constant rate of supply of a given radioisotope. The hope is that in doing so, more samples will be able to analyzed and with better accuracy than current models provide. Additionally, for samples that show sinusoidal oscillations, I aim to examine the period of oscillations and investigate the physical significance of the period. Chapter 3 will provide a derivation of this new model, called the Non-Constant Rate of Supply (NCRS) model. The CRS and NCRS models will be implemented on a fictitious data set to demonstrate the utility of the NCRS model. In Chapter 4, the NCRS model will be applied to four existing data sets and compared against the CRS model. Chapter 5

will examine 30 additional sediment samples. For the samples with sinusoidal oscillations, the period will be computed. Climate cycles will be considered as a potential cause of the oscillations. In Chapter 6, I will draw some conclusions and offer recommendations for future work.

CHAPTER 3
A NEW TECHNIQUE FOR RADIOMETRIC DATING

3.1 Deriving the Non-Constant Rate of Supply Model

I developed a Non-Constant Rate of Supply (NCRS) model in an effort to expand the scope of samples that can be analyzed using radiometric dating. The method closely follows the techniques used by Appleby and Oldfield in the development of their CRS model [36]. The main difference between the two approaches is the initial assumption. Instead of assuming that the rate of supply of lead-210 is constant, I assumed that it was allowed to fluctuate.

Suppose that instead of a constant supply rate, the lead-210 rate varies by some known functions of time. In other words,

$$C_0(t)r(t) = \zeta + f_1(t) + f_2(t) + \cdots + f_n(t), \tag{3.1}$$

where ζ in $\frac{Bq}{cm^2yr}$ is constant, C_0 in $\frac{Bq}{g}$ is the initial concentration of unsupported lead-210 in the sediment, $r(t)$ in $\frac{g}{cm^2yr}$ is the dry mass sedimentation rate at time t, and $f_1(t), f_2(t) \cdots f_n(t)$ in $\frac{Bq}{cm^2yr}$ are arbitrary functions of time. If x is the depth of the sediment of age t, then the concentration of lead-210 at depth x is given by

$$C(x) = C_0(t)e^{-kt}, \tag{3.2}$$

where $k = .03114$ is the radioactive decay constant of lead-210 in inverse years. Then, rearranging the concentration equation,

$$C_0(t) = C(x)e^{kt}. \tag{3.3}$$

For the same reason as outlined in Chapter 2 in the derivation of the CRS model, the rate of change of depth is given by

$$\dot{x} = \frac{r(t)}{\rho(x)}, \tag{3.4}$$

where $\rho(x)$ is again the dry mass per unit wet volume of the sediment at depth x in $\frac{g}{cm^3}$. Solving for $r(t)$,

$$r(t) = \rho(x)\dot{x}. \tag{3.5}$$

Substituting (3.3) and (3.5) into (3.1),

$$C(x)e^{kt}\rho(x)\dot{x} = \zeta + f_1(t) + f_2(t) + \cdots + f_n(t) \tag{3.6}$$

or, rearranging,

$$C(x)\rho(x)\dot{x} = e^{-kt}(\zeta + f_1(t) + f_2(t) + \cdots + f_n(t)). \tag{3.7}$$

Let

$$A(x) = \int_x^\infty \rho(s)C(s)ds, \tag{3.8}$$

where A in $\frac{Bq}{cm^2}$ is the total residual unsupported lead-210 beneath sediment layers of depth x. Observe that, by the Fundamental Theorem of Calculus,

$$\dot{A} = \frac{d}{dt}(\int_x^\infty \rho(s)C(s)ds) = [\rho(s)C(s)]_{s=\infty} - \rho(x)C(x)\dot{x}. \tag{3.9}$$

The unsupported lead-210 concentration decreases with depth, meaning that $[\rho(s)C(s)]_{s=\infty} = 0$, and hence

$$\dot{A} = -\rho(x)C(x)\dot{x} = -e^{-kt}(\zeta + f_1(t) + f_2(t) + \cdots + f_n(t)). \tag{3.10}$$

Thus,

$$-\int_{-\infty}^t \rho(x)C(x)\dot{x}ds = -\int_{-\infty}^t e^{-ks}(\zeta + f_1(s) + f_2(s) + \cdots + f_n(s))ds. \tag{3.11}$$

Absorbing the negative sign into the limits of integration,

$$\begin{aligned} &-\int_{-\infty}^t e^{-ks}(\zeta + f_1(s) + f_2(s) + \cdots + f_n(s))ds \\ &= \int_t^\infty e^{-ks}(\zeta + f_1(s) + f_2(s) + \cdots + f_n(s))ds \end{aligned} \tag{3.12}$$

and thus

$$A(x) = \zeta \int_t^\infty e^{-ks} ds + \int_t^\infty f_1(s) e^{-ks} ds + \int_t^\infty f_2(s) e^{-ks} ds + \cdots + \int_t^\infty f_n(s) e^{-ks} ds$$
$$= -\zeta[-\frac{1}{k} e^{-ks}]_t^\infty + \int_t^\infty f_1(s) e^{-ks} ds + \int_t^\infty f_2(s) e^{-ks} ds + \cdots + \int_t^\infty f_n(s) e^{-ks} ds. \quad (3.13)$$

In general,

$$A(x) = \frac{\zeta}{k} e^{-kt} + \int_t^\infty f_1(s) e^{-ks} ds + \int_t^\infty f_2(s) e^{-ks} ds + \cdots + \int_t^\infty f_n(s) e^{-ks} ds, \quad (3.14)$$

where t is the age in years of the sediment layer of depth x.[1] Given an initial condition A(0) and functions $f_1, f_2, \cdots f_n$, this equation can be written explicitly, as demonstrated in the following sections. For a given sample, the age can be estimated from $A(x)$, although if the rate of supply is non-constant, that is, $f_i \neq 0$ for any i, numerical techniques may be required to determine t.

3.2 The NCRS Model with Sinusoidal and Linear Terms

If the rate of supply of a radioisotope is assumed to be non-constant, the natural question would be what sort of functions may describe it. Some data, such as shown in Figure **??**, suggest that the rate of supply may fluctuate sinusoidally. The potential causes of these sinusiodal fluctuations are not fully understood, but will be discussed in later chapters. Another possible non-constant change would be a linear change. Such a change may occur, for example, if there is inflow or outflow to the body of water from which the core sample was collected, or if the radioisotope is able to migrate through the layers of soil.

Suppose that a plot of concentration versus depth for a given sample suggests that in addition to exponential decay, the concentration rate shows both sinusoidal and linear fluctuations. In other words,

$$C_0(t) r(t) = \zeta + a \sin(bt + c) + gt, \quad (3.15)$$

[1]Note that $A(x)$ is used here to be consistent with Appleby and Oldfield's notation, since their notation was used for the CRS derivation. However, $A(t)$ might make more sense. While the accumulation of lead-210 does vary with depth, that variation is a direct consequence of the nuclear decay process, which progresses with time.

where a, b, c, g, and ζ are constant. Then

$$C_0(t)r(t) = C(x)\rho(x)\dot{x}e^{kt} = \zeta + a\sin(bt+c) + gt \tag{3.16}$$

and therefore

$$C(x)\rho(x)\dot{x} = e^{-kt}(\zeta + a\sin(bt+c) + gt). \tag{3.17}$$

Then

$$A(x) = \int_t^\infty C(x)\rho(x)\dot{x}ds = \int_t^\infty e^{-ks}(\zeta + a\sin(bs+c) + gs)ds. \tag{3.18}$$

Thus,

$$\begin{aligned} A(x) &= \zeta\int_t^\infty e^{-ks}ds + a\int_t^\infty \sin(bs+c)e^{-ks}ds + g\int_t^\infty se^{-ks}ds \\ &= \frac{\zeta}{k}e^{-kt} + a\int_t^\infty \sin(bs+c)e^{-ks}ds + g\int_t^\infty se^{-ks}ds. \end{aligned} \tag{3.19}$$

Integrating,

$$\begin{aligned} A(x) &= \frac{\zeta}{k}e^{-kt} + \frac{a}{k^2+b^2}(k\sin(bt+c) + b\cos(bt+c))e^{-kt} + g(\frac{t}{k} + \frac{1}{k^2})e^{-kt} \\ &= e^{-kt}(\frac{\zeta}{k} + \frac{g}{k^2} + \frac{gt}{k} + \frac{a}{k^2+b^2}(k\sin(bt+c) + b\cos(bt+c)). \end{aligned} \tag{3.20}$$

If a sample has only sinusoidal variance in the rate of supply of the radionuclide, then $g = 0$ in [3.20]. If it displays only linear variance, then $a = 0$ in [3.20]. While sinusoidal and linear changes to the concentration are some of the more common changes that might be observed, this method will work for many mathematical functions.

3.3 Modeling a Pulse

Another possible occurrence that could affect the rate of supply would be if a large quantity of a radioisotope was introduced into a lake in a short amount of time. This may be found, for example, in a body of water into which nuclear reactor effluent is released, such as was shown in [54]. Mathematically, such an influx might be modeled with a delta function.

Suppose that a pulse is released at some time t_0. Assume that

$$C_0(t)r(t) = \zeta + h\delta(t - t_0), \tag{3.21}$$

where h in $\frac{Bq}{cm^2 yr}$ is constant. Then

$$C_0(t)r(t) = C(x)\rho(x)\dot{x}e^{-kt} = \zeta + h\delta(t - t_0), \tag{3.22}$$

and thus

$$C(x)\rho(x)\dot{x} = e^{-kt}(\zeta + h\delta(t - t_0)). \tag{3.23}$$

Therefore

$$A(x) = \int_t^\infty C(x)\rho(x)\dot{x}dt = \int_t^\infty e^{-ks}(\zeta + h\delta(s - t_0)ds). \tag{3.24}$$

Integrating,

$$A(x) = \frac{\zeta}{k}e^{-kt} + h\int_t^\infty e^{-ks}\delta(s - t_0)ds. \tag{3.25}$$

The results of integration depend on whether the depth (or, correspondingly, the time) at which the pulse was released is included in the limits of integration. For older sediment, which accumulated before the pulse was released, there will be no contribution from the pulse term, as is consistent with the mathematical definition of an integral over a delta function. For newer sediment which has accumulated after the pulse, however, recalling that

$$\int_{-\infty}^\infty f(s)\delta(s - t_0) = f(t_0), \tag{3.26}$$

then

$$h\int_t^\infty e^{-ks}\delta(s - t_0)ds = he^{-kt_0}. \tag{3.27}$$

Therefore,

$$A = \begin{cases} \frac{\zeta}{k}e^{-kt} & t > t_0 \\ \frac{\zeta}{k}e^{-kt} + he^{-kt_0} & t < t_0. \end{cases} \tag{3.28}$$

Recall that $A(x)$ is defined as the accumulation of all sediment layers below the depth x. The pulse contributes excess radionuclides only to the sediment layer corresponding to the

time t_0, but because A is cumulative, the introduction of the pulse of radioisotopes will be reflected in the A values for the upper sediment layers.

3.4 Restating the NCRS Model

Before an attempt is made at modeling the data, it is important to demonstrate the equivalency between the approach outlined in previous sections and the one that will be utilized in the following sections. Observe that

$$C_0(t)r(t) = \zeta + a\sin(bt+c) + gt = \zeta(1 + \frac{a}{\zeta}\sin(bt+c) + \frac{g}{\zeta}t). \tag{3.29}$$

Note that $\frac{a}{\zeta}$ and $\frac{g}{\zeta}$ are constant, so they could be renamed in some fashion such as this:

$$C_0(t)r(t) = \zeta(1 + a_1\sin(bt+c) + g_1t). \tag{3.30}$$

By equations (3.3) and (3.5),

$$C(x)\rho(x)\dot{x} = \zeta e^{-kt}(1 + a_1\sin(bt+c) + g_1t). \tag{3.31}$$

Next, suppose that

$$C_0(t)r(t) = \zeta. \tag{3.32}$$

Suppose also that

$$C(x) = (C_0 + a\sin(bt+c) + gt)e^{-kt} = C_0e^{-kt}(1 + \frac{a}{C_0}\sin(bt+c) + \frac{g}{C_0}). \tag{3.33}$$

Once again, since $\frac{a}{C_0}$ and $\frac{g}{C_0}$ are constants, the equation can be rewritten thusly:

$$C(x) = C_0(t)e^{-kt}(1 + a_1\sin(bt+c) + g_1t). \tag{3.34}$$

This is an equivalent way of stating that the rate of supply is not constant, as can be seen by substituting (3.34) and (3.5) into (3.32),

$$C(x)\rho(x)\dot{x} = \zeta e^{-kt}(1 + a_1\sin(bt+c) + g_1t). \tag{3.35}$$

The equation for $A(x)$ will then have a slightly modified form,

$$A(x) = \zeta e^{-kt}(\frac{1}{k} + \frac{g_1}{k^2} + \frac{g_1 t}{k} + \frac{a_1}{k^2 + b^2}(k \sin(bt + c) + b \cos(bt + c)). \tag{3.36}$$

One further clarification must be made before the modeling can begin. The data that was measured directly was lead-210 concentration versus depth, as you see in Figure 2.4. To be able to use the NCRS model, the depth data must be related to time. It will be assumed that there is a linear relation between the two. The rationale behind this assumption will be discussed in Section 3.6.

3.5 Testing the NCRS Model with Simulated Data

Before the NCRS model is applied to experimental data, it may be useful to see how it performs on a simulated data set. To generate this data set, it will be assumed that the concentration of lead-210 in a sample is given by the equation

$$c(x) = .5e^{.4x}(1 + .1 \sin(x) + .8x) \tag{3.37}$$

Note that equation [3.37] has no physical significance and is merely used for illustrative purposes.

R was used to generate the simulated data. R is a statistical software package that is frequently used in the fields of mathematics and statistics. I chose it for much of the research I have done in this paper primarily because of its nonlinear modeling capabilities, which I will demonstrate in this section. While R does have some downsides in areas such as memory management, none of its weaknesses have seemed to adversely affect its performance regarding the fitting and generation that I have needed to do for this paper.

Depths 1 cm through 11 cm were chosen in .5 cm increments and substituted into equation [3.37] to obtain concentration values, given in Table 3.1. R gave concentration values to eight significant digits. However, to introduce some variability into the data so that the equation fitted by R would not be a perfect fit, only one or two significant digits were used in the simulated data, which are given in Table 3.1. The data are shown in

Table 3.1. Simulated concentration data.

Depth (cm)	**Concentration from R** ($\frac{Bq}{cm^2}$)	**Rounded Concentration** ($\frac{Bq}{cm^2}$)
1.0	.63149078	.63
1.5	.63106464	.63
2.0	.60455634	.60
2.5	.56282744	.56
3.0	.51415539	.51
3.5	.46420913	.46
4.0	.41634290	.42
4.5	.37210821	.37
5.0	.33184939	.33
5.5	.29525972	.30
6.0	.26181466	.26
6.5	.23104698	.23
7.0	.20267078	.20
7.5	.17678975	.18
8.0	.15283658	.15
8.5	.13148816	.13
9.0	.11259029	.11
9.5	.09611026	.10
10.0	.08192217	.08
10.5	.06981963	.07
11.0	.05954510	.06

Figure 3.1 in red. After simulating the data, the curve fitting principles behind the CRS and NCRS models were used to fit the data. First, to find the CRS model fit, an exponential curve of the form

$$C(x) = ae^{-bx} \tag{3.38}$$

was fitted to the data using the nonlinear fit function in R (see Appendix C for sample R code), with initial parameters $a = .63$ and $b = .4$. The resulting curve was given as

$$C(x) = .8746e^{-.2050x}, \tag{3.39}$$

shown in Figure 3.1 in green.

To estimate the error, the residual sum of squares (RSS) will be used. Mathematically, the RSS is defined as

$$RSS = \sum_{i=1}^{n} (y_i - f(x))^2, \tag{3.40}$$

where y_i is the measured value and $f(x_i)$ is the value that would be predicted by the equation [55]. The RSS works well to compare between models on the same data set. The smaller the RSS value, the lower the deviation from the model. However, it cannot necessarily be used to compare models across data sets because the number of data points greatly influences the RSS value. The more non-zero terms there are, the larger the resulting RSS value. Thus, if the RSS values are larger for one set of data than for another, it does not necessarily mean that the model is a better fit in one case than in the other. However, throughout this paper, the goal will be to test the performance of the NCRS model against the CRS model on a given data set. Since the models are being compared on the same data set, the RSS will work fine for this purpose.

The qprC package was installed in R. This allowed for utilization of the RSS function. For the CRS model, the RSS value was found to be $RSS = .01895$.

For the NCRS model fit, a curve of the form

$$C(x) = ae^{-bx}(1 + d\sin(x) + fx) \tag{3.41}$$

was fitted to the data using the initial parameters $a = .5$, $b = .4$, $d = .1$, and $f = .8$. The resulting fit was

$$C(x) = .5137e^{-.3978x}(1 + .0822\sin(x) + .7585x), \tag{3.42}$$

shown in Figure 3.1 in blue. Observe that the coefficients in this equation are close to the coefficients in equation [3.37], as would be expected. The RSS value given was $RSS = .0001246$. Since the RSS value for the NCRS model was much lower than the RSS value for the CRS model, this suggests that the NCRS model is a better fit for the data.

To obtain the CRS solution, the cumulative activity must first be determined. To do so, all of the activities in Table 3.1 must be summed, which yields $A(0) = 6.38\ \frac{Bq}{cm^2}$. (For the purposes of this exercise, it was assumed that $M_d = 1\ \frac{g}{cm^2}$ for each data point, so the activities and modified activities are interchangeable, save for units.) Substituting this

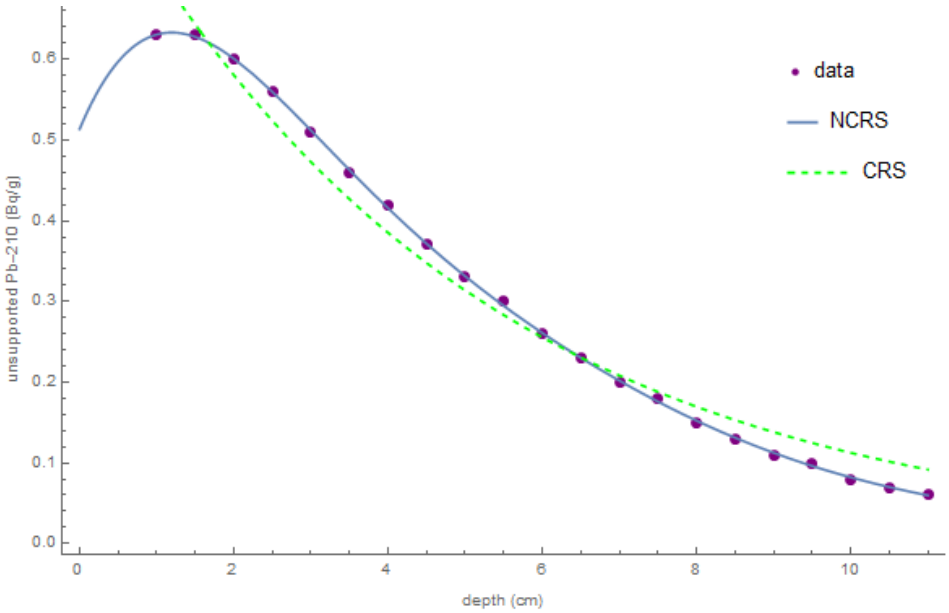

Figure 3.1. Plot of the simulated data with CRS and NCRS fits.

initial condition into equation [2.36],

$$A(t) = 6.38e^{-.03114t}, \tag{3.43}$$

which is shown in Figure 3.2 in green.

To estimate the age using the NCRS model, a conversion between x and t must be made. Equation [3.42] can be rewritten as

$$C(x) = e^{-.6661-.3978x}(1 + .0822\sin(x) + .7585x). \tag{3.44}$$

Assuming that x and t are linearly related,

$$-.6661 - .3978x = -.03114t + c_t. \tag{3.45}$$

To convert between depth and time, we need an initial condition. Since the top layer of sediment corresponds to the accumulation of sediment during a small window of time that dates to approximately the time at which the core sample was taken, this layer of sediment is considered to correspond to $t = 0$. There is some ambiguity as to what the corresponding depth should be, since each sediment layer has some thickness to it. Generally the

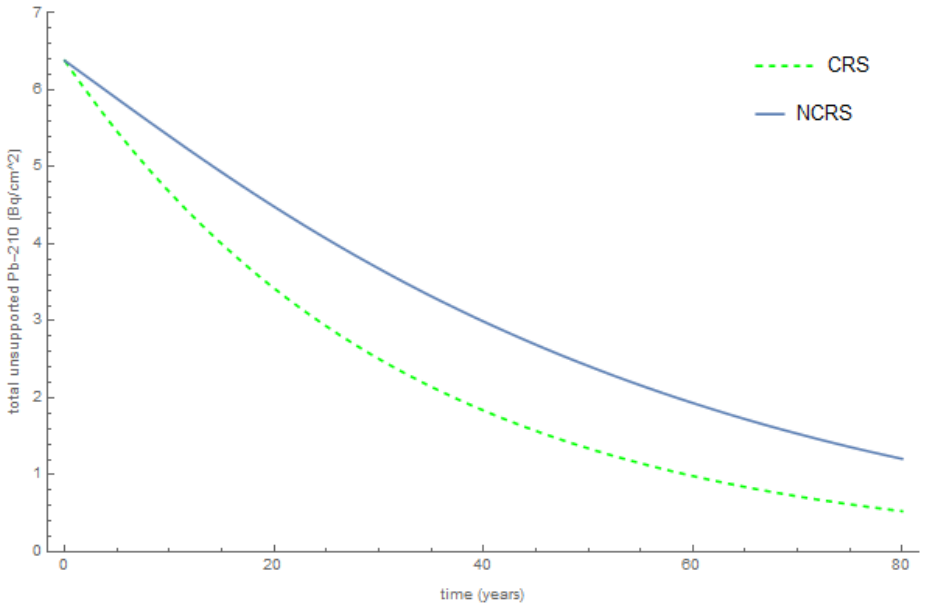

Figure 3.2. Age estimates of the simulated data with CRS and NCRS fits.

midpoint of the slice is used for the depth, as the researcher is looking for the average age of the sample. For example, if a slice is .5 cm thick, it would be considered to have a depth of .25 cm. Using the $x = 1$ cm depth as the depth at $t = 0$,

$$-.6661 - .3978(1) = -.03114(0) + c_t, \tag{3.46}$$

and hence

$$c_t = -1.064. \tag{3.47}$$

Furthermore,

$$x = \frac{1}{-.3978}(-.03114t - 1.064 + .6661) = .07828t + 1 \tag{3.48}$$

Thus,

$$\begin{aligned} C(x) &= e^{-1.064-.03114t}(1 + .0822\sin(.07828t + 1) + .7585(.07828t + 1)) \\ &= e^{-1.064-.03114t}(1.759 + .0822\sin(.07828t + 1) + .05938t) \\ &= C_0 e^{-.03114t}(1 + .0467\sin(.07828t + 1) + .03376t), \end{aligned} \tag{3.49}$$

where

$$C_0 = \frac{1}{1.759}e^{-1.064}. \tag{3.50}$$

Table 3.2. RSS and age estimates for the CRS and NCRS Models with simulated data.

	CRS	NCRS
RSS	.01895	.0001246
Age ($A = 4\frac{Bq}{cm^2}$)	15.0 years	25.8 years
Age ($A = 3\frac{Bq}{cm^2}$)	24.2 years	39.9 years
Age ($A = 2\frac{Bq}{cm^2}$)	37.3 years	58.5 years
Age ($A = 1\frac{Bq}{cm^2}$)	59.5 years	87.7 years

Thus, by equation [3.36],

$$A(x) = \zeta e^{-.03114t}(32.11 + 34.81 + 1.084t + 6.580(.03114\sin(.07828t + 1) + .07828\cos(.07828t + 1)))$$

$$= \zeta e^{-.03114t}(66.92 + 1.084t + .2049\sin(.07828t + 1) + .5151\cos(.07828t + 1)). \quad (3.51)$$

Using the initial condition $A(0) = 6.38$,

$$6.38 = \zeta(66.92 + .2049\sin(1) + .5151\cos(1)) = \zeta(67.37) \quad (3.52)$$

and hence

$$\zeta = .09470. \quad (3.53)$$

Thus,

$$A(x) = .09470e^{-.03114t}(66.92 + 1.084t + .2049\sin(.07828t + 1) + .5151\cos(.07828t + 1)). \quad (3.54)$$

This age estimate is shown in Figure 3.2 in blue. While the sinusoidal terms do not have much of an effect on the age estimate due to their small coefficients, Figure 3.2 shows that the linear term does in fact noticeably change the age estimate. Table 3.2 includes a comparison of the approximate age of the sample for four different cumulative activities for the two models, and the results differ by decades, in some cases. For example, a sample with cumulative activity of 3 $\frac{Bq}{cm^2}$ would be estimated to be about 24 years old using the CRS model, but with the NCRS model, that same sample would be estimated to be about 40 years old. Thus, the CRS model may in fact be a poor fit for samples with linear changes in the concentration of the radioisotope that is being used for dating.

3.6 Assessing the Linearity Assumption

Before delving into the linearity assumption, it is worth noting that the linearity assumption is implicitly built into the CRS and CFCS models. Recall that the concentration data is obtained as a function of depth, and that $C(x)$ is plotted versus x, not t. Thus, the equation for $C(x)$ could be written as

$$C(x) = C_0' e^{-\alpha x + \beta}, \tag{3.55}$$

where α and β are constant. By invoking

$$C(x) = C_0 e^{-kt}, \tag{3.56}$$

this necessarily means that x and t are related through some linear transformation, as each one appears in the exponent of the exponential and C_0 is constant.

As was mentioned in a previous section, it is assumed that x and t are linearly related. However, it is reasonable to wonder whether this assumption is necessarily true. The linear assumption is perhaps the most natural starting assumption, as it seems probable that in many environments, the amount of sediment deposited during each time step should remain constant. Each .5 cm thick slice of a core sample includes the sediment accumulation over a period of several years. For this reason, what matters to the linearity assumption is whether the volume of sediment deposits in a sample region remain constant from one year to the next.

Precipitation is one source of sediment deposits. Although precipitation may vary widely on short timescales such as from day to day, on larger timescales it often remains relatively constant. One step which may be useful to assess whether the linearity assumption is reasonable is to look up precipitation accumulations for a region over a period of several years. To access precipitation data, we will use the NOWData feature provided by the National Oceanic and Atmospheric Administration (NOAA), accessed via the site https://w2.weather.gov/climate/xmacis.php?wfo=gyx. The graph shown in Figure 3.3 is the precipitation data for Augusta, Maine.

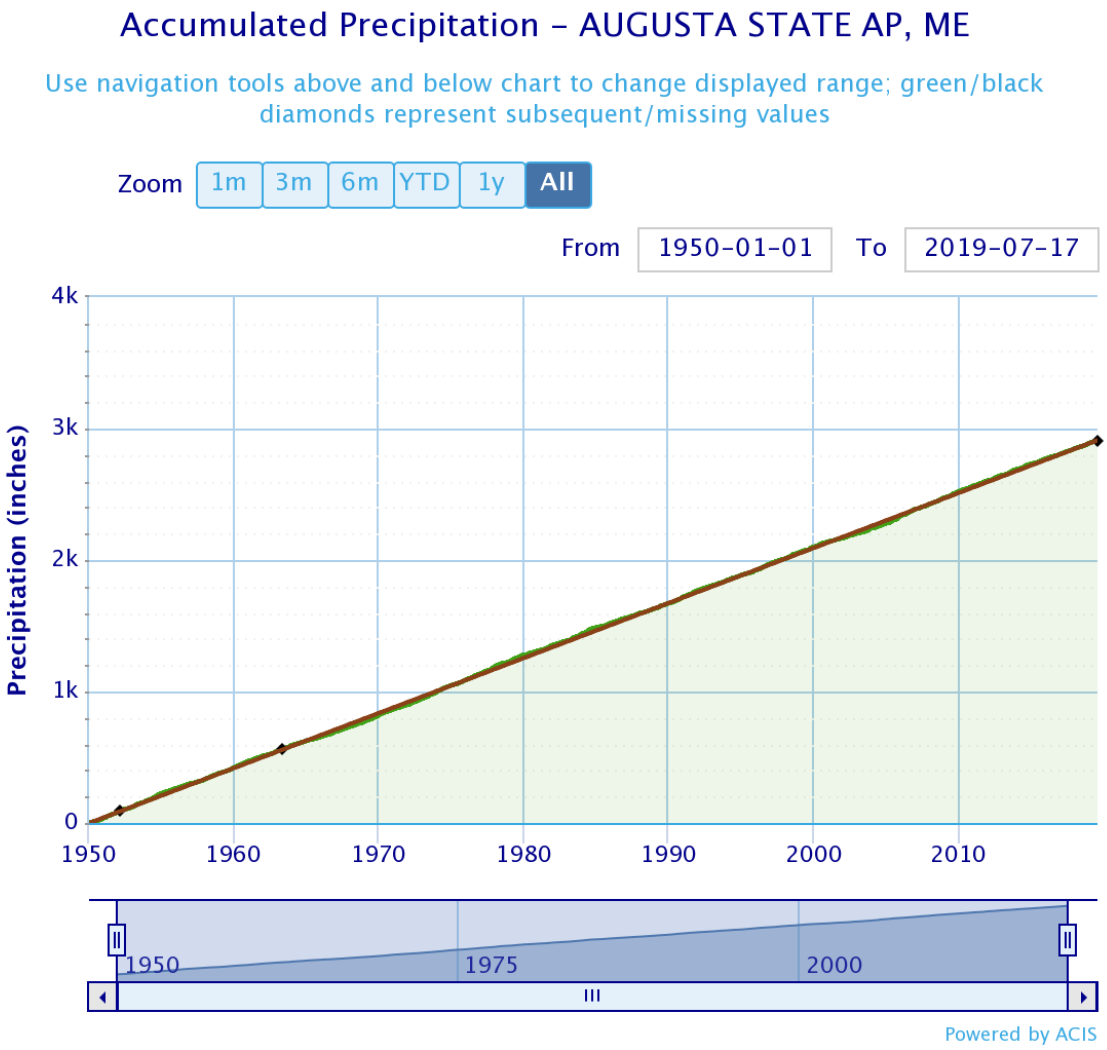

Figure 3.3. A graph showing the all time precipitation accumulation in Augusta, Maine from January 1, 1950 to July 17, 2017.
Graph obtained from NOAA's NOWData feature, available at https://w2.weather.gov/climate/xmacis.php?wfo=gyx

Figure 3.3 shows the all time accumulation of precipitation in Augusta, Maine. Although one line is partially obscured, there are two lines on the graph, one in brown and one in green. The green line shows the actual accumulation while the brown line shows the expected accumulation. While the green line does deviate slightly in places, as would be expected since weather does not behave in a perfectly predictable fashion, it very nearly fits the linear brown line. While this data does not go back for the 100-150 year period that might be represented in a lake core sample, it does provide evidence that the average

precipitation remains roughly constant over time. Thus it seems reasonable for lakes in the Augusta area to assume that the precipitation is not significantly altering the amount of sediment that is being deposited in a given time step.

Augusta, Maine was chosen for this demonstration because of its proximity to Monmouth, Maine, the location of Cochnewagon Lake. It is worth noting that the NOWData feature does not differentiate between types of precipitation. Since different forms of precipitation carry sediment differently, it is reasonable to ask whether rainfall and snowfall individually remain constant over time. This may be especially important since the changing climate is affecting the forms of precipitation in some geographical locations. Although perhaps not as easily accessible, data differentiating between rain and snow accumulations does exist for many locations and can likely be acquired by contacting a local National Weather Services branch office. However, unless there have been noticeable shifts in the types of precipitation in a location, it may be reasonable to assume that the annual occurrences of rain and snow remain roughly constant if the annual precipitation remains constant.

Inflow and outflow to a body of water may also carry in and remove sediment. If a barrier is created that restricts the inflow or outflow, or if there are changes to the climate that could significantly affect the flow of the waterways, such as rapid melting of glaciers, then it may be worth examining whether the change has affected the rate of sediment deposit. However, in relatively stable environments, inflow and outflow should not affect the rate at which sediment accumulates.

While wind is harder to quantify than precipitation, it is again reasonable to assume that over a sufficiently long period of time, wind will deposit the same amount of sediment into the body of water each time step. What tends to occur with wind is that it changes direction. Since different soils are made up of different types of organic and inorganic matter, changes in wind direction may change the type of matter that is being deposited, but it may not change the overall amount of matter that is being deposited. It may, for

example, increase or decrease the amount of lead-210 being introduced into the lake bed without affecting the overall sediment depositions. Since several years are represented in a .5 cm thick core sample, as long as there are not sustained, large scale changes in the wind patterns, the wind likely will not change the sediment deposition rate.

Generally, a linear assumption is likely warranted. However, in cases in which there are changes that would affect the rate at which sediment is being deposited, the question remains whether the NCRS model could still be implemented. As long as the change could be mathematically modeled, the NCRS model will still work. For example, assume that a dam is constructed that reduces the amount of sediment that is being deposited annually. The relationship between depth and time will likely still be linear in the years after the dam is constructed, although the coefficients will be different. To take into account the effect of the dam, two distinct calculations would have to be made, one for the years prior to the introduction of the dam and one for the years following the dam's completion. Even in instances in which the linearity assumption would not hold, the NCRS model could still be used, just with a different assumption.

CHAPTER 4
IMPLEMENTING THE NCRS MODEL

4.1 Testing the CRS Model on the Cochnewagon Lake Data

Consider the data presented in Figure 2.4 of the concentration of unsupported lead-210 as a function of depth, taken from Cochnewagon Lake. Cochnewagon Lake, also known as Cochnewagon Pond, is a body of water located in Monmouth Township, Maine.

The CRS model assumes that the concentration of lead-210 decays exponentially, so to find an equation for the data, the natural logarithm of concentration can be plotted against depth and a best fit line can be determined. The resulting plot is shown in Figure 4.1. Mathematica was used to generate the best fit line,[1]

$$\log(C) = -.513 - .244x. \tag{4.1}$$

Exponentiating,

$$C(x) = e^{-.513-.244x}. \tag{4.2}$$

This equation is shown in Figure 4.4 in green. R was used to calculate the RSS value to determine the fitness of the CRS model for the Cochnewagon Lake data. It was found that $RSS = .01263$.

Assuming that depth and time have a linear dependence,

$$-.513 - .244x = -.03114t + c_t, \tag{4.3}$$

where c_t is constant. Using the assumption that the first data point is the concentration at $t = 0$,

$$-.513 - .244(.25) = -.03114(0) + c_t, \tag{4.4}$$

[1]Note that all coefficients in the following sections have been rounded to three significant digits. The actual equations produced by Mathematica and R included more digits, which were retained until the end of the calculations, at which point the coefficients were rounded.

and thus

$$c_t = -.574. \tag{4.5}$$

Hence,

$$-.513 - .244x = -.03114t - .574. \tag{4.6}$$

Substituting equation [4.6] into equation (4.2),

$$C(x) = e^{-.574-.03114t} = .563e^{-.03114t} = C_0e^{-.03114t}. \tag{4.7}$$

From equation (3.14), using the initial condition that $A(0) = .1501$ in $\frac{Bq}{cm^2}$,

$$A(x) = .150e^{-.03114t}. \tag{4.8}$$

4.2 Implementing the NCRS Model with Sinusoidal Terms on the Cochnewagon Lake Data

R was used to find the best fit curve including sinusoidal fluctuations. The curve was given by the equation

$$C(x) = .519e^{-.197x}(1 + .150\sin(1.79x + 3.13)). \tag{4.9}$$

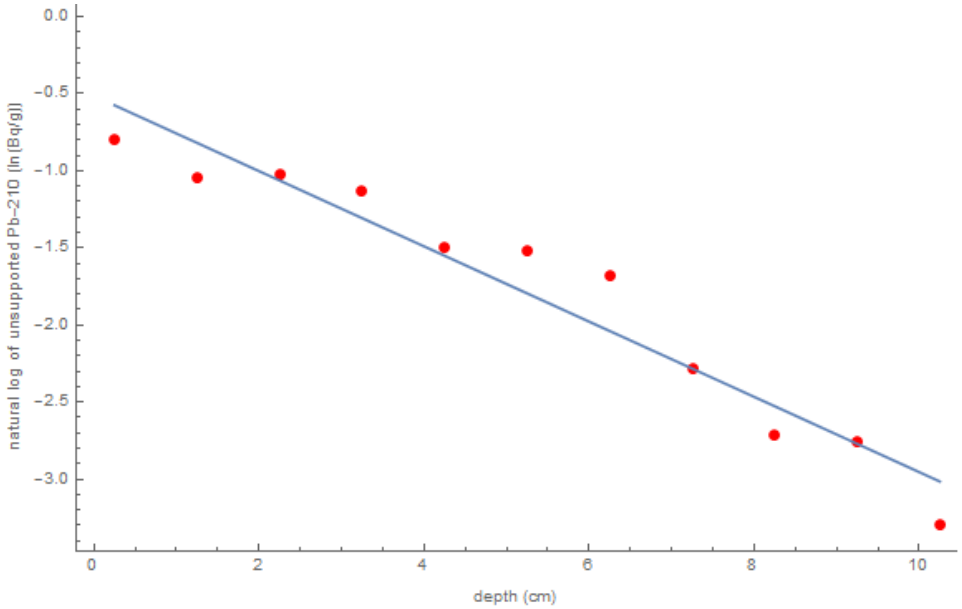

Figure 4.1. Natural logarithm of unsupported lead-210 vs. depth.

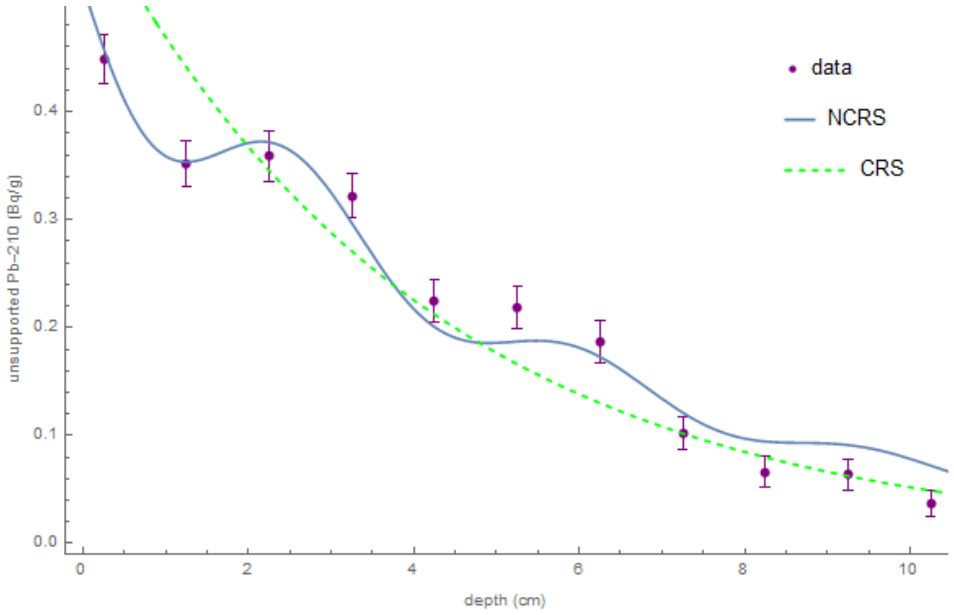

Figure 4.2. A comparison of CRS and NCRS model with no linear term.

Equation (4.9) is shown in Figure 4.2 in blue. The RSS value was found using R to be $RSS = .006966$.

$C(x)$ can be rewritten as

$$C(x) = .519e^{-.197x-.655}(1 + .150\sin(1.793x + 3.13)). \tag{4.10}$$

Using the same technique as outlined in the previous sections, it was found that

$$-.197x - .655 = -.03114t + c_t, \tag{4.11}$$

and thus,

$$c_t = -.704. \tag{4.12}$$

Thus,

$$x = .158t + .25 \tag{4.13}$$

and hence,

$$\begin{aligned} C(x) &= .519e^{-.03114t-.0493}(1 + .150\sin(.283t + .448)) \\ &= C_0e^{-.03114t-.0493}(1 + .150\sin(.283t + .448)). \end{aligned} \tag{4.14}$$

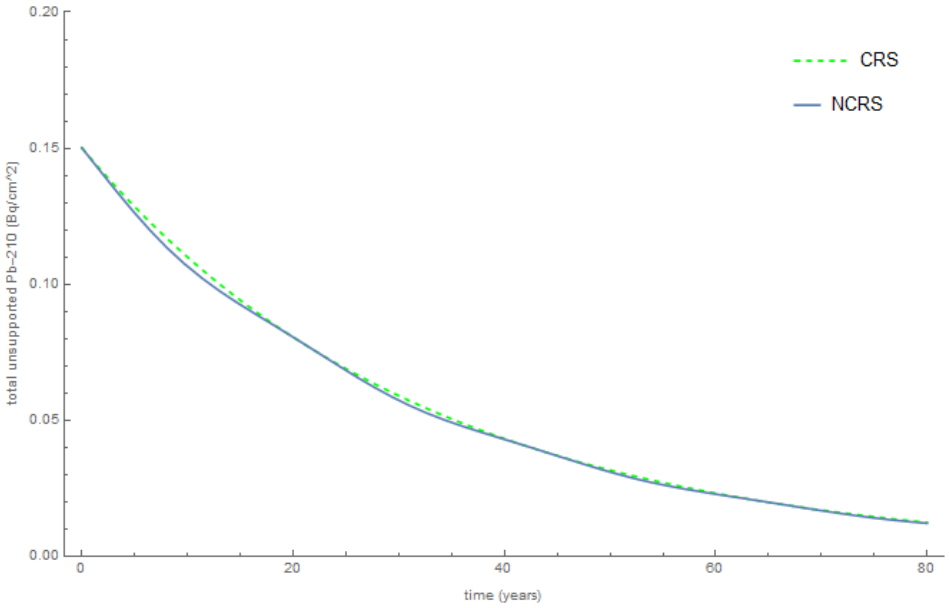

Figure 4.3. A comparison of CRS and NCRS model results with no linear term.

By equation (3.36),

$$A(x) = \zeta e^{-.03114t}(32.1 + 1.84(.0311\sin(.283t + .448) + .283\cos(.283t + .448).)) \tag{4.15}$$

Using the initial condition $A(0) = .1501$ in $\frac{Bq}{cm^2}$,

$$\zeta = .00460 \tag{4.16}$$

and thus,

$$A(x) = .00460e^{-.03114t}(32.1 + .184(.0311\sin(.283t + .448) + .283\cos(.283t + .448).)) \tag{4.17}$$

Equation (4.17) is shown in Figure 4.3 in blue. In this case, the two models seem to be in good agreement. This is not unexpected, as the sinusoidal term is small due to the small coefficients, and with the exponential term necessarily the same, the linear term was the only term significantly shifting the estimate. Note, however, that there are places where the two models diverge. For example, for a concentration of .11 $\frac{Bq}{cm^2}$, the CRS model

estimates the age to be 9.98 years, while the NCRS model estimates the age to be 9.43 *years*, a difference of about half a year. The sine term is particularly muted in this lake, however. In subsequent examples, more pronounced sinusoidal effects will be seen.

Observe also that the NCRS model shows some small, periodic oscillations that the CRS model does not account for. This too will merit further study in subsequent sections.

4.3 Implementing the NCRS Model with Sinusoidal and Linear Fluctuations

Several small streams, including Wilson Stream, flow into or out of Cochnewagon Lake [56]. Since there is inflow and outflow, it is possible that the lead-210 deposits could be fluctuating linearly. It is also possible that there is some other mechanism in the lake that is causing a linear change. For this reason, the NCRS model was redone including both sinusoidal and linear terms.

The nonlinear regression feature in R was used to find best fit curve for the unsupported lead-210 data using the following model equation:

$$C(x) = C_0 e^{k_1 x}(1 + a_1 \sin(bx + c) + g_1 x). \tag{4.18}$$

The given best fit curve was

$$C(x) = .348e^{-.401x}(1 + .269 \sin(2.16x + 1.39) + .694x). \tag{4.19}$$

Equation (4.19) is shown in Figure 4.4 in blue. The RSS value was found using R to be $RSS = .002180$, which is less than a fifth of the size of the RSS value found using the CRS model, suggesting that the NCRS model is a better fit.

Equation [4.19] can be rewritten in the following form:

$$C(x) = e^{-.401x-1.05}(1 + .269 \sin(2.16x + 1.39) + .694x). \tag{4.20}$$

Assuming again that depth and time are linearly related,

$$-.401x - 1.05 = -.03114t + c_t, \tag{4.21}$$

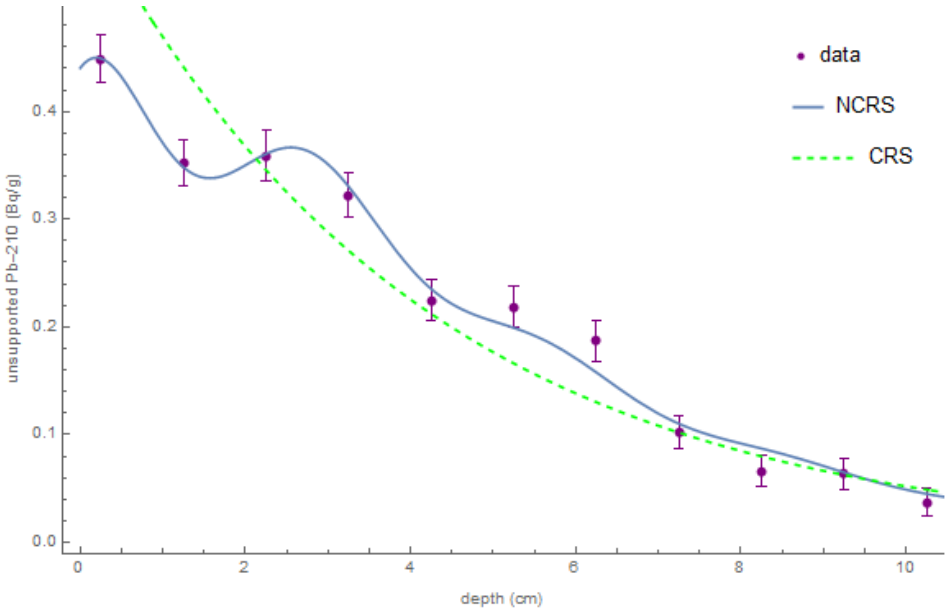

Figure 4.4. Data from Douglas Cahl's thesis with CRS and NCRS fit lines.

where c_t is an arbitrary constant distinct from the constant determined in the previous section. Using the same assumption as previously that when $t = 0$, $x = .25$,

$$-.401(.25) - 1.05 = c_t, \tag{4.22}$$

and hence

$$c_t = -1.16. \tag{4.23}$$

Solving for x,

$$x = .0778t + .25. \tag{4.24}$$

Thus,

$$C(x) = e^{-.401x-1.05}(1 + .269\sin(2.16x + 1.39) + .694x) \tag{4.25}$$

$$= e^{-.401(.0778t+.25)-1.05}(1 + .269\sin(2.16(.0778t + .25) + 1.39)$$

$$+.694(.0778t + .25))$$

$$= e^{-.03114t-.955}(1.17 + .269\sin(.168t + 1.92) + .0540t)$$

$$= .385e^{-.03114t}(1.17 + .269\sin(.168t + 1.92) + .0540t)$$

$$= .452e^{-.03114t}(1 + .230\sin(.168t + 1.92) + .0460t)$$

$$= C_0e^{-.03114t}(1 + .230\sin(.168t + 1.92) + .0460t)$$

By equation (3.36),

$$A(x) = \zeta e^{-.03114t}(\frac{1}{.03114} + \frac{.0460}{.03114^2} + \frac{.0460t}{.03114} \tag{4.26}$$

$$+\frac{.230}{.03114^2 + .168^2}(.03114\sin(.168t + 1.92)$$

$$+.168\cos(.168t + 1.92)))$$

$$= \zeta e^{-.03114t}(32.1 + 47.4 + 1.48t + 7.87(.03114\sin(.168t + 1.92)$$

$$+.168\cos(.169t + 1.92)))$$

$$= \zeta e^{-.03114t}(79.5 + 1.48t + 7.87(.03114\sin(.168t + 1.92)$$

$$+.168\cos(.168t + 1.92))).$$

Given the initial condition $A(0) = .1501\ \frac{Bq}{cm^2}$,

$$.150 = \zeta(79.5 + 7.87(.03114\sin(1.92) + .168\cos(1.92))). \tag{4.27}$$

Thus,

$$\zeta = .00189. \tag{4.28}$$

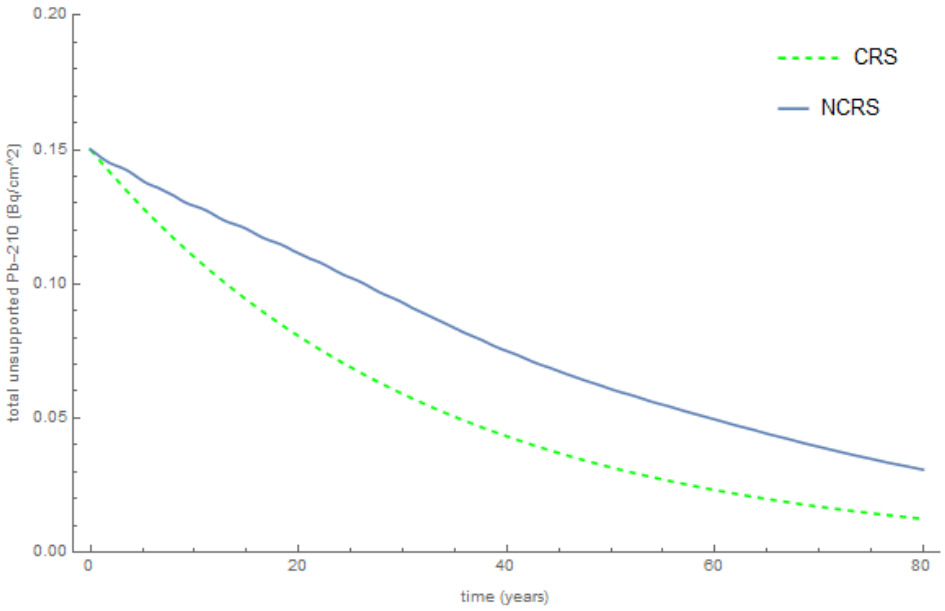

Figure 4.5. A comparison of CRS and NCRS age estimates.

Therefore,

$$A(x) = .00189e^{-.03114t}(79.5 + 1.48t \tag{4.29}$$
$$+7.87(.03114\sin(.168t + 1.92)$$
$$+.168\cos(.168t + 1.92))).$$

Equation (4.29) is shown in Figure 4.5 in blue, compared to the CRS solution, which is shown in green. This model deviates quite a bit from the CRS solution. Since a mechanism that would cause linear changes in the rate of supply of lead-210 has not yet been established for Cochnewagon Lake (although inflow and outflow are potential contenders), the results presented in this section should not necessarily be taken as a better estimate for the age of Cochnewagon Lake data. However, should such a mechanism be confirmed, then the NCRS model should be considered seriously as a potential better fit.

4.4 Modeling SS15 in Greenland: The Physically Unrealistic Linear Term

The next body of water we will analyze is lake SS15 in Greenland. I obtained the data for this lake from the ERL computer amongst a collection of lake data that had been

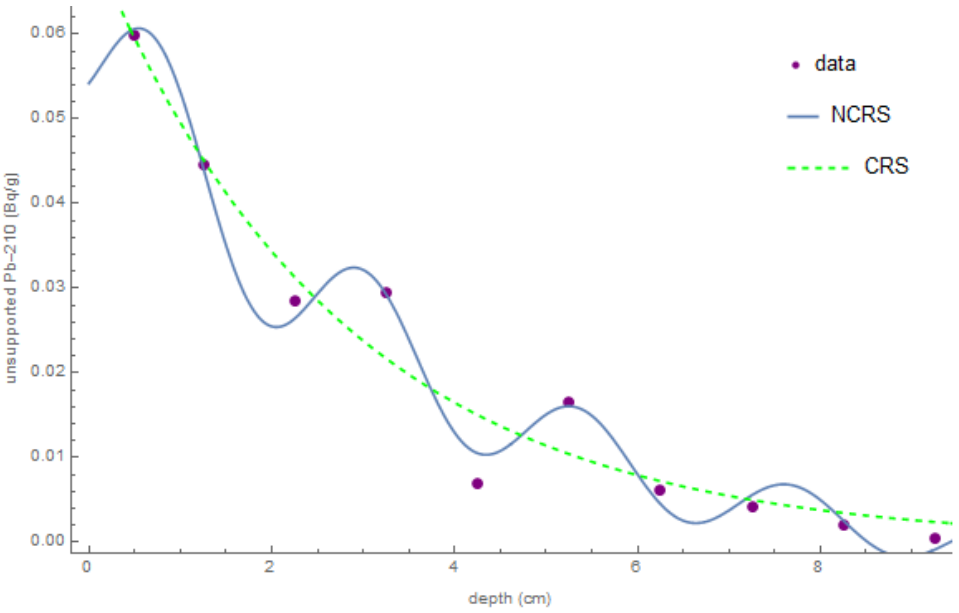

Figure 4.6. A comparison of CRS and NCRS fits for the lake SS15 in Greenland lead-210 data.

analyzed previously. I selected SS15 because it appeared to show evidence of sinusoidal fluctuations similar to the fluctuations seen in the Cochnewagon Lake data.

The lead-210 data collected from lake SS15 is shown in Figure 4.6 in red. Note that error bars are absent from this graph. This is because the error estimates were too small to be visible on the graph. Error estimates for this sample are included in Table A.3.

To begin the analysis, CRS and NCRS fits of the data were obtained using R. The unsupported lead-210 data was imported into R and two nonlinear models were implemented, one for the CRS model and the other for the NCRS model. For the CRS fit, the exponential decay equation

$$C(x) = e^{ax+b} \tag{4.30}$$

was used. R generated the optimal coefficients, resulting in the fit equation

$$C(x) = e^{-2.64-.367x}. \tag{4.31}$$

This equation is shown in Figure 4.6 in green. The residual sum of squares for the CRS fit was calculated to be $RSS = .0001788$.

For the NCRS model, equation [4.18] was inputted into the nonlinear fit function in R. R outputted the optimal coefficients, resulting in the equation

$$C(x) = .0595e^{-.165x}(1 + .202\sin(2.71x - .459) - .104x). \tag{4.32}$$

This equation is shown in Figure 4.6 in blue. The residual sum of squares was found to be $RSS = 2.431 \times 10^{-5}$. Comparing the ratios of the two RSS values, the NCRS model's error estimate is more than 7 times smaller than the CRS model's error estimate, suggesting that the NCRS model is a better fit for the data.

To obtain the CRS solution, the cumulative activity at the surface layer must be known. For the data presented in this chapter, the cumulative accumulations were provided in the spreadsheet from which the concentration data was obtained. The cumulative activity was given to be $A(0) = .1372\ \frac{Bq}{cm^2}$. The CRS solution is thus obtained by substituting this initial condition into the exponential decay equation

$$A(x) = A(0)e^{-.03114t}. \tag{4.33}$$

Thus, age estimates for the CRS model can be obtained from the equation

$$A(x) = .137e^{-.03114t}. \tag{4.34}$$

This CRS age estimate is shown in Figure 4.7 in green.

Before the NCRS solution can be obtained, Equation [4.32] must be rewritten so that a conversion between depth and time can be made. Note that

$$\begin{aligned} C(x) &= .0595e^{-.165x}(1 + .202\sin(2.71x - .459) - .104x) \\ &= e^{-2.81-.165x}(1 + .202\sin(2.71x - .459) - .104x), \end{aligned} \tag{4.35}$$

and thus to switch from x to t,

$$-2.82 - .165x = -.03114t + c_t. \tag{4.36}$$

Using the initial depth $x = .5$ as the depth estimate for $t = 0$,

$$-2.82 - .165(.5) = -.03114(0) + c_t, \tag{4.37}$$

and hence

$$c_t = -.290. \tag{4.38}$$

Solving equation [4.37] for x,

$$x = .5 + .188t. \tag{4.39}$$

Rewriting equation [4.35] in terms of time,

$$\begin{aligned} C(x) &= e^{-.2.90-.03114t}(1 + .202\sin(2.71(.5 + .188t) - .459) \\ &\qquad -.104(.5 + .188t)) \\ &= e^{-2.91-.03114t}(.948 + .202\sin(.496t + .894) - .0195t) \\ &= .948e^{-2.90-.03114t}(1 + .213\sin(.496t + .894) - .0206t). \end{aligned} \tag{4.40}$$

Thus,

$$C(x) = C_0 e^{-.03114t}(1 + .213\sin(.496t + .894) - .0206t). \tag{4.41}$$

Now that equation [4.41] is in the correct form, the coefficients can be substituted into equation [3.36]. This results in the model equation,

$$\begin{aligned} A(x) &= \zeta e^{-.03114t}(\frac{1}{-.03114} + \frac{-.0206}{.03114^2} + \frac{-.0206t}{.03114} \\ &+ \frac{.213}{.03114^2 + .496^2}(.03114\sin(.496t + .894) + .496\cos(.496t + .894)). \end{aligned} \tag{4.42}$$

Simplifying,

$$\begin{aligned} A(x) = \zeta e^{-.03114t}(10.9 - .662t + .864[&.03114\sin(.496t + .894) \\ &+.496\cos(.496t + .894)]). \end{aligned} \tag{4.43}$$

The constant ζ remains to be determined. Using the initial condition $A(0) = 0.1372\ \frac{Bq}{cm^2}$,

$$0.137 = \zeta(10.9 + .864(.03114\sin(.894) + .496\cos(.894))) = 11.3. \tag{4.44}$$

Then

$$\zeta = \frac{.137}{11.3} = .0121. \tag{4.45}$$

Therefore equation [4.32] becomes

$$A(x) = .0121e^{-.03114t}(10.9 - .661670t + .864[.03114\sin(.496t + .894) + .496\cos(.496t + .894)]). \quad (4.46)$$

Equation [4.46] is shown in Figure 4.7 in blue. Due to the decreasing linear term, the initial NCRS fit would seem to suggest that the entire sample is less than 20 years old, which is not consistent with the generally accepted age estimates for lake sediment samples of a similar depth. For this reason, the NCRS model was recomputed without the linear term.

Using R, the coefficients for the best fit curve were recalculated excluding the linear term. The resulting equation was

$$C(x) = .0608e^{-.316x}(1 + .278\sin(2.78x - .669)). \quad (4.47)$$

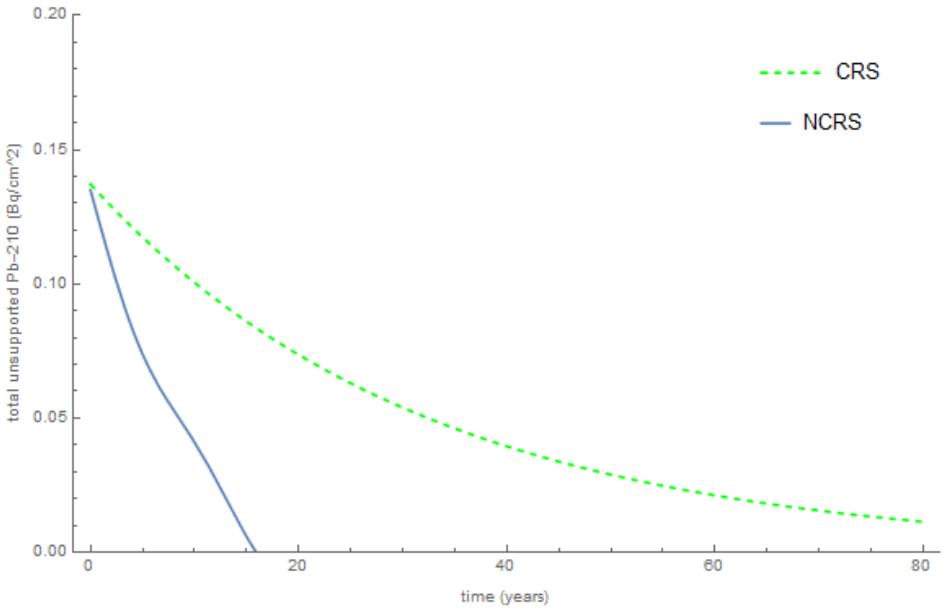

Figure 4.7. A comparison of CRS and NCRS age estimates for the lake SS15 in Greenland lead-210 data including a linear term in the NCRS model.

The RSS value was calculated to be $RSS = 6.77 \times 10^{-5}$. While not as close a fit as the original NCRS model, this modified model is still a better fit than the purely exponential CRS fit. Equation [4.47] is shown in Figure 4.8 in blue.

Equation [4.47] can be rewritten as

$$C(x) = e^{-2.80-.316x}(1 + .278\sin(2.78x - .669)). \tag{4.48}$$

Assuming that x and t are linearly related,

$$-2.80 - .316x = -.03114t + c_t. \tag{4.49}$$

Using the condition that $x = .5\ cm$ when $t = 0\ s$, $c_t = -2.96$. Therefore,

$$x = .5 + .0985t, \tag{4.50}$$

and thus

$$\begin{aligned} C(x) &= e^{-.03114t-2.96}(1 + .278\sin(2.78(.5 + .0985t) - .669)) \\ &= e^{-.03114t-2.96}(1 + .278\sin(.274t + .721)) \end{aligned} \tag{4.51}$$

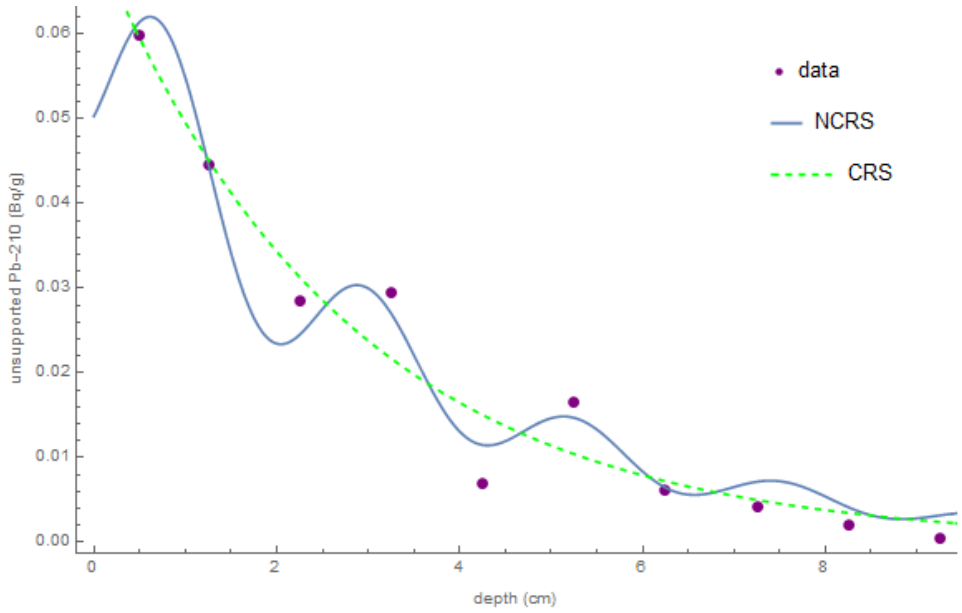

Figure 4.8. A comparison of CRS and NCRS fits for the lake SS15 in Greenland lead-210 data excluding a linear term from the NCRS model.

Therefore,

$$C(x) = C_0 e^{-.03114t}(1 + .278\sin(.274t + .721)). \tag{4.52}$$

Substituting the coefficients of equation [4.52] into equation [3.36],

$$A(x) = \zeta e^{-.03114t}(32.1 + .278(.03114\sin(.274t + .721) \\ +.274\cos(.274t + .721))). \tag{4.53}$$

Solving for ζ in the same manner as before, using the initial condition $A(0) = .1372$ $\frac{Bq}{cm^2}$, $\zeta = .00416$, and hence

$$A(x) = .004164e^{-.03114t}(32.1 + .278(.03114\sin(.274t + .721) \\ +.274\cos(.274t + .721))). \tag{4.54}$$

Equation [4.54] is shown in Figure 4.9 in blue, compared to the CRS fit, shown in green. While the sinusoidal fluctuations are relatively small, the age estimates differ by about a year in places. For example, for a concentration of .095 $\frac{Bq}{cm^2}$, the NCRS model estimates the age to be about 10.9 years, while the CRS model estimates the age to be about 11.8 years. A difference of a year on a time scale of about 10 years is not insignificant.

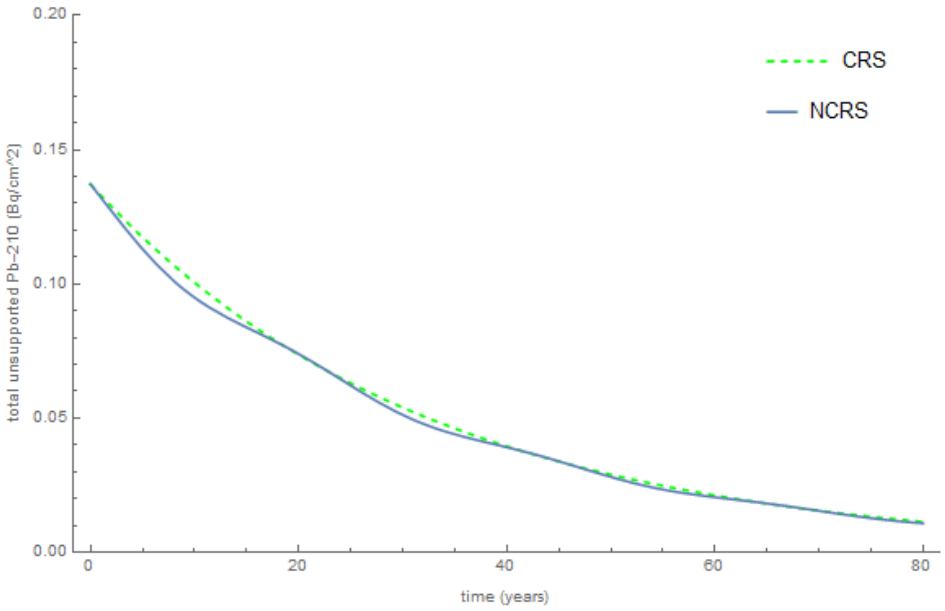

Figure 4.9. A comparison of CRS and NCRS models for the lake SS15 in Greenland lead-210 data, excluding a linear term from the NCRS model.

Further, as mentioned previously, the NCRS model does provide information that the CRS model does not. The period of the oscillations can easily be obtained from the NCRS model, the significance of which will be discussed in Section 5.2.

4.5 Modeling Gardner Pond

The next body of water I selected for modeling was Gardner Pond in Gardner, Maine. This sample's data was included in a set of lake sample data contained on the computer in the ERL. I selected it because it appeared to have some data points that did not lie along an exponential decay curve. The data for this pond is shown in Figure 4.10 in red.

R was used to obtain the CRS and NCRS fits. For the CRS fit, an exponential model was used. The coefficients of the best fit exponential were generated in R, resulting in the equation

$$C(x) = e^{.671-.625x}. \tag{4.55}$$

Equation [4.55] is shown in Figure 4.10 in green. The RSS value was found to be $RSS = .0196$. Using the initial condition $A(0) = .408\ \frac{Bq}{cm^2}$, the CRS solution is

$$A(x) = .408e^{-.03114t}. \tag{4.56}$$

Equation [4.56] is shown in Figure 4.11 in green.

For the NCRS model, an initial fit including both a sinusoidal and a linear term was implemented in R. The coefficients generated in R corresponded to the equation

$$C(x) = 1.39e^{-.451x}(1 + .244\sin(1.64x + .0959) - .0257x). \tag{4.57}$$

This model was a much better fit than the initial model, with an RSS value $RSS = .00214$.

A secondary NCRS fit without the linear term was also considered. The coefficients for this equation were generated in R, producing the equation

$$C(x) = 1.37e^{-.474x}(1 + .263\sin(1.66x + .0202)). \tag{4.58}$$

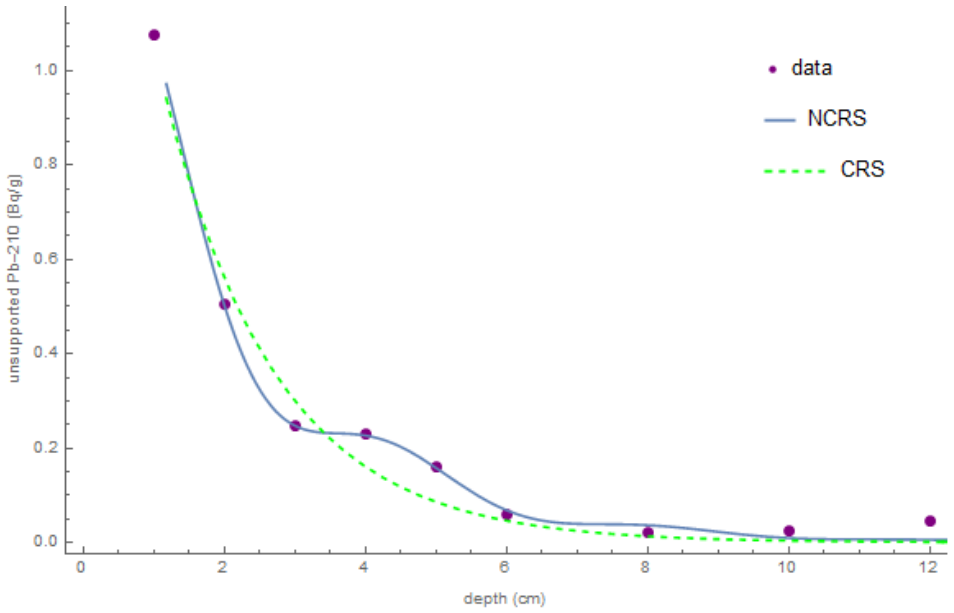

Figure 4.10. A comparison of CRS and NCRS fits for Gardner Pond lead-210 data

This equation was about as good a fit as the model including the linear term, with $RSS = .00215$. Since the linear term did not seem to improve the fit of the model any, it was omitted, and equation [4.58] was used. Equation [4.58] is shown in Figure 4.10 in blue.

Equation [4.58] can be rewritten as

$$C(x) = e^{-.315-.474x}(1 + .263\sin(1.66x + .0202)). \tag{4.59}$$

A conversion between depth and time can then be made, using

$$.315 - .474x = .03114t + c_t. \tag{4.60}$$

Since the depth $x = 1\ cm$ corresponds to $t = 0$, $c_t = -.158$. Therefore,

$$x = .0658t + 1. \tag{4.61}$$

Equation [4.10] can thus be rewritten as

$$C(x) = e^{-.159-.03114t}(1 + .263\sin(1.66(.0658t + 1) + .0202)), \tag{4.62}$$

which reduces to

$$C(x) = C_0 e^{-.03114t}(1 + .263\sin(.109t + 1.68)). \tag{4.63}$$

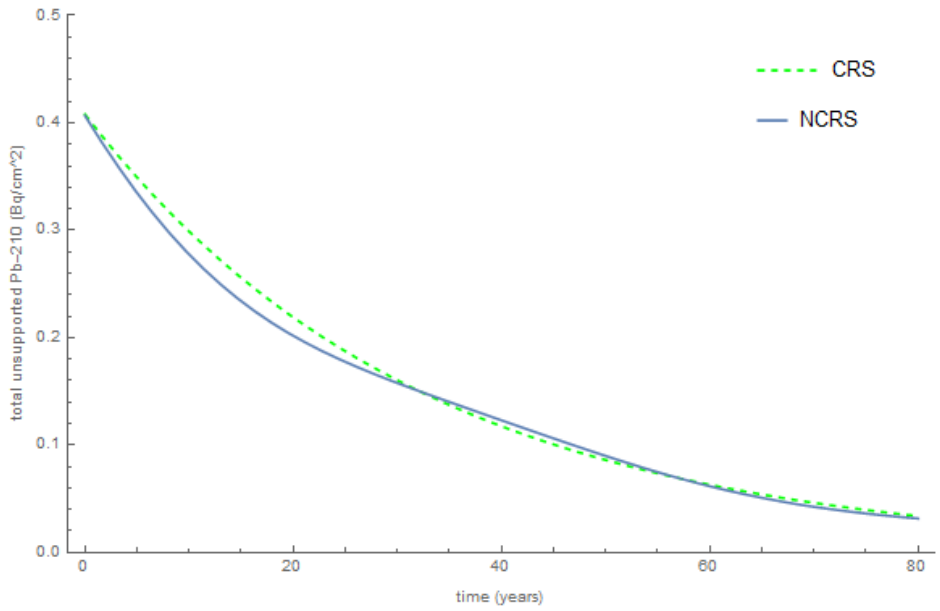

Figure 4.11. A comparison of CRS and NCRS models for Gardner Pond lead-210 data

Substituting the coefficients of equation [4.63] into [3.36],

$$A(x) = \zeta e^{-.03114t}(32.1 + 20.3(.03114\sin(.109t + 1.68) \\ +.109\cos(.109t + 1.68))). \tag{4.64}$$

Using the initial condition $A(0) = .4080\ \frac{Bq}{cm^2}$, it can be determined that $\zeta = .0125$, and hence

$$A(x) = .0125e^{-.03114t}(32.1 + 20.3(.03114\sin(.109t + 1.68) \\ +.109\cos(.109t + 1.68))). \tag{4.65}$$

Equation [4.65] is shown in Figure 4.11 in blue. Here we see a fairly large divergence in the two models for some of the upper sediment samples. For example, for a concentration of .23 $\frac{Bq}{cm^2}$, the NCRS model yields an age estimate of about 15.5 years, while the CRS model provides an age estimate of about 18.4 years. A nearly three year difference between estimates on such a short time scale suggests that oscillatory behavior must be considered to obtain an accurate age estimate for the upper sediment layers.

Another point of interest for the Gardner Pond model is the period of oscillations. Note that a longer period was needed to fit the concentration versus depth data compared to the

two previously discussed models, and correspondingly, the oscillations in the time estimate have a longer period. The potential significance of this will be discussed in Section 5.2.

4.6 Modeling Golden Lake

The next body of water we will analyze is Golden Lake. This was another data set from the ERL computer that appeared to show fluctuations in the data points. The lead-210 data collected from Golden Lake is shown in Figure 4.12 in red. No error bars are present because the measurement uncertainty was too small to be represented on this graph.

After initial fitting attempts were made for the Golden Lake data using both the CRS and NCRS models, it became clear that the first data point deviated from the trend followed by the remaining points in the series. The first data point corresponds to the lead-210 in the surface layer of sediment. There are many issues that could potentially lead to inaccurate measures in the surface layer of sediment, since this is the sediment that comes into direct contact with plants and animals in the lake, as well as moving water currents. Since this data point was so different from the remaining points, it was omitted from the later fitting attempts.

The lead-210 specific activities were imported into R and two nonlinear fit models were implemented. The first was an exponential fit,

$$C(x) = e^{ax+b}, \tag{4.66}$$

which was used for the CRS fit. R outputted the optimal coefficients for a and b, yielding

$$C(x) = e^{-.303x-2.83}. \tag{4.67}$$

This curve is shown in Figure 4.12 in green. The RSS value for this curve was computed as $RSS = 5.579 \times 10^{-5}$. For the NCRS fit, equation [4.18] was used. R outputted the optimal coefficients, which yielded the equation

$$C(x) = .0510e^{-.142x}(1 + .0950\sin(2.37x - 1.79) - .0899x). \tag{4.68}$$

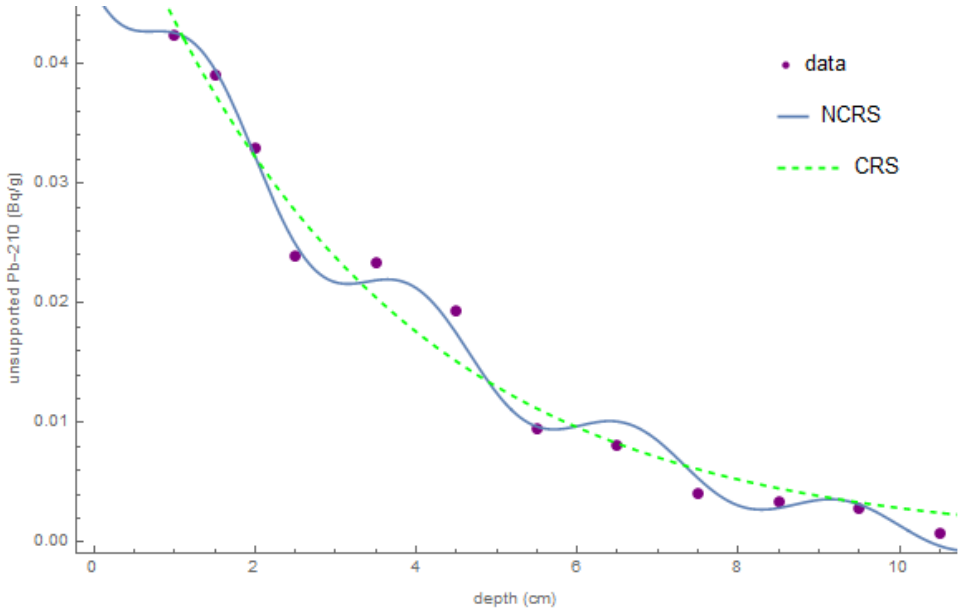

Figure 4.12. A comparison of CRS and NCRS fits for the Golden Lake lead-210 data.

This curve is shown in Figure 4.12 in blue. The RSS value was $RSS = 1.465 \times 10^{-5}$. Note that the NCRS fit is almost four times better a fit by the RSS metric. Note also that the NCRS model seems to match the periodicity of the data well, something that the CRS model cannot account for.

Once the CRS and NCRS fits were obtained, the age estimates could be computed. For the CRS model, equation [2.36] will be utilized. For the initial condition $A(0) = 0.289\ \frac{Bq}{cm^2}$,

$$A(x) = .289e^{-.03114t}. \tag{4.69}$$

Equation [4.69] is shown in Figure 4.13 in green.

To estimate the age using the NCRS model, first a conversion between depth and time must be made. Rewriting equation [4.68],

$$C(x) = e^{-2.98-.142x}(1 + .0950\sin(2.37x - 1.79) - .0899x). \tag{4.70}$$

Employing the linearity assumption,

$$-2.98 - .142x = -.03114t + c_t. \tag{4.71}$$

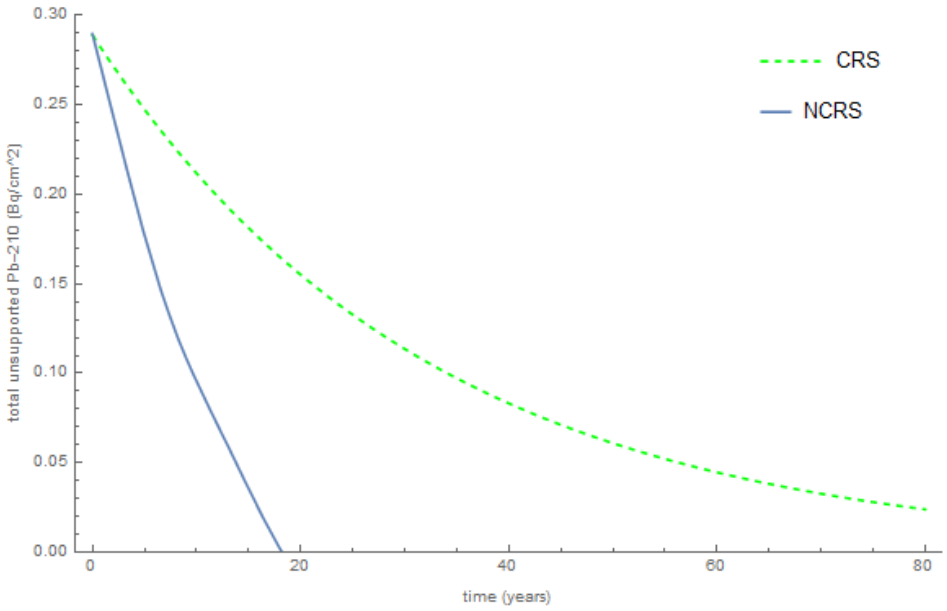

Figure 4.13. A comparison of CRS and NCRS estimates for the Golden Lake lead-210 data including a linear term in the NCRS model.

Since the depth $x = .5\ cm$ corresponds to $t = 0$,

$$-2.98 - .142(.5) = -.03114(0) + c_t, \tag{4.72}$$

and thus

$$c_t = -3.05. \tag{4.73}$$

Substituting equation [4.73] into equation [4.71] and solving for x,

$$x = .220t + .5. \tag{4.74}$$

Now equation [4.70] can be rewritten in terms of time:

$$\begin{aligned} C(x) &= e^{-2.98-.142x}(1 + .0950\sin(2.37x - 1.79) - .0899t) \qquad (4.75)\\ &= e^{-2.98-.142(.220t+.5)}(1 + .0950\sin(2.37(.220t + .5) - 1.79)\\ &\qquad -.0899(.220t + .5))\\ &= e^{-.03114t-3.05}(.955 + .0950\sin(.520t - .611) - .0198t)\\ &= .955e^{-.03114t-3.05}(1 + .0995\sin(.520t - .611) - .0198t)\\ &= C_0e^{-.03114t}(1 + .0995\sin(.520t - .611) - .0198t). \end{aligned}$$

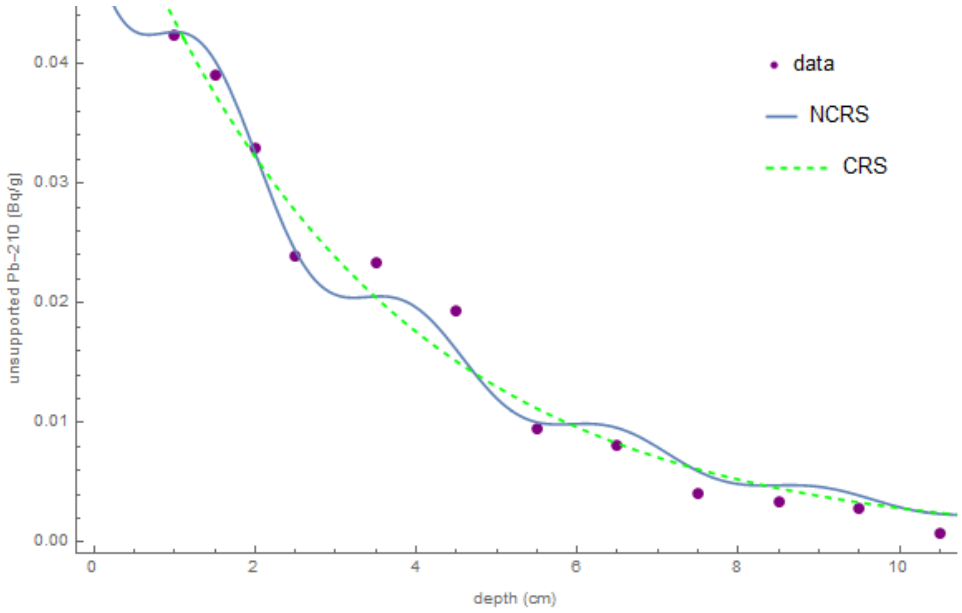

Figure 4.14. A comparison of CRS and NCRS fits for the Golden Lake lead-210 data excluding the linear term from the NCRS model.

Now that equation [4.75] is in the correct form, the coefficients can be substituted into equation [3.36], yielding

$$A(x) = \zeta e^{-.03114t}\left(\frac{1}{.03114} - \frac{.0198}{(.03114)^2} - \frac{.0198t}{.03114}\right. \tag{4.76}$$
$$\left. + \frac{.0995}{(.03114)^2 + (.520)^2}(.03114\sin(.520t - .611) + .520\cos(.520t - .611))\right)$$
$$= \zeta e^{-.03114t}(11.7 - .635t + .366(.03114\sin(.520t - .611)$$
$$+.520\cos(.520t - .611))).$$

Using the initial condition $A(0) = 0.2892\ \frac{Bq}{cm^2}$, it was determined that $\zeta = .0244$, and thus

$$A(x) = .0244e^{-.03114t}(11.7 - .635t + .366(.03114\sin(.520t - .611) \tag{4.77}$$
$$+.520\cos(.520t - .611))).$$

Equation [4.77] is shown in Figure 4.13 in blue.

Since the linear term seems to yield an unrealistic age estimate, the NCRS model was recomputed in R without the linear term. R generated coefficients, resulting in the equation

$$C(x) = .0551e^{-.287x}(1 + .126\sin(2.47x - 2.21)). \tag{4.78}$$

The RSS value was found to be $RSS = 3.19 \times 10^{-5}$, which is better than the CRS fit, although not as close as the original NCRS fit. Equation [4.78] is shown in Figure 4.14 in blue.

Using the same process as outlined in the previous examples, it was found that the linearity condition is given by

$$x = .109t + .5, \tag{4.79}$$

and thus

$$C(x) = e^{-2.04-.03114t}(1 + .126\sin(.262t - 1.01)). \tag{4.80}$$

Therefore,

$$C(x) = C_0 e^{-.03114t}(1 + .126\sin(.262t - 1.01)). \tag{4.81}$$

Substituting the coefficients from [4.81] into [3.36],

$$A(x) = \zeta e^{-.03114t}(32.1 + 1.81(.03114\sin(.262t - 1.01) + .262\cos(.262t - 1.01))). \tag{4.82}$$

Using the initial condition $A(0) = .2892\ \frac{Bq}{cm^2}$, $\zeta = .00895$, and hence

$$A(x) = .00895e^{-.03114t}(32.1 + 1.81(.03114\sin(.262t - 1.01) + .262\cos(.262t - 1.01))). \tag{4.83}$$

Equation [4.83] is shown in Figure 4.15 in blue.

4.7 The NCRS Model: A Discussion

In this chapter, the NCRS model was tested against the CRS model on four different lake sediment samples. Upon analyzing these four lake samples, several distinctions become apparent. The first is that when a linear term is introduced into the NCRS model, the age estimates of the CRS and NCRS models can diverge by as much as several decades. This may suggest that the linear term is not generally useful for estimating the age of sediment

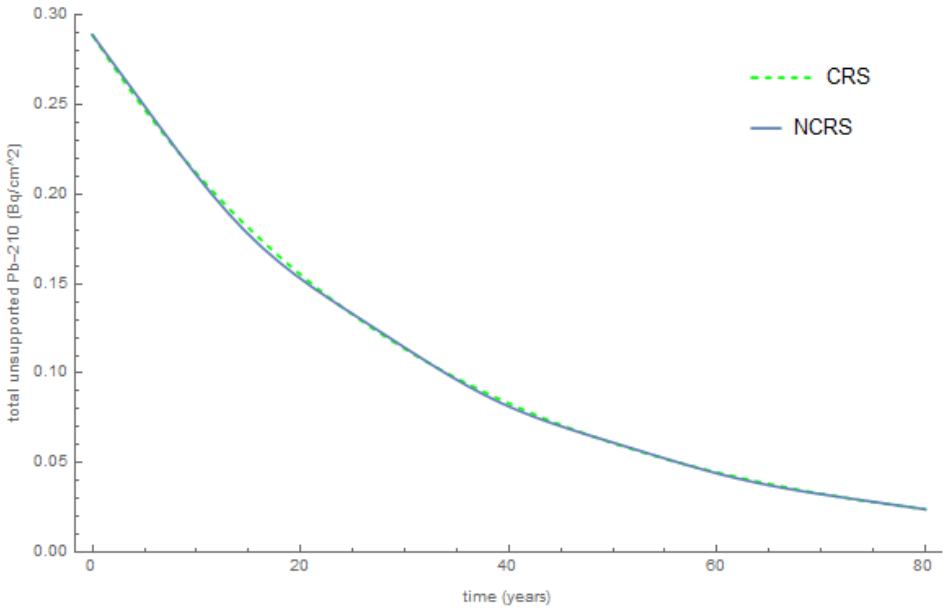

Figure 4.15. A comparison of CRS and NCRS models for the Golden Lake lead-210 data excluding the linear term from the NCRS model.

samples. However, it is worth noting that many age estimates made using the CRS model are not verified by alternative means, such as pollen markers. Thus, it remains to be determined whether the CRS models are indeed accurate age models for the given bodies of water. Potential validation techniques will be discussed in Chapter 6.

It may be that linear increases or decreases are more gradual than would be predicted by a curve fitting function, and more information about the body of water in question would be needed to determine an accurate coefficient for the linear term. Because the linear term has the ability to change the age estimates so drastically, it would be worth pursuing whether its inclusion is in fact warranted.

When the linear term is omitted from the NCRS model, the CRS and NCRS age estimates align more closely. However, for the upper sediment layers, the two models can yield age estimates that differ by several years. Since the upper sediment layers are relatively new, such a discrepancy is nontrivial and suggests that for bodies of water which seem to exhibit oscillatory behavior, such behavior needs to be incorporated into the models to yield accurate age estimates.

Further, the NCRS model provides some information that the CRS model cannot. The sinusoidal fluctuations in the NCRS model could be used to estimate the period of oscillations for each body of water. If the periods are similar, this may suggest a common physical phenomenon is responsible for creating the oscillations.

In the following chapter, data from additional samples will be fitted using the NCRS model without the linear term. While sufficient details will be provided such that the equations can be checked, intermediary steps will be omitted in the interest of readability. Once a critical number of bodies of water have been analyzed, the periods of each, as well as of the lakes considered in this chapter, will be estimated and analyzed.

CHAPTER 5
FURTHER INVESTIGATIONS OF THE NCRS MODEL

5.1 Testing the NCRSFitModelSoftware on More Lead-210 Data

An algorithm, NCRSFitModelSoftware, was developed to compute approximate coefficients for the NCRS model. The algorithm was developed by Dr. Brian Toner, in conjunction with the author. The code is included in Appendix

Although NCRSFitModelSoftware was developed such that a linear term could be included, it was not utilized in these models. The rationale was that because the linear term can drastically alter the age estimates, it should only be included when there is clear physical evidence that it is needed.

NCRSFitModelSoftware was run on the data for the four lakes investigated in Chapter 4 and produced similar results to those presented previously. The results were not identical, and varied slightly for different runs of the algorithm on the same data set. This is due to the inherent difficulty associated with nonlinear fitting, where the initial parameters influence the fit that is chosen. There may be many locally good fits, but finding a universal best fit can be challenging. Thus a good fit that agreed closely with, but perhaps not identically to, the model produced by the fitting mechanisms devised in Chapter 4 was what was sought.

The data used in this section was core data that had been obtained by members of the Environmental Research Lab (ERL) previously. Different samples may have been acquired and processed by different individuals. While the ERL has data for many of the lake cores analyzed in the lab over the years, not all data sets proved useful for this analysis. Some of the lake core data appeared to follow a pure exponential decay curve, while others demonstrated erratic behavior that did not appear to be sinusoidal in nature. However, the NCRSFitModelSoftware was run on most samples (33 in total), regardless of the perceived

Table 5.1. Bodies of water modeled by the NCRSFitModelSoftware and their classifications.

Failure on CRS	Failure on NCRS	Questionable Fit	Reasonable Fit
Laguna Negra	Black Pond	Bullen Merri	Barsjon
Laguna Schmoll	Furbosjon	Damariscotta River 1	Bracey Lake
Laguna Toncek	Lilla	Damariscotta River 2	Gardner Pond
Laguna Verde	Long Lake	Greenland	Golden Lake
Second Pond 2	Damariscotta River 3	HiddenBT	Highland Lake
Ysjon	Pike	Jellison Pond	Lake Purrumbete
	SS32	Michi Lake	Salmon Pond
		Seal Cove Pond	SS15
		Second Pond 1	Warner Lake
		Tilden Pond	
		Tunk Lake	

fit, to see what the software would do when the chosen model was likely a poor fit for the data. Of the data sets tested by the NCRSFitModelSoftware, 9 of the 33 data samples were able to be reasonably fit using the NCRS model with sinusoidal fluctuations. (Cochnewagon Lake was also able to be modeled using NCRSFitModelSoftware, but it came from a different set of data sets and thus was not included in the 33.)

There were three issues that could arise when the NCRSFitModelSoftware was run. The algorithm could error out when attempting to fit the data using a purely exponential fit (the CRS fit). The algorithm could also perform the exponential fit, but error out when implementing the NCRS fit. In both of these cases, the algorithm failed to produce a result. The other issue that cropped up was questionable fitting of the data. In some instances, the NCRSfitModelSoftware produced a NCRS fit that visibly seemed to be a poor fit for the data, such as by fitting a sinusoidal curve to a data set for which there appeared to be no oscillatory behavior. Table 5.1 shows the distribution of bodies of water in terms of fit failure or success. Some of the curves for which the NCRSFitModelSoftware produced a good sinusoidal fit were discussed in Chapter 4, and thus will not be revisited in this section. The remainder of the reasonable sinusiodal fits, as well as some examples of data sets for which the NCRSFitModelSoftware did not produce a reasonable sinusoidal fit,

will be considered in the subsequent subsections. While for each of the samples considered below the NCRS model appeared to be a better fit than the CRS model based on the RSS value, in some cases neither appears to be a particularly good fit, suggesting that a different set of curves may be needed.

5.1.1 Highland Lake

The Highland Lake data appeared to show some fluctuations, although it did not have the clear sinusoidal trend that the lake samples considered in Chapter 4 showed. Nonetheless, NCRSFitModelSoftware was run on the data. The CRS model equation was found to be

$$C(x) = e^{-0.216x+2.17}, \tag{5.1}$$

shown in Figure 5.1 in black, while the NCRS fit was

$$C(x) = exp{-0.275x + 2.40(1 - 0.335\sin(1.93x + 0.231))}, \tag{5.2}$$

shown in Figure 5.1 in blue. The RSS value for the CRS model computed by the NCRSFitModelSoftware was $RSS = 16.70$, while for the NCRS model it was $RSS = 8.009$.

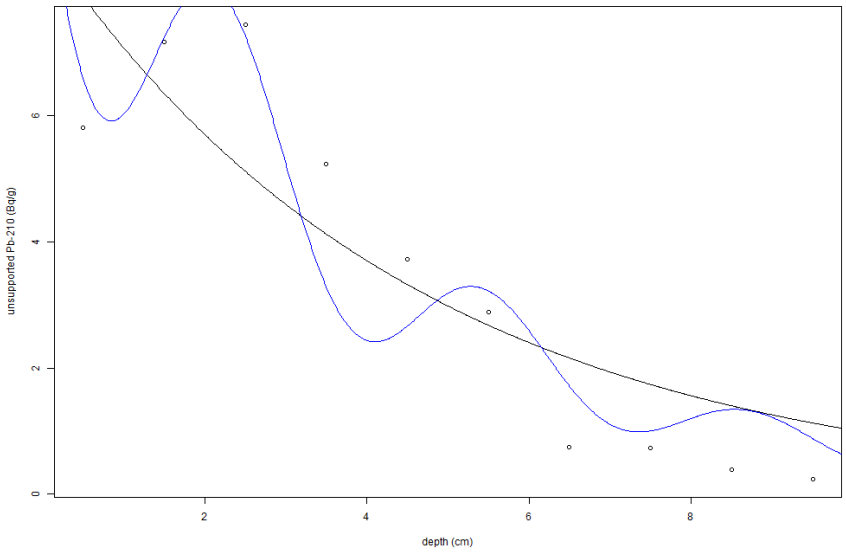

Figure 5.1. Unsupported lead-210 versus depth for Highland Lake.

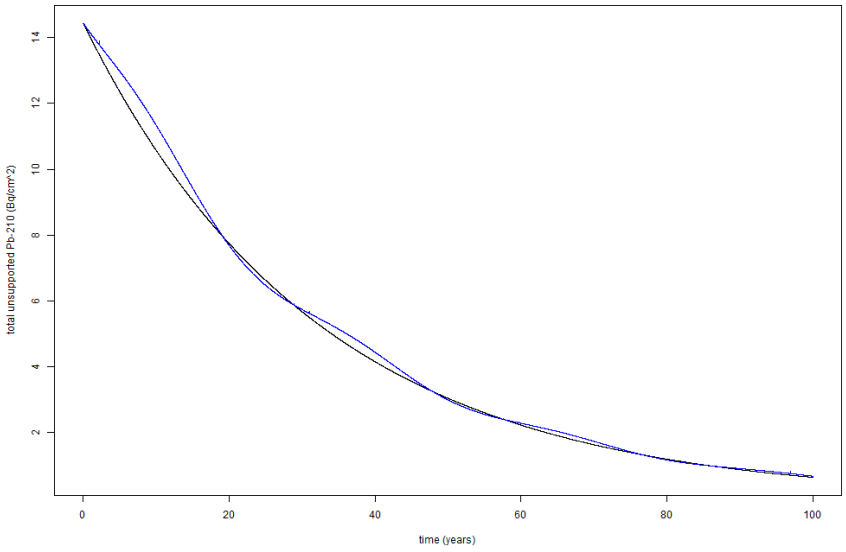

Figure 5.2. Age estimates for Highland Lake.

For the NCRS model, the linear transformation between depth and time was

$$-0.275x + 2.40 = -.03114t + 2.26, \tag{5.3}$$

and thus

$$C(x) = C_0 e^{-0.03114t}(1 - 0.335\sin(0.218t + 0.116)). \tag{5.4}$$

$A(x)$ for the CRS and NCRS models were found numerically and are shown in Figure 5.2 in black and blue, respectively.

5.1.2 Salmon Pond

For Salmon lake, the CRS fit was found to be

$$C(x) = e^{-0.284x+0.0960}, \tag{5.5}$$

shown in Figure 5.3 in black, while the NCRS fit was

$$C(x) = e^{-0.379x+0.415}(1 + 0.408\sin(2.96x - 3.84)), \tag{5.6}$$

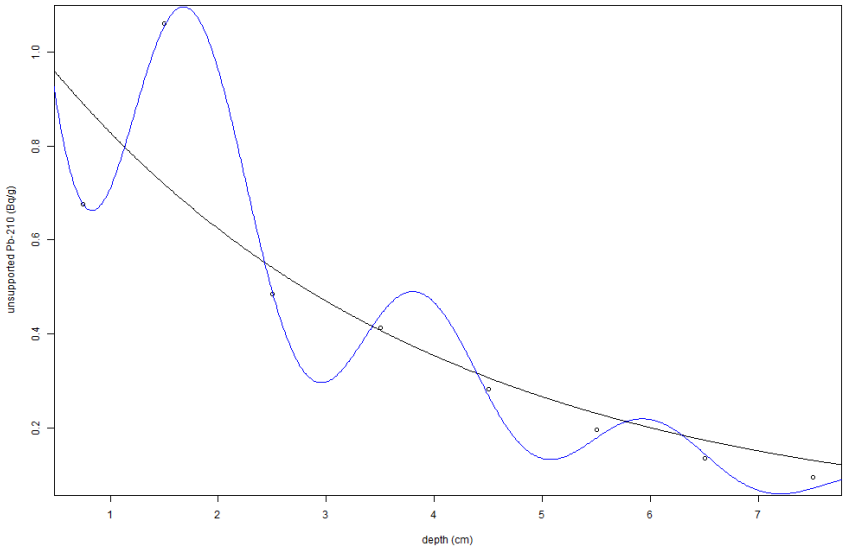

Figure 5.3. Unsupported lead-210 versus depth for Salmon Pond.

shown in Figure 5.3 in blue. The RSS values were computed to be $RSS = 0.1707$ for the CRS model and $RSS = 0.001978$ for the NCRS model.

The conversion between depth and time was given as

$$-0.379x + 0.415 = -.03114t + 0.130, \tag{5.7}$$

leading to

$$C(x) = e^{-0.03114t}(1 + 0.408\sin(0.243t - 2.88)). \tag{5.8}$$

$A(x)$ plots for the CRS and NCRS estimates are shown in Figure 5.8 in black and blue, respectively.

5.1.3 Lake Purrumbete

For Lake Purrumbete, for the CRS model,

$$C(x) = e^{-0.427x-0.465}, \tag{5.9}$$

shown in Figure 5.5 in black, and for the NCRS model,

$$C(x) = e^{-0.533x-0.172}(1 + 0.514\sin(4.08x + 0.992)), \tag{5.10}$$

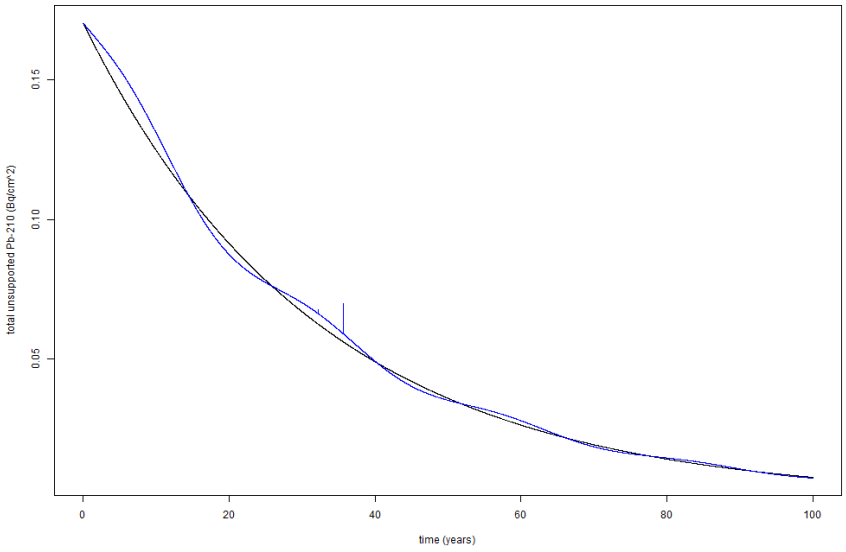

Figure 5.4. Age estimates for Salmon Pond.

shown in Figure 5.5 in blue. The RSS values were $RSS = 0.0137$ for the CRS model and $RSS = 0.00267$ for the NCRS model.

For the NCRS model, it was determined that

$$-0.533x - 0.172 = -.03114t - 0.838, \tag{5.11}$$

and thus,

$$C(x) = C_0 e^{-0.03114t}(1 + 0.514\sin(0.239t + 1.24)). \tag{5.12}$$

The $A(x)$ curves are shown in Figure 5.6, with the CRS fit in black and the NCRS fit in blue.

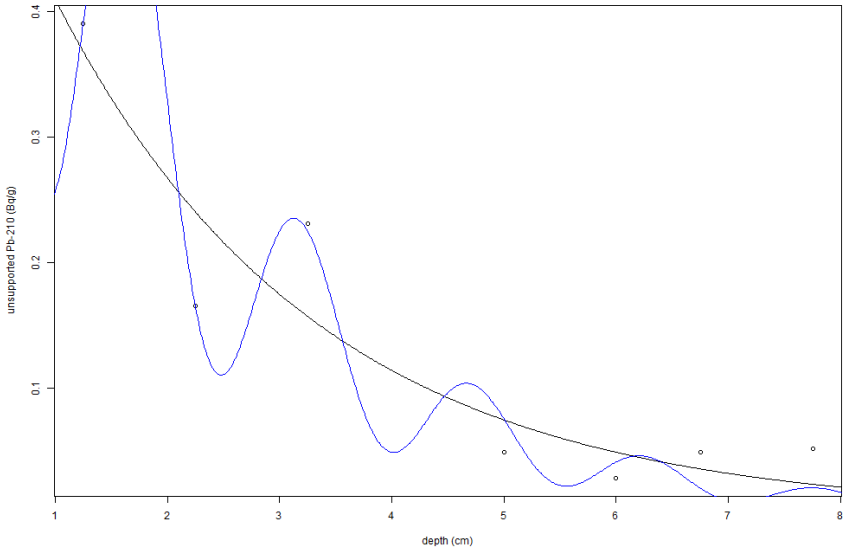

Figure 5.5. Unsupported lead-210 versus depth for Lake Purrumbete.

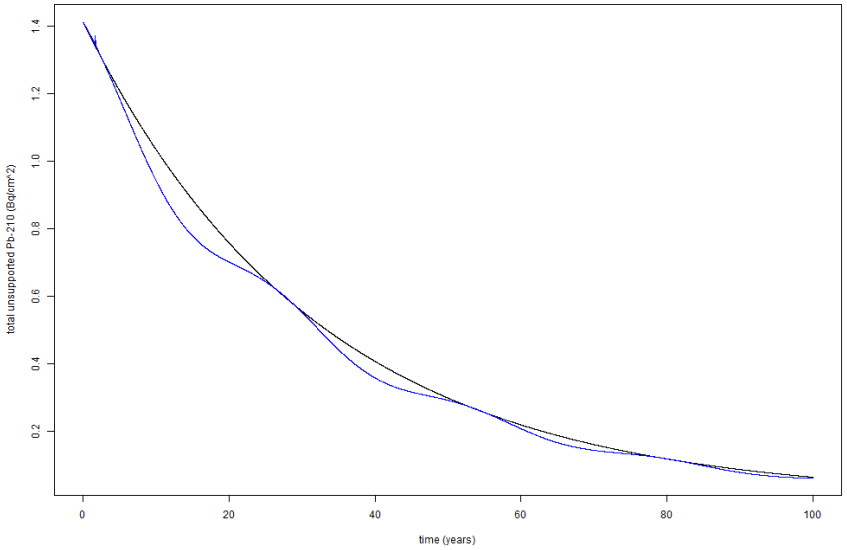

Figure 5.6. Age estimates for Lake Purrumbete.

5.1.4 Warner Lake

Once it had been confirmed that NCRSFitModelSoftware produced results similar to those obtained in Chapter 4, it was implemented on the data for Warner Lake in Peru. While there are some fluctuations present in the data, it is not clear that they are necessarily sinusoidal in nature. Nonetheless, the NCRSFitModelSoftware was run to see if a fit including sinusoidal fluctuations better fit the data than a purely exponential model. The first data point had inadvertently been excluded in the initial run, but this exclusion seemed to provide a good fit for the potential periodic behavior, so it was excluded from successive runs as well. For the exponential fit, NCRSFitModelSoftware produced the equation

$$C(x) = e^{-0.609x+3.45}, \tag{5.13}$$

shown in Figure 5.7 in black, and for the NCRS fit with sinusoidal fluctuations it produced the equation

$$C(x) = e^{-0.405x+2.97}(1 + 0.589\sin(2.80x - 0.942)), \tag{5.14}$$

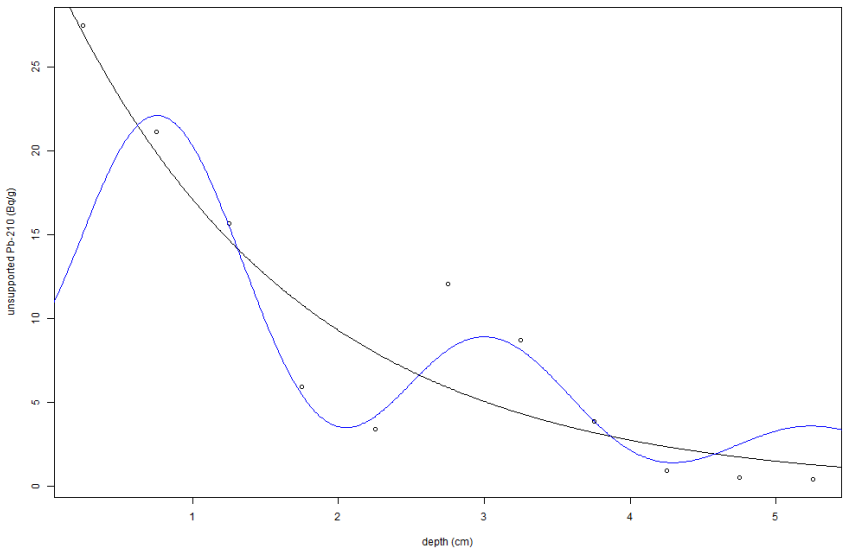

Figure 5.7. Unsupported lead-210 versus depth for Warner Lake in Peru.

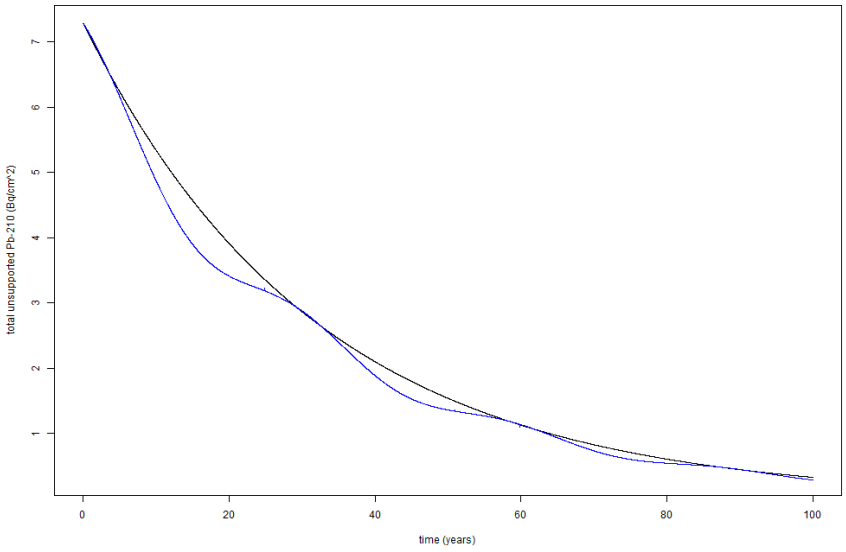

Figure 5.8. Age estimates for Warner Lake in Peru.

shown in Figure 5.7 in blue. For the relationship between x and t, it determined that

$$-0.405x + 2.97 = -.03114t + 2.77, \tag{5.15}$$

resulting in the equation

$$C(x) = C_0 e^{-0.03114t}(1 + 0.589\sin(0.215t - 0.471)) \tag{5.16}$$

$A(x)$ was determined numerically for the CRS and NCRS fits. The results are shown in Figure 5.8, with the CRS fit in black and the NCRS fit in blue. Note that because NCRSFitModelSoftware was developed using R, the figures are produced in R rather than Mathematica, which is why the images appear different than in previous sections.

5.1.5 Bracey Lake

The NCRSFitModelSoftware was then implemented on the Bracey Lake lead-210 data. The CRS fit was found to be

$$C(x) = e^{-0.239x-0.0722}, \tag{5.17}$$

shown in Figure 5.9 in black, while the NCRS fit was found to be

$$c(x) = e^{-0.245x-0.0418}(1 + 0.113\sin(1.86x + 1.50)), \tag{5.18}$$

shown in Figure 5.9 in blue. The linearity condition was found to be

$$-0.245x - 0.0418 = -.03114t - 0.226, \tag{5.19}$$

and thus

$$C(x) = C_0 e^{-0.03114*t}(1 + 0.589\sin(0.215t - 0.236)). \tag{5.20}$$

$A(x)$ was determined numerically. The CRS and NCRS results are shown in Figure 5.10 in black and blue, respectively.

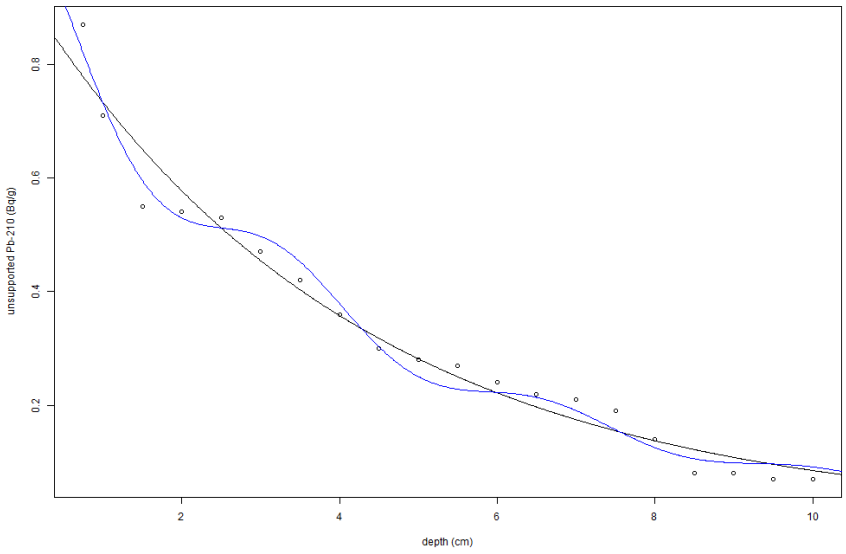

Figure 5.9. Unsupported lead-210 versus depth for Bracey Lake.

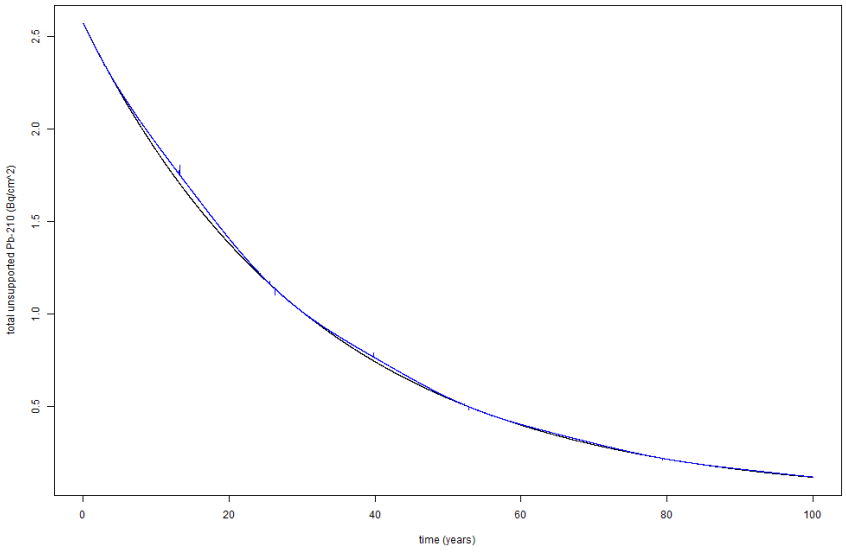

Figure 5.10. CRS and NCRS Age estimates for Bracey Lake.

5.1.6 Barsjon Lake

Barsjon Lake in Sweden also seemed to be modeled reasonably well using the NCRSFitModelSoftware. The algorithm produced the CRS fit

$$C(x) = e^{-0.179x-2.74}, \tag{5.21}$$

shown in Figure 5.11 in black, and the NCRS fit

$$C(x) = e{-}0.211x - 2.58(1 + 0.239\sin(2.82x + 2.51)), \tag{5.22}$$

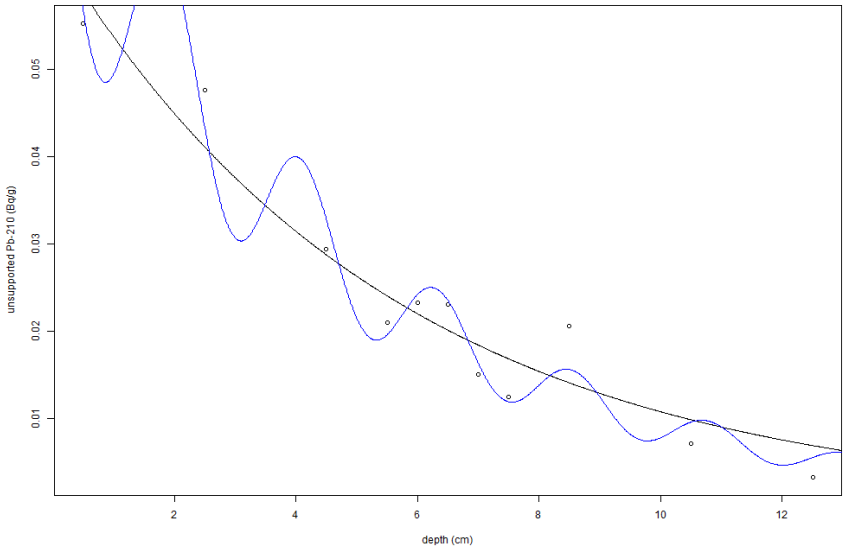

Figure 5.11. Unsupported lead-210 versus depth for Barsjon Lake.

shown in Figure 5.11 in blue. The RSS values were computed to be $RSS = 0.0001681$ and $RSS = 7.372 \times 10^{-5}$ for the CRS and NCRS fits, respectively.

The linearity condition was found to be

$$-0.211x - 2.58 = -.03114t - 2.68, \tag{5.23}$$

yielding the equation

$$C(x) = e^{-0.03114t}(1 + 0.239\sin(0.417t + 1.25)). \tag{5.24}$$

The CRS and NCRS age curves were computed numerically and are shown in Figure 5.12 in black and blue, respectively.

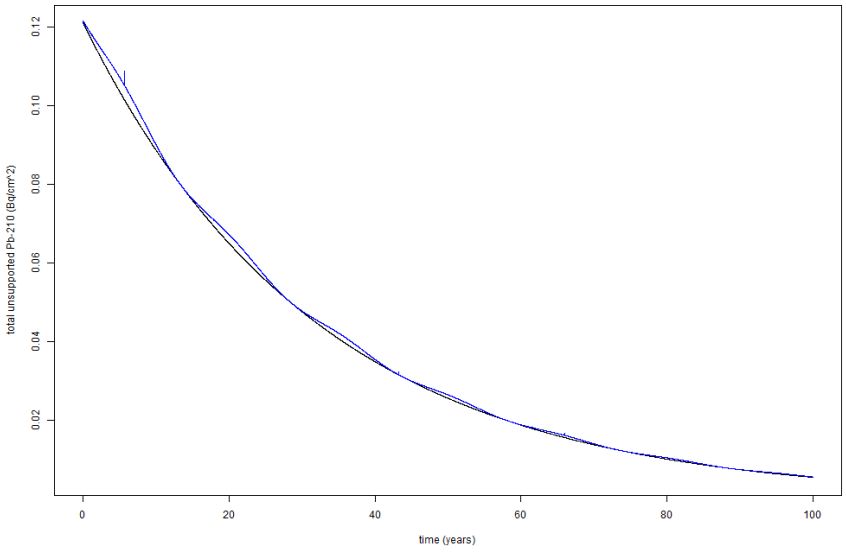

Figure 5.12. CRS and NCRS Age estimates for Barsjon Lake.

5.1.7 Laguna Negra: Failure in Modeling CRS Fit

While the NCRSFitModelSoftware produced an output for many of the data sets, in some instances it failed to produce a result. The first place where it could run into trouble was in modeling the exponential fit, which would be used for the CRS model. One such example of this is the sample from Laguna Negra in Argentina. As shown in Figure 5.13, the data appears to follow an exponential curve reasonably well, although the tail of the curve skews upward a little.

When NCRSModelFitSoftware was run on the data, an error message appeared, shown in Figure 5.14. The message stated, “Missing value or an infinity produced when evaluating the model." The x and y data values were checked and no missing data points were found, so presumably the algorithm ran into issues with an infinite value somehow.

The data was able to be fitted with an exponential curve using the nls function in R, the solution of which is shown plotted against the data points in Figure 5.13. Since the data does not seem to exhibit any clear oscillatory behavior, no attempt was made to manually fit it using the NCRS model with sinusoidal fluctuations.

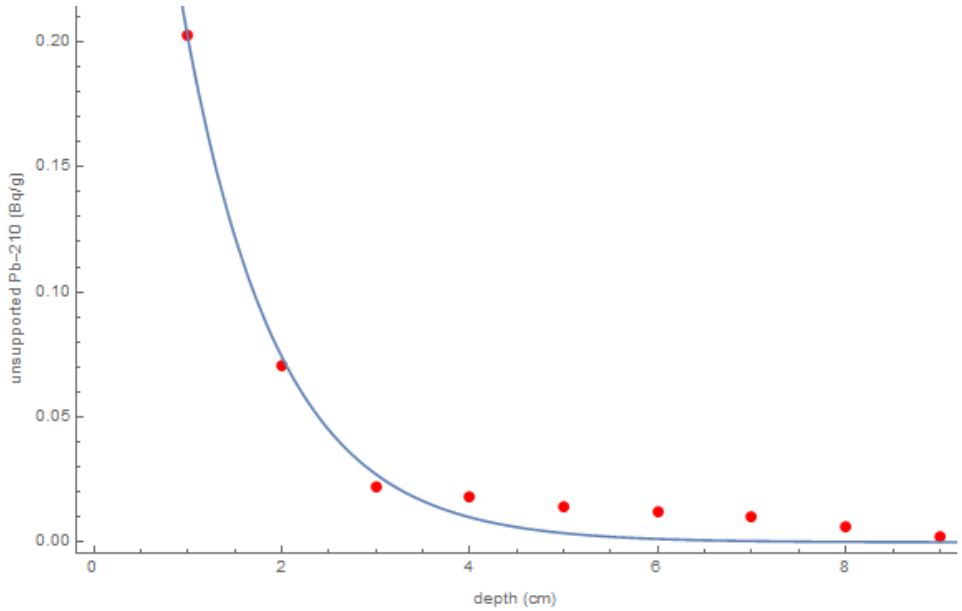

Figure 5.13. Unsupported lead-210 versus depth for Laguna Negra in Argentina.

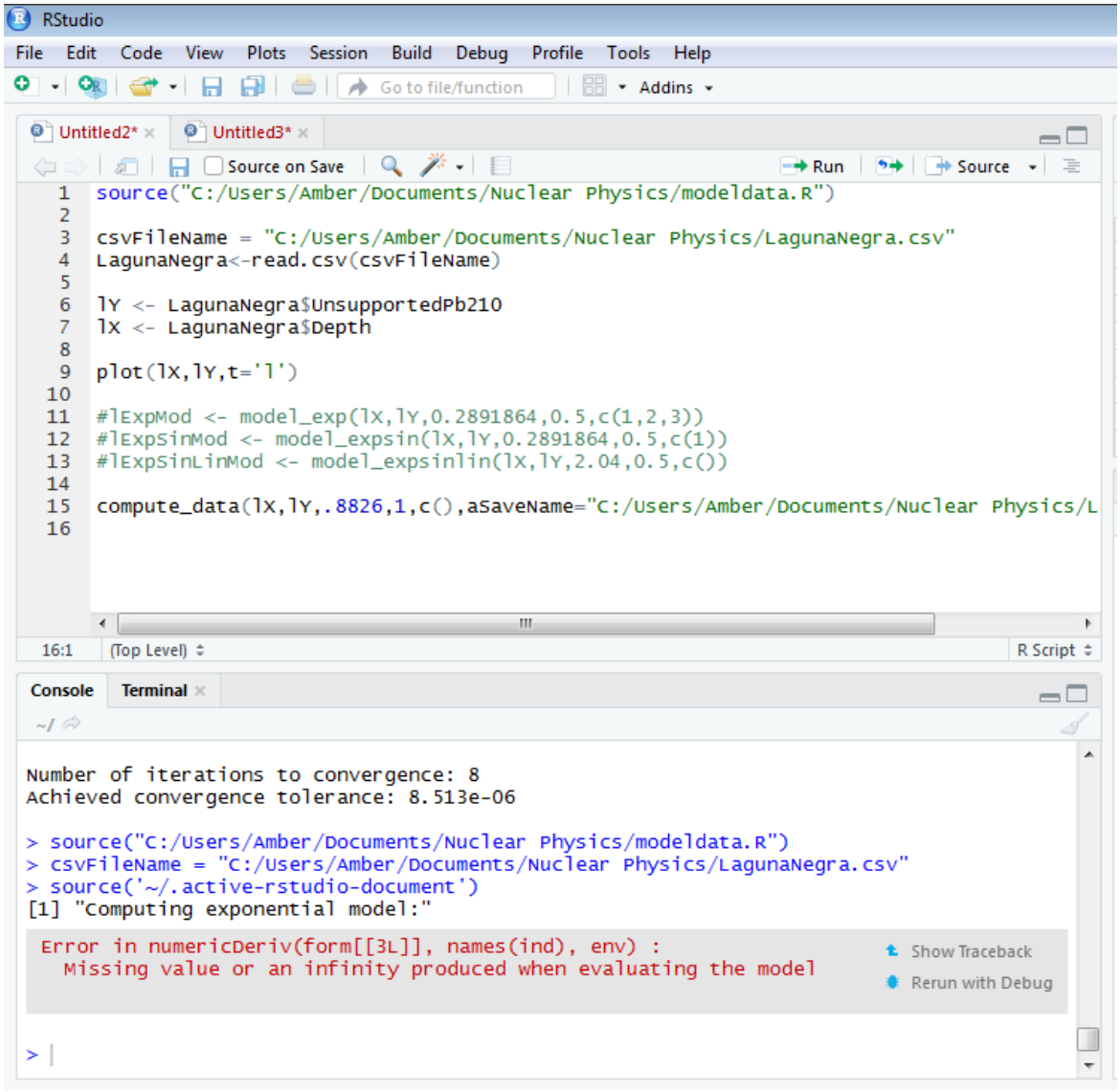

Figure 5.14. Error message received when modeling Laguna Negra data.

5.1.8 Long Lake: Failure to Produce the NCRS Fit

Another possible outcome was that the NCRSModelFitSoftware would produce a result for the exponential fit, but not for the NCRS fit. An example of this can be seen in the modeling of Long Lake. The Long Lake data is shown in Figure 5.15.

When the NCRSFitModelSoftware was run on the Long Lake data, an exponential solution was produced. However, when the algorithm searched for an NCRS fit, an error was produced, as shown in Figure 5.16. The following message was given, “number of iterations exceeded maximum of 50." This issue can arise when the set of initial conditions chosen for the nls function are not well suited to the data, and sometimes can be remedied by a different choice of initial conditions. However, it can also arise when the function is not well suited to the data. Note that one data point deviates quite a bit from the others, which likely made it difficult for the software to fit the data with a curve. Aside from one errant initial data point, the Long Lake data appears fairly close to exponential decay, so a manual fit using the nls function was not attempted at this time.

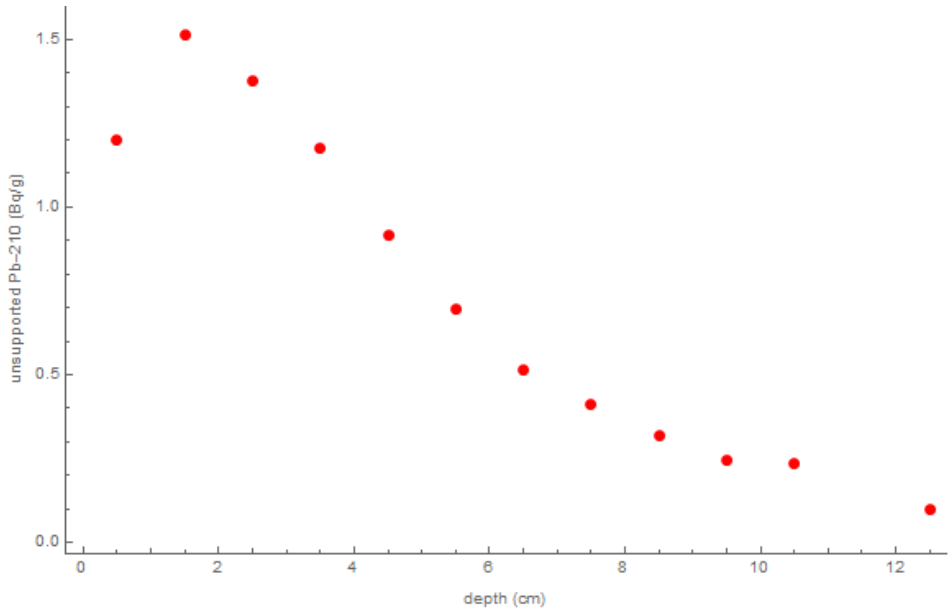

Figure 5.15. Unsupported lead-210 versus depth for Long Lake.

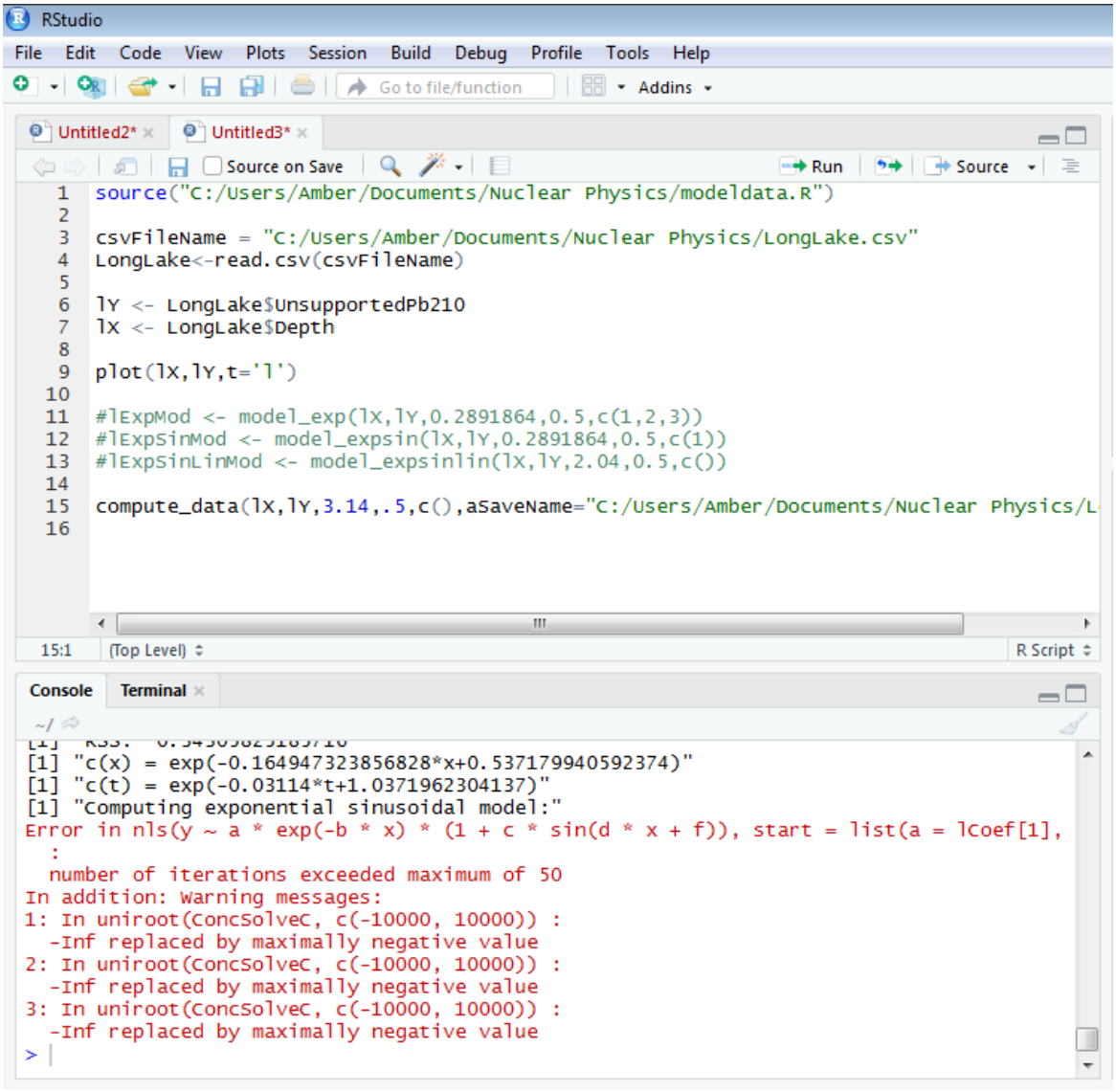

Figure 5.16. Error message received when modeling Long Lake data.

5.1.9 Bullen Merri: A Questionable Fit

Lake Bullen Merri is a lake in Australia. It is not clear from the distribution of the data points that a sinusoidal fit is the ideal choice here. However, because the NCRSFitModelSoftware was able to fit a sinusoidal curve to the data that fit well, it was included anyway. It seems likely that the fit is coincidental, since the data appears exponential with the exception of one discrepant data point, and when the discrepant data

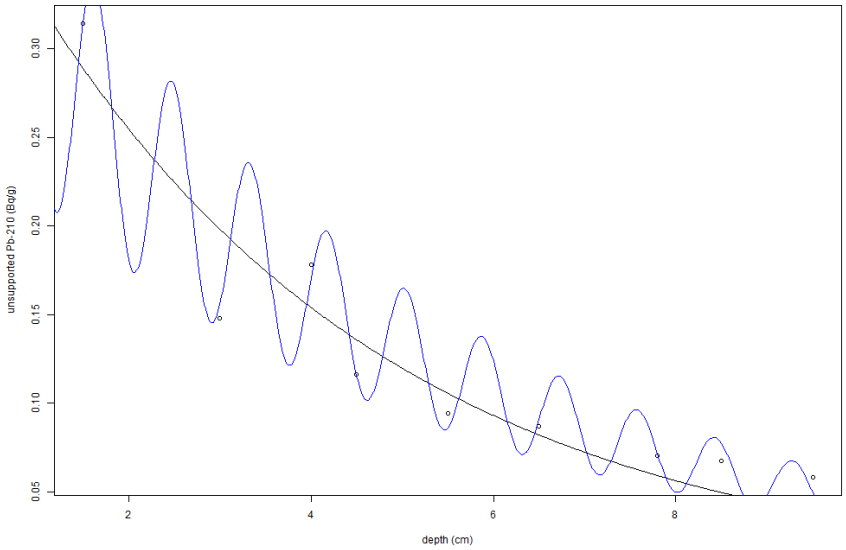

Figure 5.17. Unsupported lead-210 versus depth for Lake Bullen Merri in Australia.

point was removed, the algorithm gave an error message. Nonetheless, it is worth examining how the modeling software handles such situations.

The NCRSFitModelSoftware determined the CRS fit to be

$$C(x) = e^{-0.252*x-0.864}, \tag{5.25}$$

shown in Figure 5.17 in black, while the NCRS fit was found to be

$$C(x) = e^{-0.210x-0.993}(1 - 0.278\sin(7.38x - 13.6)), \tag{5.26}$$

shown in Figure 5.17 in blue. The RSS values were $RSS = 0.00513$ for the CRS fit and $RSS = 0.000369$ for the NCRS fit.

The conversion between depth and time was found to be

$$-0.210x - 0.993 = -.03114t - 1.31, \tag{5.27}$$

and thus the NCRS fit in terms of time was

$$C(x) = C_0 e^{-0.03114t}(1 - 0.278\sin(1.10t - 20.4)). \tag{5.28}$$

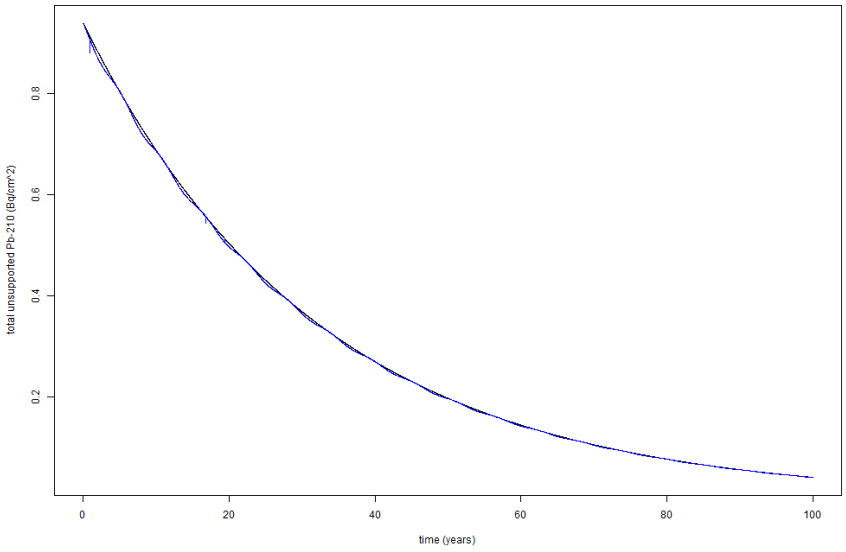

Figure 5.18. CRS and NCRS Age estimates for Lake Bullen Merri in Australia.

The $A(x)$ curves were computed numerically and plotted in Figure 5.17, with the CRS curve in black and the NCRS curve in blue.

While a fit curve and age estimate were able to be produced using the NCRSFitModelSoftware, the fit here does not appear to be a particularly good fit. Thus, discretion must be used when implementing the NCRSFitModelSoftware. If a fit does not look reasonable, it is worth questioning whether it is useful for the data set in question.

5.1.10 Other Questionable Fits

While Lake Bullen Merri provides a good example of a fit provided by the NCRSFitModelSoftware that upon closer inspection does not seem to fit the data well, I thought it might be useful to provide a few more examples. Some of these data sets may in fact have some periodic behavior, but due to some discrepancies in the data, the algorithm was not able to correctly deduce the periodic nature. These data sets may benefit from a manual fitting. Others, like Lake Bullen Merri seem to exhibit no clear periodic trend at all. The Damariscotta River core 1 data sample (Figure 5.19) appears to follow an exponential curve fairly well. There is one data point at $x = 7.5cm$ that does deviate from

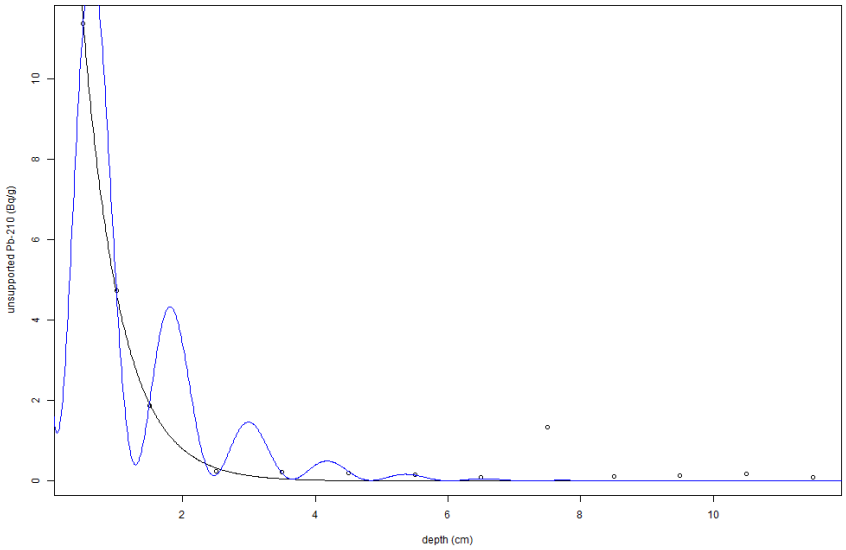

Figure 5.19. Unsupported lead-210 versus depth for the Damariscotta River Core 1.

the exponential curve, but it is not fitted any better by the sinusoidal curve the algorithm chose. The second Damariscotta River core sample (Figure 5.20) does not fit an exponential curve quite as well as the first core seems to. However, the fluctuations in the data do not really appear to be sinusoidal in nature, suggesting that the NCRS model with a sinusoidal term is not the best choice for a fit curve.

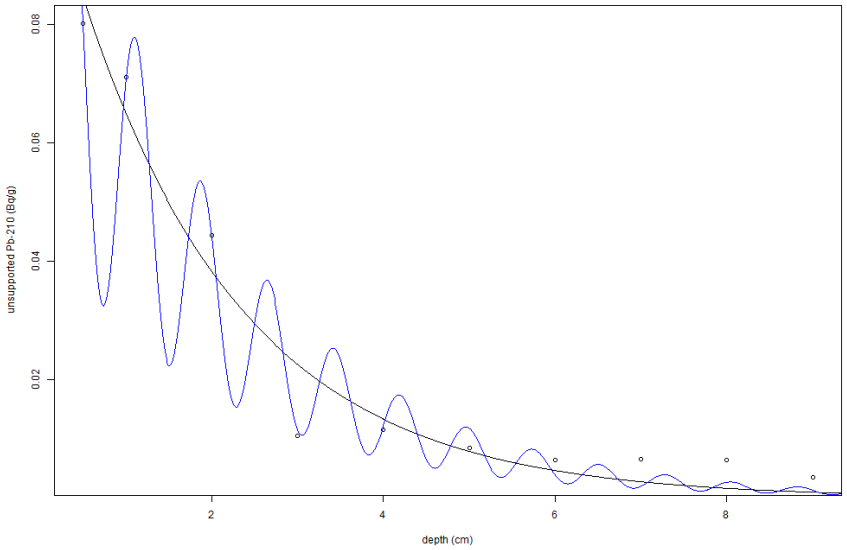

Figure 5.20. Unsupported lead-210 versus depth for the Damariscotta River Core 2.

The next sample (Figure 5.21) was labeled only with the country of origin, Greenland, so it is not clear which body of water it came from. For this sample, while it appears that there may be some periodic behavior, the peaks of the data do not match with the peaks of the selected function, and the period of the fit function seems shorter than the one exhibited by the data. This may be an instance in which manual fitting could potentially provide a more informative result.

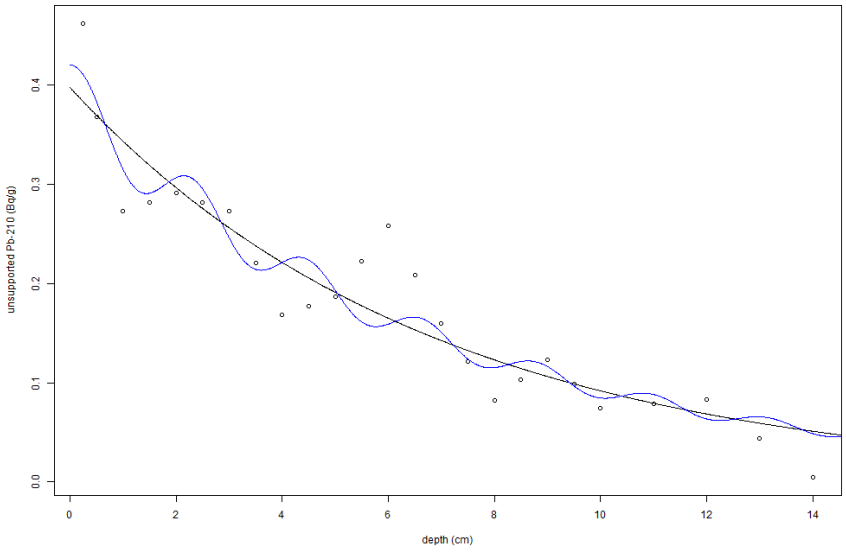

Figure 5.21. Unsupported lead-210 versus depth for a body of water in Greenland.

For the next data set (Figure 5.22), labeled Hidden BT, the NCRS fit seems to fit the first three data points well. However, for the remaining data points, it does not seem to fit at all, although the exponential fit isn't particularly good either. It is not clear that this data is periodic, and thus the NCRS fit with sinusoidal fluctuations is likely not the optimal choice of fit function here.

5.2 Examining the Period of Oscillations

One potential benefit of the NCRS model is that it allows for an estimation of the period of oscillations for data exhibiting sinusoidal fluctuations. If the periods of several models fall within a similar range, it may suggest that a common phenomenon is responsible for the oscillations. Being able to provide an approximate number for that period could potentially help to narrow down the cause of the oscillatory behavior.

To determine the period, the $C(x)$ equation solved for time was used. That is, the equation of the form

$$C(x) = C_0 e^{-kt}(1 + c \sin dt + f). \tag{5.29}$$

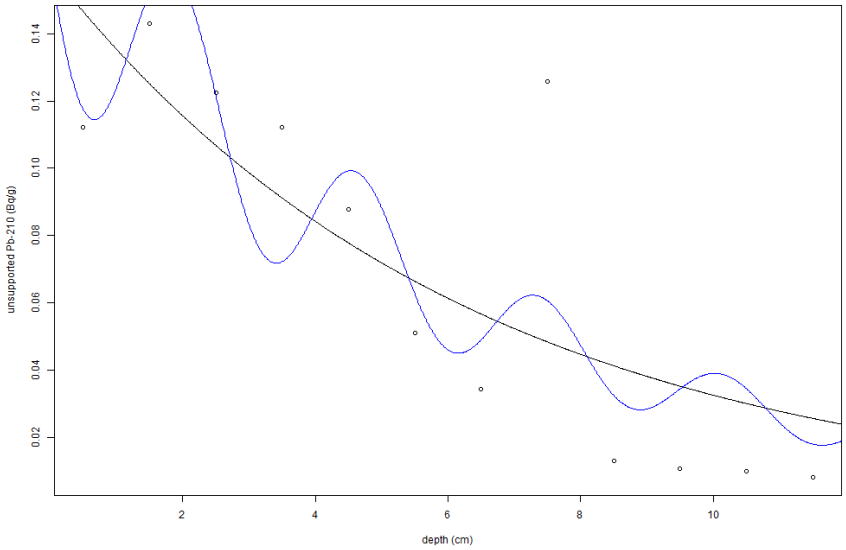

Figure 5.22. Unsupported lead-210 versus depth the Hidden BT data set.

The period was computed by dividing 2π by the coefficient of the time term inside the sin function. Using the notation above, this could be described mathematically as

$$T = \frac{2\pi}{d}. \tag{5.30}$$

For the bodies of water considered in Chapter 5, the period was computed using NCRSFitModelSoftware.

Table 5.2. Period of oscillations for bodies of water considered in Chapters 4 and 5.

Body of Water	Period (years)	Equation
Cochnewagon Lake	22	4.14
SS15	23	4.52
Gardner Pond	57	4.63
Golden Lake	24	4.81
Highland Lake	29	5.4
Salmon Pond	26	5.8
Lake Purrumbete	26	5.12
Warner Lake	29	5.16
Bracey Lake	27	5.20
Barsjon Lake	15	5.24

The period of oscillations for each of the bodies of water described in Chapters 4 and 5 which had a reasonable NCRS fit was computed and compiled in Table 5.2. All but two of the bodies of water, Barsjon Lake and Gardner Pond, have periods between 20 and 30 years. Before we examine the potential implications of the computed periods, however, it is worthwhile to consider the uncertainty in the period calculations.

5.2.1 Estimating the Error in the Period of Oscillations

While there historically have been trends in weather data, there also is some variance, some noise. Thus obtaining a precise equation for the deposition of lead-210 in a lake core sample is infeasible. Thus there is no "true" value to which the generated equations can be compared. However, an estimate of the error could be obtained through simulations using noisy data.

To estimate the error properly, the experimental error for each data point must be known. This could be obtained by taking multiple cores from the same body of water, analyzing the slices, and determining the mean and standard deviation of the lead-210 content at each depth. However, none of these ten bodies of water had multiple cores taken, so the experimental error could not be determined. An alternate approach was needed.

To estimate the error, I chose a generating equation to create a set of "true" data points. The equation I chose was

$$C(x) = .5e^{-.2x}(1 + .15\sin(1.8x + 3)). \tag{5.31}$$

You may notice that this model equation is close to the generated concentration equation for Cochnewagon Lake. I wanted to use an equation with physically realistic parameters, so I opted to use Cochnewagon Lake's concentration equation as my starting point and then round the coefficients a little.

I generated eleven data points by substituting eleven depth values into the model equation and rounding the output to two significant digits. The values are shown in Table 5.3.

Table 5.3. Simulated concentration data without noise

Depth (cm)	Concentration ($\frac{Bq}{g}$)
.25	.454
.75	.370
1.25	.339
1.75	.345
2.25	.352
2.75	.332
3.25	.282
3.75	.241
4.25	.184
4.75	.169
5.25	.172

Table 5.4. Simulated concentration data with noise

Depth (cm)	Concentration ($\frac{Bq}{g}$)
.25	.493
.75	.360
1.25	.323
1.75	.343
2.25	.395
2.75	.334
3.25	.285
3.75	.259
4.25	.231
4.75	.147
5.25	.162

The next step was to use R to add some noise to the generated data points. To generate the noise, I modified the runif function to generate random numbers between 1 and -1. I then scaled these random numbers by .05 and added them to the original data points. The results are given in Table 5.4. The code used for this process is given in Appendix C.2.

The coefficient used to determine the amplitude of the noise depends largely on the sample in question. For some samples, the data points almost perfectly fit a curve, so it would be anticipated that there is little noise in the data. For other data sets, the data points may deviate quite a bit from the best fit curve, and thus it would be expected that

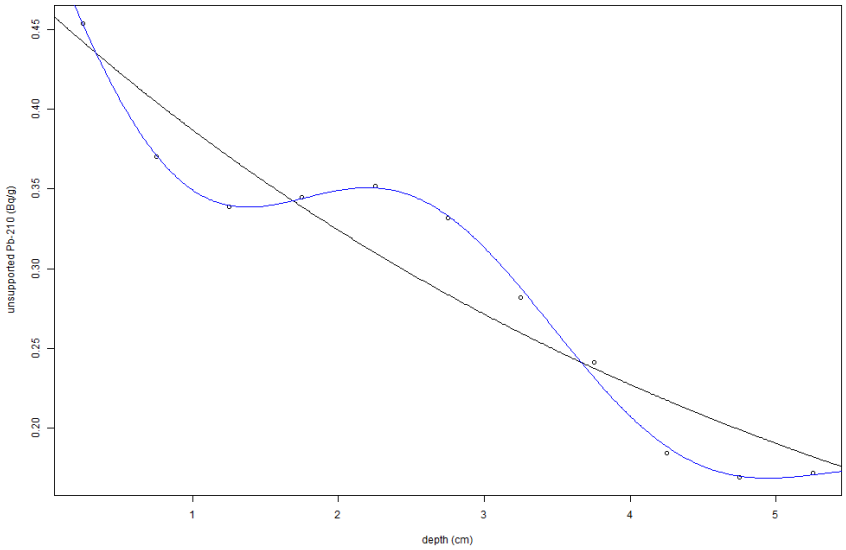

Figure 5.23. The fit function for the simulated concentration data without noise.

the data is noisier. To estimate the coefficient, then, one method would be to determine the mean error for all of the data points in a sample and multiply that number by 2. The error is doubled because, taking the magnitude of the random numbers generated, the mean of these random numbers would be on average about .5. Thus by doubling the random numbers, the mean error of the simulated data points should be comparable to the mean error of the original data points. I did not use this process for the purposes of this example. Rather, I chose a coefficient, .05, that visually looked like it produced an appropriately large error. However, for the error estimates for the ten bodies of water considered in this section, I took the more rigorous approach.

Once I had obtained the two sets of data, one without noise and one with, I ran the NCRSFitModelSoftware on both data sets. Plots of the fit functions for the simulated concentration data without and with noise are shown in Figures 5.23 and 5.24, respectively. The software produced the equation for the concentration as a function of time for the simulated data without noise:

$$C(t) = e^{-0.03114t}(1 + 0.147\sin(0.280t + 0.752)). \tag{5.32}$$

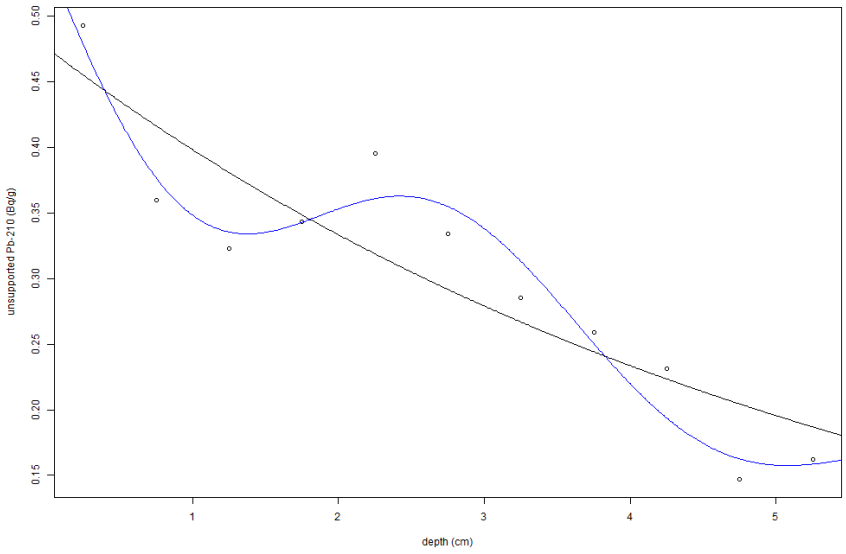

Figure 5.24. The fit function for the simulated concentration data with noise.

For the data with noise, the equation was given as

$$C(t) = e^{-0.03114t}(1 - 0.187\sin(0.260t - 0.0509)). \tag{5.33}$$

The periods for these two data sets were thus $T_{WO} = 22.4\ years$ and $T_W = 24.1$. Thus the two period values differed by a little less than two years.

It is possible that a singular trial may produce larger or smaller deviations from the original data than would be expected on average. For this reason, I ran twenty-nine more simulations of data with noise and computed the period. The values of all thirty trials are given in Table 5.5. It is worth noting that I ran more than 30 trials to accrue this data. There were a couple of instances in which NCRSFitModelSoftware produced an error message and did not provide a period estimate. There were also a few instances in which the graph produced looked like a questionable fit, with a lot of small oscillations between data points that did not appear warranted. These fits were not included in the listed simulations.

I used R to compute the mean and standard deviation of these 30 simulations. The mean was $\mu = 21.7\ years$, while the standard deviation was $3.51\ years$. Since the mean

Table 5.5. Thirty simulations with random noise and the resulting period

Data run	Period ($Years$)
Original	22.4
Simulation 1	24.1
Simulation 2	16.7
Simulation 3	26.4
Simulation 4	27.4
Simulation 5	19.9
Simulation 6	28.7
Simulation 7	27.8
Simulation 8	15.9
Simulation 9	18.7
Simulation 10	18.8
Simulation 11	17.0
Simulation 12	23.4
Simulation 13	19.3
Simulation 14	22.4
Simulation 15	22.4
Simulation 16	25.5
Simulation 17	16.7
Simulation 18	26.2
Simulation 19	23.0
Simulation 20	18.9
Simulation 21	22.0
Simulation 22	21.1
Simulation 23	23.3
Simulation 24	19.0
Simulation 25	24.6
Simulation 26	19.6
Simulation 27	21.4
Simulation 28	20.0
Simulation 29	20.6
Simulation 30	19.8

was generated from simulated data, it is not a better estimate of the period, and is useful primarily as a check to make sure the simulation process is running correctly. For 30 simulations, we would expect to see that the mean is similar to the “original" period (the period determined from the NCRSModelFitSoftware), but because of the small sample size, we would not expect them to be close to identical. Since the original period was 22.4

Table 5.6. Period of oscillations for bodies of water considered in Chapters 4 and 5.

Body of Water	Period (years)
Cochnewagon Lake	22.4 ± 6.7
SS15	22.9 ± 3.1
Gardner Pond	$N/A \pm N/A$
Golden Lake	24.0 ± 4.1
Highland Lake	28.9 ± 11
Salmon Pond	25.9 ± 1.5
Lake Purrumbete	$N/A \pm N/A$
Warner Lake	29.2 ± 8.5
Bracey Lake	26.6 ± 5.4
Barsjon Lake	15.1 ± 6.3

years, the mean of the simulated period data 21.7 *years* seems reasonably close, given that for a 95% confidence interval around the simulation mean, the original value falls within that range.

There are many techniques that can be used to estimate the error of a sample. I opted to use twice the standard deviation as my error estimation technique. My preference is to overestimate the error rather than potentially underestimate it, which this technique should accomplish. Thus for this example, the error would be about 7.0 *years*, meaning that the period for this fictional data set would be 22.4 ± 7.0 *years*.

5.2.2 Results

I ran 30 simulations for each of the 10 bodies of water considered in this section. The results of these simulations are shown in Appendix B. I used these simulations to compute the error in the same manner outlined for this example, by computing the standard deviation and doubling it. The results of these computations are shown in Table 5.6. For two of the bodies of water, Gardner Pond and Lake Purrumbete, the means of the simulations were different enough (using a 95% confidence interval) from the period values obtained from the actual data that the two means could not be said to be the same. For both of these bodies of water, a handful of the trials yielded periods on the order of $50 - 60$

years that visually appeared to fit the data well. Interestingly, even though the Gardner Pond simulated data was generated using a curve that should have produced a 57 *year* period, once the noise was introduced, the majority of the trials yielded periods on the order of $20 - 30$ *years*. Because the noisy simulations were so different from the periods generated from the data, I decided that we do not have enough information to say what the period of oscillations is for these two lakes.

For the remaining eight bodies of water, the period generated from the data did fall within a 95% confidence interval around the mean of the simulated noisy data. The uncertainty, which was computed by doubling the standard deviation, varied widely from one lake to the next. This is unsurprising, given that some lake data appeared to be noisier than the other lakes. Once uncertainty was accounted for, seven of the bodies of water had periods that overlapped with one another. The one exception was Barsjon, which had a period that overlapped with some, but not all, of the lakes.

One thing to be aware of is that these results are only as good as the original fit curves. Because of the conversion between depth and time, it is not only the sinusoidal piece but also the exponential piece that have to be fit well to get an accurate estimate for the period. Improved curve fitting techniques could yield better period estimates.

5.3 Oceanic Oscillations

For the bodies of water considered in the previous section, almost all had a period between $20 - 30$ *years*. This raises the question as to what could be causing such oscillations in lead-210 sediment content.

One possibility is that such fluctuations could be caused by climate cycles. Climate cycles are periodic changes in things such as atmospheric temperature, air pressure, winds, ocean surface temperature, and precipitation amounts. In particular, since the majority of the bodies of water considered are in proximity to the Atlantic Ocean, for such bodies of water, it is possible that one or more of the oceanic climate cycles is influencing lead-210

deposits. Despite extensive research, oceanic oscillations are still not fully understood. Recently, efforts have been made to estimate the period of oceanic oscillations (e.g., [57, 58]). Rather than exhibiting a single distinct period, it has been shown that the processes behind such oscillations may have several distinct periods.

Of particular interest to this research are the North Atlantic Oscillation (NAO), the Atlantic meridional overturning oscillation (AMOC), and the Atlantic mutidecadal oscillation (AMO), which will be collectively referred to as the North Atlantic Oscillations (NAOs). Each of these oscillations operates in the North Atlantic Ocean.

Seip et al. [57] found cycles for the NAOs with lengths of 7, 13, 20, 26, and 34 *years*. Observe that, after accounting for uncertainty, almost all of the bodies of water considered in the previous section had a period of 20 or 26 *years*, the one exception being Barsjon, which could be said to have a period of 13 or 20 *years*. It is possible, then, that one particular mechanism behind the oscillations with a period of $20 - 26$ *years* governs the lead-210 deposits. It is also possible that all of the mechanisms affect lead-210 deposits to some degree, some perhaps more so than others, and that if multiple sinusoidal functions were used in the NCRS model instead of a single one, that a better fit could be found. Such a process would require more sophisticated modeling software than the default nonlinear fit function in R, but could be a good avenue for future research.

CHAPTER 6
CONCLUSIONS AND FUTURE RESEARCH

In this paper, I have derived a new model for radiometric dating, the non-constant rate of supply (NCRS) model. It is a generalized model such that the commonly used constant rate of supply (CRS) model could be viewed as a special case of the NCRS model when the rate of supply of a given radionuclide is constant. It can be utilized whenever the concentration data for a radioisotope in a given sample can be modeled by a combination of mathematical functions (e.g., the concentration data may be modeled as an exponential decay curve with sinusoidal fluctuations).

6.1 Summary and Conclusions

I applied the NCRS model to lead-210 data for 34 bodies of water. For four of these bodies of water, I performed the NCRS analysis by hand (see Chapter 4). Initially I included both sinusoidal and linear fluctuations in my concentration modelings. While the inclusion of the linear term provided a better fit than sinusoidal and exponential terms alone, it soon became apparent that the linear term significantly shifted the age estimates, in some cases by decades. While it would be expected that the linear term should affect the age estimates some, in a couple of cases the age estimates it provided appeared to be physically unrealistic. Thus, for future applications of the NCRS model, I removed the linear term. Even though the linear term proved troublesome in certain cases, it did raise some important questions for radiometric dating. If there is downward migration of lead-210 in the soil, then conventional dating techniques may not accurately estimate the age of the sediment. The linear term may still be useful in some instances, particularly in bodies of water in which there is significant migration of lead-210, but more information about the body of water would be needed so that an accurate linear term could be appended to the concentration equation.

To model the other bodies of water, Dr. Brian Toner and I developed the NCRSModelFitSoftware, which automated the NCRS modeling process. Although the software has the capability to include a linear term, I included only sinusoidal fluctuations in addition to exponential decay. I pulled 33 bodies of water (including three that I had modeled by hand previously) from a collection of processed data contained on the ERL computer. While not all bodies of water exhibited sinusoidal fluctuations, for nine of the samples, the NCRSModelFitSoftware was able to produce a fit curve with sinusoidal fluctuations that appeared to fit the data reasonably well. Cochnewagon Lake was also able to be fit by the software, but it came from a separate collection of data. In total, this left 10 bodies of water with sinusoidal fluctuations to be further analyzed.

The sinusoidal oscillations did shift the age estimates, in some instances by a matter of years. This effect was most pronounced for the upper layers of sediment, as the exponential decay dampened out much of the sinusoidal term's effect in deeper sediment. On such a short timescale, a difference of a few years matters when it comes to estimating the age of the sediment. If there truly are sinusoidal fluctuations, which the data seems to support in at least some bodies of water, it is imperative that these are considered in dating models.

An important future step will be to validate the model using samples of known age. Often validation is done using a secondary radioisotope such as cesium-137 or hallmark features of the sediment, such as pollen markers. While the cesium-137 content for each sample is collected in the ERL, for many if not most of the bodies of water considered in this paper, the lead-210 and cesium-137 dates do not align when the CRS model is used. This issue was explored in [37], and was part of the inspiration for this paper, to reconcile the two estimates by accounting for the potential downward migration of cesium-137. The difficulties with direct application of the NCRS model to cesium-137 will be discussed later in this chapter, but if those difficulties can be accounted for, this may be a fruitful avenue for future research.

Since the CRS and NCRS models produce similar estimates for the deeper sediment layers when considering only sinusoidal fluctuations, however, using a fallout radionuclide as a calibration tool may not be a fine grained enough technique to see differences between the two models. Physical markers, such as pollen markers, could potentially be useful here, if they could be located in the upper sediment layers. However, this would likely require the introduction of a new plant species to a geographic region within the past 15-20 years in order to see differences between the age estimates of the two models. This requirement limits the number of available bodies of water from which the data could be extracted, but if such bodies of water can be found, then they may prove useful for testing the utility of the NCRS model.

Perhaps the best physical validation tool would be a varved lake. In such bodies of water, there is so little sediment mixing that the season in which a sediment layer was formed can be distinguished based on the color of the sediment. Thus, the age can be determined by counting the stripes of color in the sediment. Obtaining varved lake data is difficult, as few such lakes exist. To retain the sediment stratification, there must be virtually no plant or animal activity in the lake. However, if varved lake data could be obtained, it could provide a robust validation tool, assuming the sediment had nonconstant trends in the lead-210 data which would require the use of the NCRS model.

Another key factor I investigated was the period of oscillations. I computed the period for all 10 samples with sinusoidal fluctuations. Eight of the 10 had period values on the order of $20 - 30$ *years*. Of the remaining two bodies of water, Barsjon had a period of about 15 *years*, while Gardner Pond had a period of about 57 years. Two of the bodies of water, one of which was Gardner Pond, ended up being removed from the sample because the uncertainty was too high for the age estimate to be considered meaningful. Of the remaining eight bodies of water, all but Barsjon overlapped with the periods of one another. Barsjon's period overlapped with some, but not all, of the bodies of water in the sample.

Since the majority of the bodies of water in the sample seemed to share a common period, the natural question was, what could cause such a phenomenon? Since the introduction of lead-210 into sediment is conducted through factors such as precipitation and wind, climate cycles, which are cyclic in nature, seemed to be a probable contender. In particular, since most of the bodies of water in the sample are close to the Atlantic Ocean, I looked up the period of oscillations for the North Atlantic Oscillations (NAOs). Instead of having one period, each of these oscillations has several distinct periods. Recent research [57] suggests that the periods have lengths of about lengths of 7, 13, 20, 26, and 34 *years*. With uncertainty, all of the bodies of water except Barsjon have periods of about 20 or 26 *years*, while Barsjon has a period of about 13 or 20 years. While this does not definitively prove that climate cycles are responsible for the sinusoidal fluctuations in sediment samples, it does suggest that climate cycles could be a potential cause.

6.2 Improvements and Further Work

To build upon this work, one of the best avenues for future research would be the inclusion of more sediment samples. While it is encouraging to see that the bodies of water in this study had periods that were roughly the same, it is possible that the observed phenomenon is merely a fluke. More samples could provide further evidence that there is indeed a phenomenon leading to oscillatory behavior in some sediment deposits.

The fit of the concentration versus depth data is crucial to the success of the NCRS model. Both the exponential and sinusoidal pieces of the model must be fit well in order to determine an accurate estimate of the period of oscillations. However, the nonlinear fit function in R, which was what I used for the fits, did not always produce sensible fits (see Sections 5.1.7-5.1.10). While in some cases, this was due to either the data being purely exponential or too noisy, in other instances it was likely due to an issue with the function itself.

The function is relying on mathematical optimization alone. There may be only a small difference between two different fit curves, but the function always picks the one that has the smallest deviation from the data points, even if that fit makes less physical sense. I ran into an issue several times, of which Damariscotta River Core 2 is a good example (see Figure 5.20), where, to obtain the best possible fit, the software would produce a sinusoidal function with a very short period and thus lots of oscillations. In the case of the Damariscotta River Core 2, the data appears to be exponential, with one data point that deviates from the exponential shape. Since it is expected that there will be some amount of noise in the data, a human researcher would likely determine that a sinusoidal function was not needed and that a pure exponential function would produce the most physically realistic fit. The software, however, produced a curve that hits the outlier and comes close to hitting the other points, but which does not seem like a good fit for the general trend of the data. With enough oscillations, a function can reach nearly every data point, but the necessity of so many oscillations is often not reflected in the general shape of the data.

At present, there is no objective system for determining which fits are reasonable and which ones are not. It si up to the researcher to visually inspect the fits and discard any that seem unreasonable. In Sections 5.1.9 and 5.1.10 I have provided you with examples of the types of fits that I thought were unreasonable, but it would be better if unrealistic fits were ruled out by the fit function itself. If a better fit function could be devised, perhaps one with noise reduction, then it could make the fitting process easier and reduce chances of erroneously discarding a valid fit.

The cause of the sinusoidal oscillations could also prove to be a fruitful avenue for research. While it seems probable that climate cycles could be the cause of such fluctuations, the particular climate cycles and mechanisms that could be responsible remain an open question. Since the bodies of water considered here come from various geographic regions, investigations of individual lakes and their climates could help to better understand

the phenomenon. It is also possible that another cause aside from climate cycles is responsible for the oscillations. Alternate explanations may be worth consideration.

6.3 Cesium Dating and Other Fallout Radionuclides

One of the goals at the outset of this project was to use the NCRS model to estimate the age of samples using cesium-137. However, due to the unique shape of cesium curves, the model must be adapted to fit cesium-137, which proved to be more difficult than initially anticipated. Consider the activity data for Golden Lake, shown in 6.1, for lead-210 and cesium-137, obtained from one of the old data sheets in the ERL. (Note that total lead-210 activity, rather than unsupported lead-210 activity, is shown. Note also that activity, rather than specific activity, is on the y axis, allowing lead-210 and cesium-137 to be plotted on the same graph.) Unlike lead-210, which primarily exhibits exponential decay, the cesium-137 data has almost a bell shape, although what happens in the very middle of the graph is unclear. Unlike lead-210, which is constantly being produced, cesium-137 was introduced into the environment during the above ground nuclear weapons testing in the 1950s and 1960s. The presence of cesium-137 in pre-nuclear testing sediment suggests that the cesium has been able to migrate through the layers of sediment. After the weapons testing ended, cesium-137 continued to be deposited into waterways through wind and precipitation, but at decreasing rates. The cesium-137 data must therefore be modeled piecewise for the time prior to above ground nuclear weapons testing, the years of testing, and the years post-testing. Let's suppose that the start of testing corresponds to depth x_1 and the ending of testing corresponds to depth x_2. For the years preceding the testing, we will have approximately a decay curve, with starting amplitude S_1, as well as potentially a sinusoidal function to account for the oscillations visible in the data. For the years post-testing, we have what looks like an increasing exponential function, going from a relatively small value to maximum value S_2. To model this, what we could do would be flip the data horizontally so that it looks like an exponential decay curve (meaning that we can

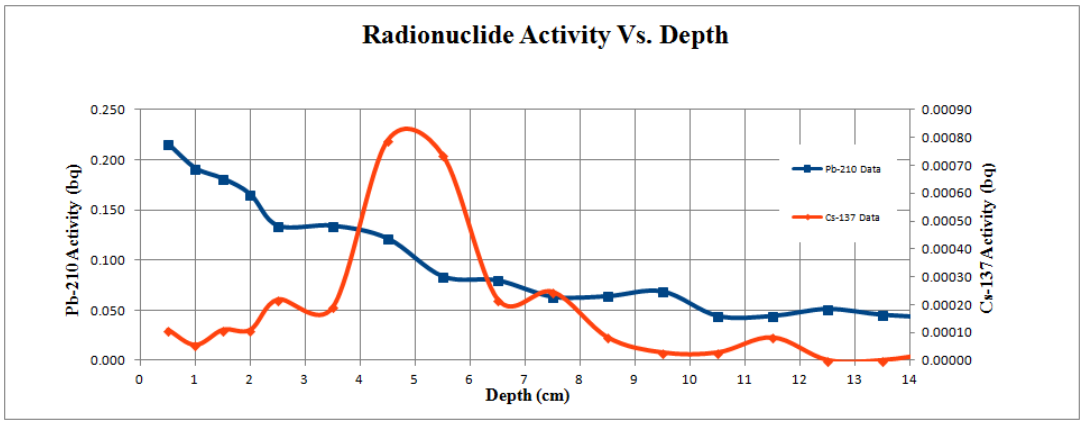

Figure 6.1. Unsupported and supported lead-210 and cesium-137 activity in Golden Lake.

have a starting value of S_2 at depth x_2). Then the depth data will correspond to rising through the layers of sediment rather than descending. Because this data is "flipped," it would have to be treated separately from the weapons testing and pre-testing years, because the information that would come from it would be in a sense reversed. The depths and times generated from this curve would be measuring from the depth at concentration S_2, so calculations would have to be performed to transform the axis back to the origin.

When considering the testing years, however, we run into some difficulties. Since cesium-137 was introduced into the atmosphere in large quantities over relatively short intervals of time, one way to model the process by which it was introduced would be through a series of pulse functions. However, since the sediment sample slices correspond to several year intervals, even if the precise dates of the pulses were known, the data isn't fine grained enough to determine information about the individual pulses. Rather, what we see is an accumulation of the effects of multiple pulses and their corresponding decays, the shape of which we cannot precisely model with our limited information.

My initial thought was that perhaps we could ignore what was happening during the testing years, since we know the dates of nuclear testing. However, because cesium-137 is able to migrate through the soil, the sharp peaks that we see in the data may not correspond exactly to the years of nuclear testing. We should be able to estimate the age of sediment on the left side of the graph from the post-testing information, but the right half

we cannot determine an accurate age from without the information for the testing years. We could make an estimate based on when nuclear testing began, but that estimate could be off by several years, introducing a large amount of uncertainty into our age estimates. There are likely many more optimal approaches which could be taken, and it should be an interesting question to be considered in future research.

Since other fallout radionuclides like strontium-190 were introduced into the environment in the same fashion as cesium-137, similar models would be used. However, for fallout radionuclides that have less ability to migrate through the soil layers, there may not be as much difficulty in modeling as there is with cesium-137. There may not even be a right half to the graph if the radioisotopes are nearly stationary, since these isotopes are not naturally occurring. While cesium-137 is likely the most commonly collected and utilized of the fallout radionuclides for radiometric dating, it would be interesting to apply the NCRS model to other radioisotopes as well.

6.4 Conclusion

The research presented here provides much promise for future research endeavors. It is intriguing to see that of the small sample of bodies of water considered, many exhibited sinusoidal oscillations. Of the bodies of water with sinusoidal oscillations, almost all had the same period, once uncertainty was accounted for. It is also notable that this period seems to line up with the period of some of the processes behind the NAOs, suggesting that perhaps climate cycles could be behind the periodic behavior.

There are many possibilities for improvement, particularly in regards to the fitting process, which could yield better results. There are also many avenues to explore, such as the cause of the oscillations and adapting the NCRS model for fallout radioisotopes. Hopefully this work will be but the start of new research in radiometric dating and will help us to better understand the world around us.

REFERENCES

[1] D. L. Cahl, "Diffusion coefficients calculated using Cs 137 profiles applied to Pb 210 dating in lake core samples," Master's thesis, University of Maine, 2012.

[2] H. R. von Gunten, "Radioactivity: A tool to explore the past," *Radiochimica Acta* **71** (1995) 305–316.

[3] B. Lindell, *Pandora's Box: The History of radiation, radioactivity, and radiological protection.* Nordic Society for Radiation Protection, Sweden, 1st ed., 1996. Translated from Swedish by Helen Johnson.

[4] G. Rosenbusch and A. Knect-van Eekelen, *Wilhelm Conrad Röntgen: The Birth of Radiology.* Springer, Switzerland, 1st ed., 2019.

[5] T. J. Jorgensen, *Strange Glow: The Story of Radiation.* Princeton University Press, Princeton, N.J., 1st ed., 2016.

[6] W. C. Röntgen, "On a new kind of rays," *Science* **3** no. 59, (1896) 227–231. Translated from German by Arthur Stanton.

[7] B. Goldsmith, *Obsessive genius: The inner world of Marie Curie.* WW Norton & Company, 2005.

[8] M. S. Curie, "Les nouvelles substances radioactives," *Revue Scientifique* **37** no. 2, (1900) 65–71.

[9] M. Malley, "The discovery of atomic transmutation: Scientific styles and philosophies in france and britain," *Isis* **70** no. 2, (1979) 213–223.

[10] W. Ramsay and F. Soddy, "Experiments in radio-activity, and the production of helium from radium," *Nature* (1903) 354–355.

[11] E. Rutherford and T. Royds, "Spectrum of the radiun emanation," *Philosophical Magazine* **16** no. 2, (1908) 313–317.

[12] E. Rutherford and F. Soddy, "The cause and nature of radioactivity - Part I," *The London, Edinburgh, and Dublin Philosophical Magazine and Journal of Science* **21** no. 4, (1902) 370–396.

[13] L. Badash, "The age-of-the-Earth debate," *Scientific American* **261** no. 2, (1989) 90–97.

[14] E. Rutherford and H. T. Barnes, "Heating effect of the radium emanation," *Nature* **68** no. 1774, (1903) 622.

[15] D. R. Prothero, *The Story of the Earth in 25 Rocks: Tales of Important Geological Puzzles and the People who Solved Them.* Columbia University Press, Columbia, N.Y., 1st ed., 2018.

[16] J. L. Powell, *Four Revolutions in the Earth Sciences: from Hersey to Truth.* Columbia University Press, Columbia, N.Y., 1st ed., 2015.

[17] B. B. Boltwood, "On the ultimate disintegration products of the radioactive elements: Part II. the disintegration products of uranium," *American Journal of Science* **23** no. 134, (1907) 77–88.

[18] E. Rutherford and B. B. Boltwood, "The relative proportion of radium and uranium in radio-active minerals," *American Journal of Science* **22** no. 127, (1906) 1.

[19] A. Holmes, "The association of lead with uranium in rock-minerals, and its application to the measurement of geological time," *Proceedings of the Royal Society of London. Series A, Containing Papers of a Mathematical and Physical Character* **85** no. 578, (1911) 248–256.

[20] Arthur Holmes, *The Age of the Earth.* Harper & Brothers, 1913.

[21] K. Swenson, *Medical women and Victorian fiction.* University of Missouri Press, 2005.

[22] M. C. Nagel, "Frederick Soddy: From alchemy to isotopes," *The Journal of Chemical Education* no. 9, (1982) 739–740.

[23] A. O. Nier, "Variations in the relative abundances of the isotopes of common lead from various sources," *Journal of the American Chemical Society* **60** (1938) 1571–1576.

[24] A. O. Nier, R. W. Thompson, and B. F. Murphey, "The isotopic composition of lead and the measurement of geological time, iii," *Physical Review* **60** no. 2, (1941) 112–116.

[25] A. Holmes, "An estimate of the age of the earth," *Nature* **157** (1946) 680–684.

[26] F. G. Houtermans, "Die Isotopen-Häufigkeiten im natürlichen Blei un das Alter des Urans," *Naturwissenchaften* **33** (1946) 185–186.

[27] C. Patterson, "Age of meteorites and the earth," *Geochimica et Cosmochimica Acta* **10** no. 4, (1956) 230–237.

[28] W. F. Libby, "Atmospheric helium three and radiocarbon from cosmic radiation," *Physical Review* **69** (1946) 671–672.

[29] W. F. Libby, *Radiocarbon Dating.* University of Chicago Press, 1952.

[30] M. Hedman, *The Age of Everything: How Science Explores the Past.* University of Chicago Press, 2007.

[31] B. R. R. Persson and E. Holm, "Polonium-210 and lead-210 in the terrestrial environment: a historical review," *Journal of Enviromental Radioactivity* **102** (2011) 420–429.

[32] K. S. Krane, *Introductory Nuclear Physics.* John Wiley & Sons, New York, 1st ed., 1988.

[33] E. D. Goldberg, "Geochronology with Pb-210 in radioactive dating," in *International Atomic Energy Agency Symposium Proceedings*, pp. 121–131. 1963.

[34] S. Krishnaswamy, D. Lal, J. M. Martin, and M. Meybeck, "Geochronology of lake sediments," *Earth and Planetary Science Letters* **11** (1971) 407–414.

[35] J.A. Sanchez-Cabeza and A.C. Ruiz-Fernández, "210pb sediment radiochronology: an integrated formulation and classification of dating models," *Geochimica et Cosmochimica Acta* **82** (2012) 183–200.

[36] P. G. Appleby and F. Oldfield, "The calculation of lead-210 dates assuming a constant rate of supply of unsupported Pb-210 to the sediment," *Catena* **5** (1978) 1–8.

[37] R. B. Davis, C. T. Hess, S. A. Norton, D. W. Hanson, K. D. Hoagland, and D. S. Anderson, "Cs-137 and Pb-210 dating of sediments from soft-water lakes in New England (U.S.A.) and Scandinavia, a failure of Cs-137 dating," *Chemical Geology* **44** (1984) 151–185.

[38] A. Lerman, "Strontium-90 in the Great Lakes: Concentration-time model," *Journal of Geophysical Research* **77** no. 18, (1972) 3256–3264.

[39] P. Van Metre, J. T. Wilson, C. C. Fuller, E. Callender, and B. J. Mahler, "Collection, analysis, and age-dating of sediment cores from 56 us lakes and reservoirs sampled by the us geological survey, 1992-2001," tech. rep., US Geological Survey, 2004.

[40] J. A. Robbins, "A model for particle-selective transport of tracers in sediments with conveyor belt deposit feeders," *Journal of Geophysical Research: Oceans* **91** no. C7, (1986) 8542–8558.

[41] E. Callender, "Geochemical effects of rapid sedimentation in aquatic systems: minimal diagenesis and the preservation of historical metal signatures," *Journal of Paleolimnology* **23** no. 3, (2000) 243–260.

[42] G. Gilmore and J. D. Hemingway, *Practical gamma-ray spectroscopy*. John Wiley & Sons, 1st ed., 1995.

[43] R. B. Firestone, C. M. Baglin, and S. Y. F. Chu, *Table of Isotopes: 1999 update*. John Wiley & Sons, 8th ed., 1999.

[44] P. A. Tanner, S. M. Pan, S. Y. Mao, and K. N. Yu, "γ-ray spectrometric and α-counting method comparison for the determination of pb-210 in estuarine sediments," *Applied Spectroscopy* **54** no. 10, (2000) 1443–1446.

[45] G. F. Knoll, *Radiation Detection and Measurement*. John Wiley & Sons, Inc., 3rd ed., 2000.

[46] V. Putyrskaya, E. Klemt, and S. Röllin, "Migration of Cs-137 in tributaries, lake water and sediment of Lago Maggiore (Italy, Switzerland) - analysis and comparison with Lago di Lugano and other lakes," *Journal of Environmental Radioactivity* **100** (2009) 35–48.

[47] J. Wang, M. Baskaran, and J. Niedermiller, "Mobility of Cs-137 in freshwater lakes: A mass balance and diffusion study of Lake St. Clair, Southeast Michigan, USA," *Geochimica et Cosmochimica Acta* **218** (2017) 323–342.

[48] J. M. Zachara, S. C. Smith, C. Liu, J. P. McKinley, R. J. Serne, and P. L. Gassman, "Sorption of Cs+ to micaceous subsurface sediments from the Hanford site, USA," *Geochimica et Cosmochimica Acta* **66** (2002) 193–211.

[49] P. G. Appleby, "Three decades of dating recent sediments by fallout radionuclides: a review," *Holocene* **18** no. 1, (2008) 83–94.

[50] M. Baskaran, J. Nix, C. Kuyper, and N. Karunakara, "Problems with the dating ot sediment core using excess (210)Pb in a freshwater system impacted by large scale watershed changes," *Journal of Environmental Radioactivity* **138** (2014) 355–363.

[51] M. Yoshimori, "Production and behavior of beryllium 7 radionuclide in the upper atmosphere," *Advances in Space Research* **36** (2005) 922–926.

[52] J. Z. Drexler, C.C. Fuller, and S. Archfield, "The approaching obsolescence of Cs-137 dating of wetland soils in North America," *Quaternary Science Review* **199** (2108) 83–96.

[53] J. Paatero, B. Veleva, and J. Hatakka, "Long-term trends of lead-210 concentrations in ground-level air in Finland and Bulgaria," in *Global Environmental Change: Challenges to Science and Society in Southeastern Europe: Selected Papers presented in the International Conference held 19-21 May 2008 in Sofia Bulgaria*, V. Alexandrov, M. F. Gajdusek, C. G. Knight, and A. Yotova, eds., pp. 229–234. Springer, 2010.

[54] C. T. Hess and C. W. Smith, "A mathematical model of the accumulation of radionuclides by oysters (C. virginia) aquacultured in the effluent of a nuclear power reactor to include major biological parameters," *Health Physics* **33** (1977) 121–130.

[55] C. Frankfort-Nachmias and A. Leon-Guerrero, *Social Statistics for a Diverse Society.* Sage Publications, 4th ed., 2006.

[56] Maine Department of Inland Fisheries and Wildlife, "Cochnewagon Pond, Monmouth Twp., Kennebec Co. U.S.G.S. Monmouth, Me." `https://www.maine.gov/ifw/docs/lake-survey-maps/kennebec/cochnewagon_pond.pdf`, 2006.

[57] Knut Lehre Seip, Øyvind Grøn, and Hui Wang, "The North Atlantic Oscillations: Cycle times for the NAO, the AMO and the AMOC," *Climate* **7** no. 3, (2019) 43.

[58] Knut L Seip and Øyvind Grøn, "Atmospheric and ocean dynamics may explain cycles in oceanic oscillations," *Climate* **7** no. 6, (2019) 77.

APPENDIX A

LAKE DATA

This appendix contains the data used for the bodies of water analyzed in this paper. Generally the data had already been processed, so the author did not need to manually compute the specific activities, but rather needed only to check that the calculations performed by previous researchers appeared to be correct, and then subtract the supported lead-210 to obtain the unsupported lead-210 values. Below are the specific activities for various lakes. Values omitted from fits are denoted with a star.

A.1 Cochnewagon Lake

Table A.1. Specific Activity of Unsupported Lead-210 and Uncertainty Values for Cochnewagon Lake.

Depth (cm)	**Specific Activity** ($\frac{Bq}{g}$)	**Uncertainty** ($\frac{Bq}{g}$))
.25	.4487	.0222
1.25	.3520	.0208
2.25	.3587	.0233
3.25	.3222	.0206
4.25	.2246	.0191
5.25	.2185	.0192
6.25	.1869	.0193
7.25	.1015	.0152
8.25	.0662	.0141
9.25	.0636	.0141
10.25	.0372	.0126

A.2 Golden Lake

Table A.2. Specific Activity of Unsupported Lead-210 and Uncertainty Values for Golden Lake.

Depth (cm)	**Specific Activity** ($\frac{Bq}{g}$)	**Uncertainty** ($\frac{Bq}{g}$))
.5*	.0567	.0001570
1	.0424	.0001338
1.5	.0390	.0001306
2	.0329	.0001199
2.5	.0239	.0001136
3.5	.0234	.0001080
4.5	.0193	.0001011
5.5	.0095	.0000905
6.5	.0081	.0000851
7.5	.0041	.0000829
8.5	.0034	.0000815
9.5	.0028	.0000764
10.5	.0008	.0000856
11.5*	-.0007	.0000759
12.5*	.0001	.0000710
13.5*	.0003	.0000778
14.5*	.0003	.0000847

A.3 SS15 Greenland

Table A.3. Specific Activity of Unsupported Lead-210 and Uncertainty Values for SS15 in Greenland.

Depth (cm)	**Specific Activity** ($\frac{Bq}{g}$)	**Uncertainty** ($\frac{Bq}{g}$))
.5	.0599005	.0000694
1.25	.0445720	.0000598
2.25	.0284988	.0000363
3.25	.0294943	.0000900
4.25	.0070382	.0000088
5.25	.0166277	.0000323
6.25	.0062154	.0000103
7.25	.0042522	.0000080
8.25	.0020304	.0000050
9.25	.0005493	.0000006

A.4 Gardner Pond

Table A.4. Specific Activity of Unsupported Lead-210 and Uncertainty Values for Gardner Pond.

Depth (cm)	**Specific Activity** ($\frac{Bq}{g}$)	**Uncertainty** ($\frac{Bq}{g}$))
1	1.0757	.0017717
2	.5035	.0012802
3	.2481	.0009118
4	.2283	.0010728
5	.1615	.0010822
6	.0592	.0008481
8	.0195	.0007759
10	.0261	.0009002
12	.0443	.0009007

A.5 Highland Lake

Table A.5. Specific Activity of Unsupported Lead-210 and Uncertainty Values for Highland Lake.

Depth (cm)	**Specific Activity** ($\frac{Bq}{g}$)	**Uncertainty** ($\frac{Bq}{g}$))
.5	5.8065	.0142
1.5	7.1761	.0121
2.5	7.4521	.0084
3.5	5.2343	.0017
4.5	3.7233	.0005
5.5	2.8816	.0090
6.5	.7423	.0103
7.5	.7341	.0065
8.5	.3921	.0026
9.5	.2361	.0011

A.6 Salmon Pond

Table A.6. Specific Activity of Unsupported Lead-210 and Uncertainty Values for Salmon Pond.

Depth (cm)	**Specific Activity** ($\frac{Bq}{g}$)	**Uncertainty** ($\frac{Bq}{g}$))
.75	.6756	.0010
1.5	1.0611	.0021
2.5	.4839	.0010
3.5	.4120	.0010
4.5	.2825	.0007
5.5	.1906	.0005
6.5	.1357	.0004
7.5	.0945	.0003

A.7 Warner Lake

Table A.7. Specific Activity of Unsupported Lead-210 and Uncertainty Values for Warner Lake.

Depth (cm)	**Specific Activity** ($\frac{Bq}{g}$)	**Uncertainty** ($\frac{Bq}{g}$))
.25*	27.5130	.0142
.75	21.1710	.0121
1.25	15.6664	.0084
1.75	5.9330	.0017
2.25	3.4262	.0005
2.75	12.0525	.0090
3.25	8.7116	.0103
3.75	3.8524	.0065
4.25	.9480	.0026
4.75	.5300	.0011
5.25	.4179	.0015

A.8 Bracey Lake

Note that uncertainty values were not given for Bracey Lake.

Table A.8. Specific Activity of Unsupported Lead-210 and for Bracey Lake.

Depth (cm)	**Specific Activity** ($\frac{Bq}{g}$)
.75	.87
1.0	.71
1.5	.55
2.0	.54
2.5	.53
3.0	.47
3.5	.42
4.0	.36
4.5	.30
5.0	.28
5.5	.27
6.0	.24
6.5	.22
7.0	.21
7.5	.19
8.0	.14
8.5	.08
9.0	.08
9.5	.07
10.0	.07

A.9 Barsjon

Table A.9. Specific Activity of Unsupported Lead-210 and Uncertainty Values for Barsjon.

Depth (cm)	**Specific Activity** ($\frac{Bq}{g}$)	**Uncertainty** ($\frac{Bq}{g}$))
.50	.055342	.0002635
2.5	.047629	.0002090
4.5	.029374	.0001700
5.5	.021024	.0001610
6.0	.023316	.0001573
6.5	.023037	.0001471
7.0	.014992	.0001616
7.5	.012472	.0001415
8.5	.02062	.0001268
10.5	.007136	.0001391
12.5	.003237	.0001245

APPENDIX B

PERIOD OF OSCILLATIONS ERROR SIMULATIONS

This appendix includes the simulation data that was used to compute the error estimates of the periods for the bodies of water considered in Chapter 5.

B.1 Cochnewagon Lake

For Cochnewagon Lake, the mean error was found to be .02301347, so the coefficient used for the error estimate was twice that value, .04602694. R was used to compute the mean and standard deviation for this simulated data. The mean was found to be $\mu = 21.5$ *years*, while the standard deviation was found to be 3.35 *years*.

B.2 SS15

For SS15, the mean error was found to be .00226476, so the coefficient used for the error estimate was twice that value, .00452952. The mean of the simulations was found to be $\mu = 22.8$ *years* and the standard deviation was found to be $\sigma = 1.55$ *years*.

B.3 Gardner Pond

For Gardner Pond, the mean error was found to be .009766963, so the coefficient used for the error estimate was twice that value, .019533926. The mean of the periods of the simulations was $\mu = 29.3$ *years*, while the standard deviation was $\sigma = 15.5$ *years*.

B.4 Golden Lake

For Golden Lake, the mean error was found to be .001360297, so the coefficient used for the error estimate was twice that value, .002720594. The mean period from the simulations was $\mu = 23.6$ *years*, while the standard deviation was $\sigma = 2.07$ *years*.

B.5 Highland Lake

For Highland Lake, the mean error was found to be .7209563, so the coefficient used for the error estimate was twice that value, 1.4419126. The mean of the simulation periods was $\mu = 26.5\ years$, while the standard deviation was $\sigma = 5.48\ years$.

B.6 Salmon Pond

For Salmon Pond, the mean error was found to be .01311514, so the coefficient used for the error estimate was twice that value, .02623028. The mean of the periods of the simulations was 25.9 *years*, while the standard deviation was $\sigma = .74\ years$.

B.7 Lake Purrumbete

For Lake Purrumbete, the mean error was found to be .006491262, so the coefficient used for the error estimate was twice that value, .012982524. The mean of the simulations was $\mu = 33.5\ years$ and the standard deviation was $\sigma = 13.3\ years$.

B.8 Warner Lake

For Warner Lake, the mean error was found to be .006491262, so the coefficient used for the error estimate was twice that value, .012982524. The mean of the simulations was found to be $\mu = 28.6\ years$, while the standard deviation was $\sigma = 4.26\ years$.

B.9 Bracey Lake

For Bracey Lake, the mean error was found to be .006491262, so the coefficient used for the error estimate was twice that value, .012982524. The mean of the simulations was $\mu = 26.4\ years$, while the standard deviation was $\sigma = 2.72\ years$.

B.10 Barsjon

For Barsjon, the mean error was found to be .002155469, so the coefficient used for the error estimate was twice that value, .004310938. The mean of the simulations was $\mu = 14.4$ $years$, while the standard deviation was $\sigma = 3.13$ $years$.

Table B.1. Thirty simulations with random noise and the resulting period for Cochnewagon Lake

Data run	Period ($Years$)
Original	22.4
Simulation 1	18.9
Simulation 2	19.3
Simulation 3	18.9
Simulation 4	16.0
Simulation 5	23.1
Simulation 6	20.5
Simulation 7	16.2
Simulation 8	25.5
Simulation 9	22.0
Simulation 10	24.2
Simulation 11	21.8
Simulation 12	16.6
Simulation 13	24.4
Simulation 14	17.1
Simulation 15	20.0
Simulation 16	27.4
Simulation 17	24.9
Simulation 18	23.8
Simulation 19	22.0
Simulation 20	21.6
Simulation 21	23.2
Simulation 22	16.7
Simulation 23	20.2
Simulation 24	22.8
Simulation 25	26.4
Simulation 26	15.7
Simulation 27	24.1
Simulation 28	23.9
Simulation 29	25.5
Simulation 30	22.1

Table B.2. Thirty simulations with random noise and the resulting period for SS15

Data run	Period ($Years$)
Original	22.9
Simulation 1	21.3
Simulation 2	23.5
Simulation 3	26.3
Simulation 4	19.9
Simulation 5	22.6
Simulation 6	20.2
Simulation 7	21.8
Simulation 8	21.5
Simulation 9	21.9
Simulation 10	21.3
Simulation 11	22.6
Simulation 12	23.4
Simulation 13	23.1
Simulation 14	26.7
Simulation 15	22.4
Simulation 16	23.4
Simulation 17	25.2
Simulation 18	23.7
Simulation 19	24.0
Simulation 20	20.8
Simulation 21	23.2
Simulation 22	21.8
Simulation 23	22.7
Simulation 24	22.0
Simulation 25	22.8
Simulation 26	23.9
Simulation 27	23.9
Simulation 28	22.3
Simulation 29	23.9
Simulation 30	22.9

Table B.3. Thirty simulations with random noise and the resulting period for Gardner Pond

Data run	Period ($Years$)
Original	57.4
Simulation 1	21.4
Simulation 2	21.2
Simulation 3	57.6
Simulation 4	21.3
Simulation 5	20.9
Simulation 6	20.6
Simulation 7	22.5
Simulation 8	21.0
Simulation 9	21.2
Simulation 10	59.7
Simulation 11	19.8
Simulation 12	19.6
Simulation 13	53.4
Simulation 14	21.6
Simulation 15	59.8
Simulation 16	20.2
Simulation 17	22.0
Simulation 18	21.2
Simulation 19	53.7
Simulation 20	20.9
Simulation 21	22.2
Simulation 22	60.3
Simulation 23	20.8
Simulation 24	19.4
Simulation 25	20.8
Simulation 26	20.1
Simulation 27	53.3
Simulation 28	21.5
Simulation 29	20.2
Simulation 30	21.9

Table B.4. Thirty simulations with random noise and the resulting period for Golden Lake

Data run	Period ($Years$)
Original	24.0
Simulation 1	23.6
Simulation 2	21.7
Simulation 3	23.7
Simulation 4	24.2
Simulation 5	21.1
Simulation 6	24.1
Simulation 7	23.0
Simulation 8	22.0
Simulation 9	25.2
Simulation 10	21.3
Simulation 11	24.0
Simulation 12	23.4
Simulation 13	26.8
Simulation 14	24.4
Simulation 15	24.0
Simulation 16	22.9
Simulation 17	27.0
Simulation 18	20.5
Simulation 19	22.2
Simulation 20	22.2
Simulation 21	22.6
Simulation 22	26.8
Simulation 23	22.8
Simulation 24	30.2
Simulation 25	24.7
Simulation 26	21.2
Simulation 27	23.7
Simulation 28	22.9
Simulation 29	21.7
Simulation 30	23.1

Table B.5. Four simulations with random noise and the resulting period for Highland Lake

Data run	Period ($Years$)
Original	28.8
Simulation 1	22.2
Simulation 2	21.7
Simulation 3	17.9
Simulation 4	22.9
Simulation 5	38.4
Simulation 6	14.5
Simulation 7	19.7
Simulation 8	19.2
Simulation 9	30.3
Simulation 10	22.7
Simulation 11	23.7
Simulation 12	25.6
Simulation 13	27.0
Simulation 14	29.2
Simulation 15	30.1
Simulation 16	34.8
Simulation 17	27.0
Simulation 18	33.2
Simulation 19	28.0
Simulation 20	25.0
Simulation 21	30.7
Simulation 22	26.3
Simulation 23	37.3
Simulation 24	24.3
Simulation 25	30.0
Simulation 26	22.5
Simulation 27	26.7
Simulation 28	27.2
Simulation 29	29.9
Simulation 30	27.2

Table B.6. Thirty simulations with random noise and the resulting period for Salmon Pond

Data run	Period ($Years$)
Original	25.9
Simulation 1	24.4
Simulation 2	26.7
Simulation 3	25.7
Simulation 4	24.4
Simulation 5	26.3
Simulation 6	25.9
Simulation 7	26.5
Simulation 8	24.8
Simulation 9	25.2
Simulation 10	26.8
Simulation 11	26.6
Simulation 12	25.9
Simulation 13	25.9
Simulation 14	25.3
Simulation 15	25.8
Simulation 16	24.7
Simulation 17	26.2
Simulation 18	26.5
Simulation 19	27.4
Simulation 20	25.4
Simulation 21	26.2
Simulation 22	25.5
Simulation 23	26.4
Simulation 24	25.6
Simulation 25	26.5
Simulation 26	26.5
Simulation 27	26.5
Simulation 28	26.0
Simulation 29	25.1
Simulation 30	26.1

Table B.7. Thirty simulations with random noise and the resulting period for Lake Purrumbete

Data run	Period ($Years$)
Original	26.3
Simulation 1	26.4
Simulation 2	52.4
Simulation 3	28.6
Simulation 4	23.9
Simulation 5	31.1
Simulation 6	25.0
Simulation 7	48.4
Simulation 8	26.6
Simulation 9	55.4
Simulation 10	26.9
Simulation 11	48.4
Simulation 12	58.0
Simulation 13	27.5
Simulation 14	55.1
Simulation 15	21.5
Simulation 16	22.2
Simulation 17	20.4
Simulation 18	56.3
Simulation 19	26.8
Simulation 20	48.5
Simulation 21	24.7
Simulation 22	20.9
Simulation 23	24.3
Simulation 24	28.8
Simulation 25	27.1
Simulation 26	22.8
Simulation 27	25.8
Simulation 28	26.2
Simulation 29	55.1
Simulation 30	20.9

Table B.8. Thirty simulations with random noise and the resulting period for Warner Lake

Data run	Period ($Years$)
Original	29.2
Simulation 1	29.3
Simulation 2	24.3
Simulation 3	25.0
Simulation 4	28.0
Simulation 5	32.4
Simulation 6	25.9
Simulation 7	38.1
Simulation 8	20.7
Simulation 9	28.9
Simulation 10	31.6
Simulation 11	30.2
Simulation 12	29.4
Simulation 13	23.5
Simulation 14	22.0
Simulation 15	25.2
Simulation 16	26.2
Simulation 17	37.2
Simulation 18	25.8
Simulation 19	37.4
Simulation 20	31.5
Simulation 21	29.3
Simulation 22	28.5
Simulation 23	29.6
Simulation 24	26.7
Simulation 25	26.3
Simulation 26	26.4
Simulation 27	26.0
Simulation 28	30.1
Simulation 29	27.2
Simulation 30	33.8

Table B.9. Thirty simulations with random noise and the resulting period for Bracey Lake

Data run	Period ($Years$)
Original	26.6
Simulation 1	21.7
Simulation 2	22.4
Simulation 3	25.7
Simulation 4	26.1
Simulation 5	29.7
Simulation 6	27.6
Simulation 7	24.1
Simulation 8	23.6
Simulation 9	24.6
Simulation 10	25.6
Simulation 11	25.0
Simulation 12	26.4
Simulation 13	27.9
Simulation 14	26.3
Simulation 15	20.2
Simulation 16	29.9
Simulation 17	32.3
Simulation 18	28.0
Simulation 19	24.2
Simulation 20	30.9
Simulation 21	29.5
Simulation 22	26.5
Simulation 23	25.5
Simulation 24	27.5
Simulation 25	28.8
Simulation 26	27.8
Simulation 27	27.8
Simulation 28	26.3
Simulation 29	23.7
Simulation 30	26.6

Table B.10. Thirty simulations with random noise and the resulting period for Barsjon

Data run	Period ($Years$)
Original	15.1
Simulation 1	17.0
Simulation 2	8.9
Simulation 3	14.6
Simulation 4	16.4
Simulation 5	12.1
Simulation 6	18.6
Simulation 7	16.4
Simulation 8	8.4
Simulation 9	11.7
Simulation 10	15.0
Simulation 11	11.5
Simulation 12	15.3
Simulation 13	14.2
Simulation 14	18.3
Simulation 15	15.8
Simulation 16	17.2
Simulation 17	15.2
Simulation 18	9.5
Simulation 19	12.9
Simulation 20	18.8
Simulation 21	14.7
Simulation 22	13.5
Simulation 23	14.5
Simulation 24	13.4
Simulation 25	9.2
Simulation 26	16.7
Simulation 27	18.1
Simulation 28	19.3
Simulation 29	10.2
Simulation 30	15.8

APPENDIX C

SAMPLE R CODE

C.1 Nonlinear Fitting

```
csvFileName = "C:/Users/Amber/Documents/Nuclear_Physics/
SampleDataforCheckingRFit.csv"
csvFileName

SampleData <- read.csv(csvFileName)
SampleData

plot(SampleData)

y = SampleData$concentration
x = SampleData$depth

nonlin_mod=nls(y~a*exp(-b*x),start=list(a=0.63,b=0.4))

summary(nonlin_mod)

library(qpcR)

RSS(nonlin_mod)

nonlin_mod
```

```
plot(x,y)

lines(x,predict(nonlin_mod),col="red")

nonlin_mod=nls(y~a*exp(-b*x)*(1+c*sin(x)+d*x),
                start=list(a=0.5,b=.4,c=.1,d=.8))

summary(nonlin_mod)

RSS(nonlin_mod)

nonlin_mod
```

C.2 Simulating Data with Noise

```
csvFileName = "C:/Users/Amber/Documents/Nuclear Physics/
SimulatedDataCochnewagonLake.csv"
SimulatedDataCochnewagonLake<-read.csv(csvFileName)

y <- SimulatedDataCochnewagonLake$UnsupportedPb210
x <- SimulatedDataCochnewagonLake$Depth



yrnd <- y+0.05*(runif(11)*2-1)

yrnd

plot(x,yrnd)
```

APPENDIX D

NCRSFITMODELSOFTWARE CODE

```
#Example for Aoft_simp, uncomment to run example after sourcing
#plot(Aoft_simp(0.5194,0.1970,function(x)(1+0.1496*sin(1.7930*x
+3.1259)),0.1501,.25),t='l')


#Uses the coefficents to compute the activity over time/depth
# @param a       - a exponential coefficient
# @param b       - b exponential coefficient
# @param fn      - The function in the form of (1+f(x)) (e.g.
(1+c*sin(d*x+f)+gx)), we are computing A(t) for
# @param A0      - A_0 the initial concentration
# @param x0      - x_0 the initial condition of x
# @param k       - The decay coefficient
# @param aYears - The number of years to integrate over
# @param aStep  - The time step to integrate over
Aoft_simp <- function(a, b, fn, A0, x0=1, k=0.03114,
aYears = 100, aStep = 0.01){

  #Build a function for a*e^(-b*x)
  expfn <- function(x)(a*exp(-b*x))

  #Solve for ct
  ConcSolve <- function(x,t,c)(expfn(x)-exp(-k*t+c))
```

```
#a*e^(-b*x)-e^(-k*t+c)
ConcSolveC <- function(c)(ConcSolve(x0,0,c))
#a*e^(-b*x)-e^(c)
ct <- uniroot(ConcSolveC,c(-10000,10000) )$root
#Solve for c

#Build a linear function for xoft
xoft <- function(t)( (-k*t+ct-log(a))/(-b) )
#x(t) = (-k*t+c-ln(a))/(-b), this is a linear function

#We have to extract C0 linear piece
#We do this by finding the intercept of our (1+c*sin(x*d+f)+g*x)
lFnPoints <- fn(xoft(0:100))
lLM <- lm(lFnPoints~c(0:100) )
lC0Lin <- lLM$coefficients[1]
#y-intercept of fn, C_0

#Solve for zeta
Coft <- function(t)(exp(-k*t)*fn(xoft(t) )/lC0Lin )
#C(t) = e^(-k*t)*(1+c*sin(x(t)*d+f)+g*x(t))/C_0
lCInt <- integrate(Coft,0,Inf)$value
#integrate C(t)dt from 0 to infinity
lZeta = A0/lCInt
= A_0/SC(t)dt

#Integrate C(T) to get A(T) we build an array of t_i and
use that to compute A(i)
```

```
  #where t_i in T
  lADataX <- seq(0,aYears,aStep)
  #Set of T values
  lADataY <- NULL
  for(i in lADataX){
    lAoft = lZeta*integrate(Coft ,i,Inf)$value
    #A(t_i) = lZeta integralC(t)dt from i to infinity
    lADataY <- c(lADataY, lAoft)
  }

  lAData <- cbind("years" = lADataX, "A(t)" = lADataY)
  #Return the A(T) data
  return(lAData)
}
```

BIOGRAPHY OF THE AUTHOR

Amber Hathaway was born in Bangor, Maine and grew up in Veazie, Maine. She graduated from Bangor High School in 2008. She completed her undergraduate studies at The University of Maine, graduating summa cum laude with a Bachelor's of Arts in Mathematics, a second major in Women's Studies, and minors in Physics and Ethics and Social and Political Philosophy. During her tenure there, she was inducted into the following honors societies: Phi Beta Kappa, Phi Kappa Phi, Pi Mu Epsilon, and Phi Sigma Tau. She earned her Master's of Arts in Mathematics from the University of Maine in May of 2014 with a dissertation entitled, "Emmy Noether's Theorem on Integral Invariants in the Context of the Calculus of Variations." She has worked as a physics instructor at the University of Maine's Upward Bound Program, as a calculus teaching assistant, and as a physics teaching assistant. Amber Emily Hathaway is a candidate for the Doctorate of Philosophy degree in Physics from the University of Maine in May 2020.